CRYOPRESERVATION EFFECTS ON A PANCREATIC SUBSTITUTE COMPRISED OF BETA CELLS OR RECOMBINANT MYOBLASTS ENCAPSULATED IN NON-ADHESIVE AND ADHESIVE ALGINATE HYDROGELS

A Dissertation
Presented to
The Academic Faculty

by

Hajira Fatima Ahmad

In Partial Fulfillment
of the Requirements for the Degree
Doctor of Philosophy in the
Department of Biomedical Engineering

Georgia Institute of Technology
August 2012

CRYOPRESERVATION EFFECTS ON A PANCREATIC SUBSTITUTE COMPRISED OF BETA CELLS OR RECOMBINANT MYOBLASTS ENCAPSULATED IN NON-ADHESIVE AND ADHESIVE ALGINATE HYDROGELS

Approved by:

Dr. Athanassios Sambanis, Advisor
School of Chemical and Biomolecular Engineering
Georgia Institute of Technology

Dr. Thomas Barker
Department of Biomedical Engineering
Georgia Institute of Technology

Dr. Kelvin Brockbank
Institute for Bioengineering and Bioscience
Georgia Institute of Technology

Dr. Nicholas Simpson
Department of Medicine, Division of Endocrinology
University of Florida

Dr. Johnna Temenoff
Department of Biomedical Engineering
Georgia Institute of Technology

Date Approved: June 17, 2012

To my Mom and Dad

ACKNOWLEDGEMENTS

First, I would like to express my deepest gratitude towards my advisor Dr. Athanassios Sambanis for all his guidance, patience, and support over the years, helping me become a better scientist and engineer. I am also grateful to my committee members, Dr. Thomas Barker, Dr. Kelvin Brockbank, Dr. Nicholas Simpson, and Dr. Johnna Temenoff, for all their constructive feedback and helpful discussions. I would like to thank Dr. Barker and Dr. Temenoff for their help in designing my second aim studies. I would like to thank Dr. Brockbank for all his helpful discussions and insight in the field of cryopreservation. I would like to thank Dr. Simpson for teaching me ^{13}C NMR and isotopomer analysis and for all his helpful feedback throughout the years. Also, I am very grateful to Dr. Leslie Gelbaum and Dr. Johannes Leisen of the Georgia Tech NMR Center for teaching me about NMR and assisting me with my NMR experiments. I would also like to thank IBB Staff Members Steve Woodard, Nadia Boguslavsky, and Andrew Shaw for their assistance with my experiments.

I would also like to express my gratitude towards the current and former members of the Sambanis lab, for all their help with experiments, useful discussions, and encouragement throughout the years. In particular, I would like to thank Fernie Goh, Alison Lawson, Kiran Durvasula, Stephanie Duncanson, Aubrey Tiernan, Sudhakar Muthyala, Saif Al-Mamari, Chun Yong, Jose Vasquez, Andrew Kim, Heather Bara, Neil Mukherjee, Angie Gulino, and Jeff Gross. I would like to especially thank Alison for working with me on developing the vitrification protocols and helping me with my large-scale vitrification experiments.

I am especially grateful to all the wonderful friends I've made over the years in IBB and Wing 1-D- Peng-Meng Kou, Jaehyung Park, Todd Rogers, Scott Wilson, Catherine Rivet Gaurav Dwivedi, Ailia Gardezi, Sangeetha Srinivasan, Sarah Griffiths, Willa Ni, Maggie Phillips, Saheli Sarkar, Nathan Hotaling, Nnenna Adimora-Finn, Casey Holliday-Ankeny, Taby Ahsan, Adele Doyle, Stacey Schutte, and Lori Norton. I've learned so much from all of them, and they have been instrumental to my success. I am also thankful for all their encouragement and support.

I would like to thank my family for their unwavering support throughout the years, especially through the many tough times in graduate school. Without their constant encouragement and support, I would not be where I am today.

Finally, I would like to acknowledge my funding source NIH R01DK73991.

TABLE OF CONTENTS

LIST OF TABLES

LIST OF FIGURES

LIST OF ABBREVIATIONS

A	Addition
ACS	Flux through acetyl-CoA synthetase
AGEs	Advanced glycated end products
APA	Alginate-poly-L-lysine-alginate
BSA	Bovine serum albumin
C1	Carbon 1
CPA	Cryoprotectant
D	Doublet
DMSO	Dimethylsulfoxide
ECM	Extracellular Matrix
EDC	1-Ethyl-3-[3-dimethylaminopropyl] carbodiimide hydrochloride
G	guluronic acid
GluC2	glutamate C2
GluC3	glutamate C3
GluC4	glutamate C4
GSIS	Glucose-stimulated insulin secretion
IDD	Insulin-dependent diabetes
iPS	Induced pluripotent stem
ISR	Insulin secretion rate
K_{ATP}	ATP-sensitive K^+
KRB	Krebs-Ringer buffer
LDH	Flux through glycolysis

M	Mannuronic acid
NMR	Nuclear magnetic resonance
PC	Pyruvate carboxylase
PD	1,2 Propanediol
PDH	Flux through pyruvate dehydrogenase
PERV	porcine endogenous retrovirus
PK	Flux through phosphoenol-pyruvate carboxykinase/pyurvate kinase or malic enzyme
PLL	Poly-L-lysine
Q	Quartet
R	Removal
RT	Room temperature
S	Singlet
SNR	Signal-to-noise ratio
Sulfo-NHS	N-hydroxysulfosuccinimide
SV40	Simian virus 40
T	Triplet
TAg	large tumor antigen
TCA	Tricarboxylic Acid
TEPS	Tissue engineered pancreatic substitute
tet	tetracycline
U-^{13}C	Uniformly ^{13}C labeled
YPC	Flux through pyruvate carboxylase
YS	Flux through non-PC anaplerosis

SUMMARY

A tissue engineered pancreatic substitute consisting of insulin-secreting cells encapsulated in alginate hydrogels may provide more physiologic control of blood glucose levels compared to current exogenous insulin therapy for patients suffering from insulin-dependent diabetes (IDD). For clinical translation of a pancreatic substitute, however, long-term storage is essential, and cryopreservation is a promising means to achieve this goal. The two main methods that may be employed for cryopreservation are conventional freezing and vitrification. Although ice formation during freezing may not necessarily be detrimental to single cells in suspension, it may have adverse affects on a 3-D construct. Vitrification, or ice-free cryopreservation, is a promising alternative method of cryopreservation. However, potential osmotic excursions as well as cytotoxicity are issues associated with vitrification due to the high concentration of cryoprotectants used in the procedure. As both methods have their potential drawbacks, both must be systematically evaluated in order to determine the appropriate method of cryopreservation.

It is currently unclear what cell type will be most appropriate for an encapsulated cell therapy for treatment of IDD, and different insulin-secreting cells may have different requirements for cell adhesion in 3-D. Cell adhesion is important for various cellular processes, including survival, proliferation, and differentiation. In particular, encapsulating beta cells or islets in an adhesive environment has been shown to be beneficial for viability and/or function, and other cell types being explored for cell-based therapies for IDD treatment may also benefit from or require adhesion in 3-D. Thus, it is

important to study the effects of cryopreservation on cells encapsulated in non-adhesive vs. adhesive hydrogels. In this thesis, we have focused on studying cryopreservation effects on two model pancreatic substitutes: murine βTC-tet insulinoma cells encapsulated in unmodified alginate and C2C12 cells, stably transfected to secrete insulin, encapsulated in partially oxidized, RGD-modified alginate. βTC-tet cells encapsulated in unmodified alginate were chosen as a model pancreatic substitute in a non-adhesive matrix, as these cells have been shown to proliferate and function in a non-adhesive environment. Stable C2C12 cells encapsulated in RGD-alginate were chosen as the model pancreatic substitute in an adhesive matrix, as C2C12 cells have been well-characterized in RGD-alginate, showing the ability to proliferate and differentiate in 3-D.

In the first part of this thesis, we studied the effects of cryopreservation on the intermediary metabolism of encapsulated βTC-tet cells by ^{13}C nuclear magnetic resonance (NMR) and isotopomer analysis, as well as the effects of cryopreservation on insulin secretory function. In order to use the ^{13}C NMR and isotopomer analysis method, we first developed the appropriate parameters and procedures for ^{13}C labeling, extraction, and isotopomer analysis from Fresh and Cryopreserved encapsulated βTC-tet cells. After the appropriate parameters and procedures were determined, relative metabolic fluxes in the tricarboxylic acid (TCA) cycle were measured from Fresh, Frozen and DPS-vitrified encapsulated cells. It was found that intermediary metabolism was maintained, as measured by ^{13}C NMR and isotopomer analysis, in cryopreserved encapsulated βTC-tet cells. Although insulin secretory function was maintained in the Conventionally Frozen group, it was impaired in the DPS-vitrified group. Small-scale glucose-stimulated and K^+-induced depolarization experiments also indicated impaired secretion from the DPS-

vitrified group, but not from the Frozen encapsulated cells. Similar stimulation indices between glucose-stimulated and depolarization-induced secretion tests post-warming, similar intracellular insulin content to Fresh controls, and impaired depolarization-induced secretion compared to Fresh controls, indicate a possible defect in late-stage insulin secretion for the DPS-vitrified group.

In the second part of this thesis, we investigated the effect of cell-matrix interactions on cellular response to cryopreservation by assessing metabolic activity and insulin secretion in Cryopreserved Stable C2C12 cells encapsulated in RGD and RGE-alginate hydrogels up to one day post-warming. In addition, to address the longer-term cellular response to cryopreservation of cells encapsulated in an adhesive hydrogel environment, Stable C2C12 cells were encapsulated in RGD-alginate hydrogels, cultured for 1 or 4 days, cryopreserved, and assayed up to 3 days post-warming for insulin secretion and metabolic activity. As cell spreading has been associated with myoblast differentiation and fusion into myotubes in RGD-alginate, cell circularity in the beads was also measured one day post-warming. Results indicate that the presence of cell-matrix interactions did not affect cellular response in terms of metabolic activity or insulin secretion up to one day post-warming. Additionally, irrespective of culture time pre-preservation, metabolic activity, insulin secretion rate, and cell morphology were maintained in Frozen, RGD-alginate encapsulated Stable C2C12 cells. Similarly, although there were differences immediately post-warming, overall, metabolic activity, insulin secretion, and cell morphology were maintained in DPS-vitrified, RGD-alginate encapsulated cells.

In conclusion, the work in this thesis presents a systematic comparison of the two cryopreservation methods, conventional freezing and vitrification, on the *in vitro* cellular aspects of insulin-secreting cells encapsulated in an adhesive vs. non-adhesive alginate environment. Results on cryopreservation effects on intermediary metabolism in encapsulated βTC-tet cells offer insight into the effects of cryopreservation on cellular bioenergetics, indicating that relative carbon flow through the TCA cycle pathways examined is unaffected by cryopreservation. Additionally, DPS-vitrification led to impaired insulin secretion from encapsulated βTC-tet cells, possibly due to a defect in late-stage insulin secretion. The results from Stable C2C12 cells encapsulated in RGD vs. RGE-alginate indicate that up to one day post-warming, cell-matrix interactions do not affect cellular response for these cells after vitrification or freezing. Although there are transient differences from the Fresh control in terms of metabolic activity and insulin for DPS-vitrified RGD-encapsulated Stable C2C12 cells, metabolic activity and insulin secretion are maintained at all time points assayed for Frozen constructs. Overall, due to results comparable to Fresh controls and simplicity of procedure, conventional freezing is appropriate for cryopreservation of βTC-tet cells encapsulated in unmodified alginate or Stable C2C12 cells encapsulated in partially oxidized, RGD-modified alginate.

CHAPTER 1

INTRODUCTION

Approximately 18.8 million people in the United States have been diagnosed with diabetes, with approximately 5 million patients suffering from insulin-dependent diabetes (IDD) [1]. Both patients with Type I diabetes as well as some with Type 2 diabetes are insulin-dependent. Current treatments for insulin-dependent diabetes (IDD), including daily glucose monitoring and insulin delivery via injections or insulin pumps, do not provide tight glycemic control. This inability to tightly control blood glucose levels often leads to various secondary complications, such as kidney disease, blindness, heart disease, and stroke [1].

Although the "Edmonton Protocol," based on intrahepatic human islet transplantation with the use of steroid-free immunosuppression, is a promising approach to the treatment of IDD, the shortage of donor islets and the need for life-long immunosuppression prevent the wide-spread application of this treatment [2]. A tissue engineered pancreatic substitute (TEPS) based on microencapsulation of xenogeneic islets or other insulin-secreting cells in an immunoprotective barrier has the potential to provide more physiologic and less invasive blood glucose control than exogenous insulin-based treatments for IDD, while potentially relaxing the limitations due to tissue availability and immunosuppression [3].

Long-term storage is essential for clinical realization of a tissue engineered pancreatic substitute, and cryopreservation is the most promising means to achieve this goal (Figure 1.1). The two main methods that may be employed for cryopreservation are

conventional freezing and vitrification. Conventional freezing leads to the formation of extracellular ice, which although not necessarily detrimental to cells in suspension, can be damaging to natural tissues as well as 3-D tissue engineered constructs [4, 5]. During vitrification, however, a glass is formed instead of ice, thereby preventing damage associated with ice formation. However, vitrification can be damaging to the cells in a construct due to cytotoxicity and potential osmotic excursions that may occur due to the high concentration of cryoprotectants used in the procedure [5, 6]. As conventional freezing and vitrification have their associated drawbacks, both cryopreservation methods must be evaluated in order to determine the optimal cryopreservation method for a pancreatic substitute.

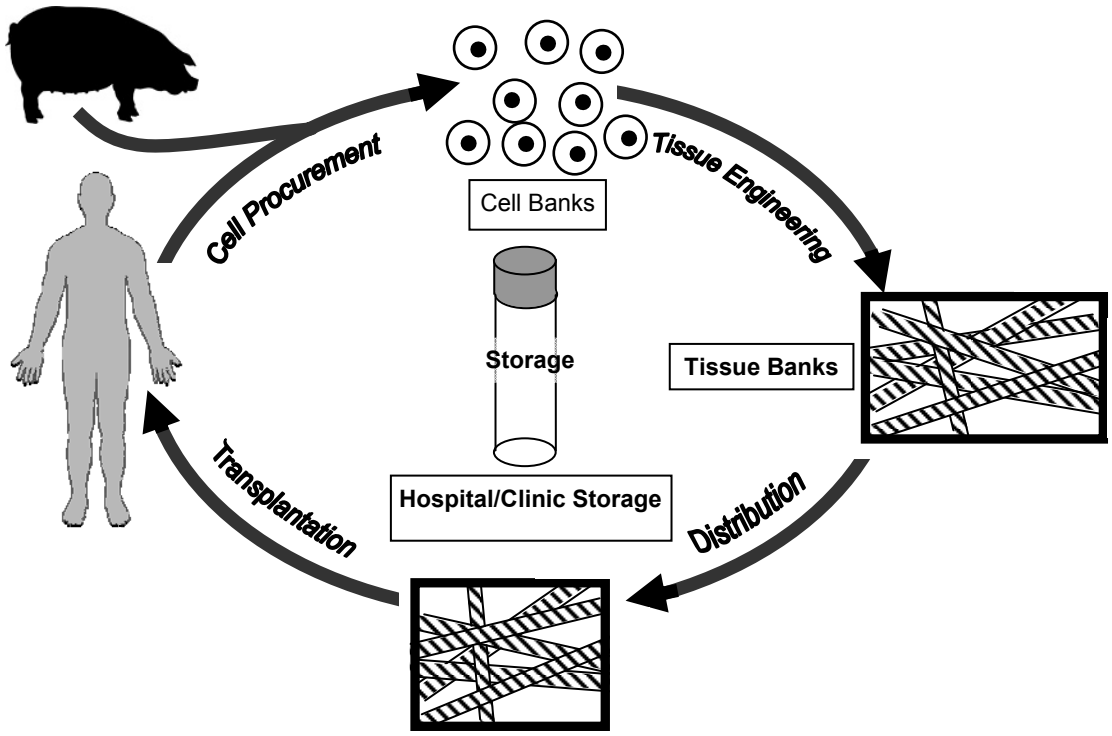

Figure 1.1 Role of cryopreservation in tissue engineering Adapted from *Life in the Frozen State* [7].

It is currently unclear what cell type will be most appropriate for an encapsulated cell therapy for treatment of IDD, and indeed different types of insulin-secreting cells may exhibit quite different requirements for cell adhesion in 3-D. Although pancreatic substitutes often consist of cells encapsulated in unmodified alginate hydrogels [8, 9], studies have suggested that pancreatic substitutes may benefit from an adhesive 3-D environment [10-12]. For anchorage-dependent cells, adhesion to the matrix is important for various cellular processes, including cell signaling, differentiation, and proliferation [13]. The added complexity of cell-matrix interactions between cells and the matrix may affect the outcome of the cryopreservation procedure, as compared with cells that are essentially suspended within a hydrogel matrix, as evidence in the cryopreservation literature indicates that adhesion has affects cryopreservation outcome [14-17]. Thus, in order to gain a fundamental understanding of the effects of cryopreservation on systems of encapsulated insulin-secreting cells as a whole, it is important to study the effects of cryopreservation on both cells encapsulated in an adhesive hydrogel matrix as well as cells encapsulated in a non-adhesive hydrogel matrix. Two model pancreatic substitutes that can be used to study this are βTC-tet cells encapsulated in unmodified alginate and C2C12 cells, stably transfected to secrete insulin, encapsulated in adhesive alginate (Figure 1.2). Murine insulinoma βTC-tet cells were used as the model pancreatic substitute in a non-adhesive environment, as they have been shown to proliferate and function well in a non-adhesive alginate system [18, 19]. On the other hand, C2C12 cells have been well-characterized in an adhesive (RGD-alginate) based system, and have been shown to proliferate and differentiate in this 3-D adhesive environment [20]. Thus, C2C12 cells, stably transfected to secrete insulin [21] and encapsulated in partially

oxidized, RGD-modified alginate, were studied as the model pancreatic substitute in a 3-D adhesive alginate system. Hence, the ***overall goal*** of this thesis was to investigate cryopreservation effects on model pancreatic substitutes consisting of cells encapsulated in non-adhesive and adhesive 3-D alginate hydrogels.

To address this overall goal, the first specific aim is to evaluate the effects of cryopreservation on intermediary metabolism and secretory function in βTC-tet cells encapsulated in unmodified alginate. As cryopreservation effects on cell viability and function in encapsulated beta cells [22, 23] have already been evaluated, and recent studies have indicated impairment in insulin secretion post-warming from encapsulated islets [24, 25] and beta cells [22], it is important to understand how fundamental aspects of glucose-stimulated insulin secretion, such as intermediary metabolism, are affected by cryopreservation. The ***hypothesis*** of this aim is that cryopreservation produces a significant change in the intermediary metabolism of encapsulated, insulin-secreting cells that survive the cryopreservation procedure.

The second specific aim of this thesis is to examine the effects of cryopreservation on cell survival and function in recombinant C2C12 cells encapsulated in adhesive alginate. Previous literature has suggested adhesion affects cell response to cryopreservation in various ways [16, 17, 26, 27], with some studies indicating an increased likelihood of cryoinjury due to adhesion [26, 27], and others indicating benefits to cryopreservation of attached cells compared to cells cryopreserved in suspension [17] or in non-adhesive matrices [16]. For example, adhesion has been shown to increase the likelihood of intracellular ice formation for cells cryopreserved while attached in 2-D compared to cells cryopreserved in suspension [26, 27]. However, studies have also

indicated benefits to adhesion in 3-D in terms of increased viability compared to cells cryopreserved in suspension or in a non-adhesive matrix [16]. Thus, although perhaps conflicting with respect to cryopreservation outcome, evidence in the literature points to adhesion affecting cryopreservation response. The ***hypothesis*** of this aim is that the presence of cell-matrix interactions between insulin-secreting cells and the matrix will affect cellular response to cryopreservation in terms of cell survival and function.

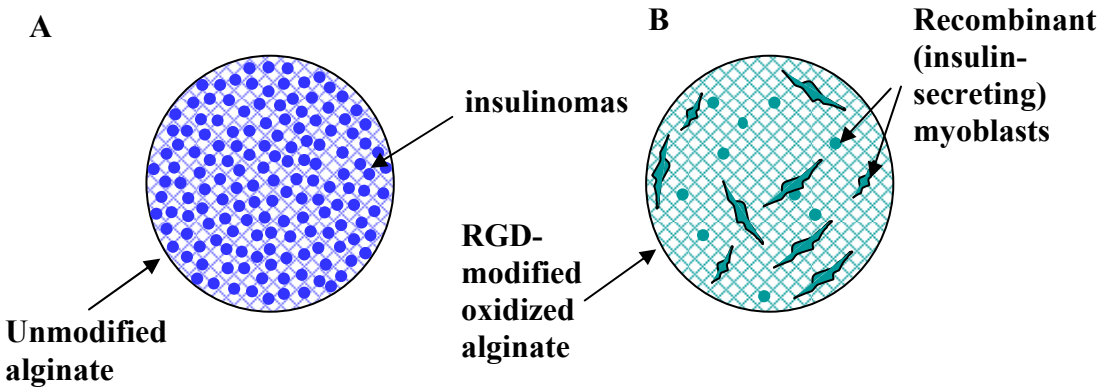

Figure 1.2 Model pancreatic substitutes studied in this thesis. A). βTC-tet cells encapsulated in unmodified alginate and B). Stably transfected C2C12 cells encapsulated in RGD-modified oxidized alginate.

An important first step in setting up a vitrification protocol for encapsulated cells is choosing the appropriate cryoprotectant solution for vitrification. In order to determine the appropriate cryoprotectant solution for vitrification of encapsulated βTC-tet cells, pre-developed cryoprotectant cocktails were added and removed from encapsulated βTC-tet cells. A previously developed math model was used to develop addition/removal protocols for the solutions [28]. The results of the cryoprotectant addition/removal study as well as initial vitrification studies are found in APPENDIX A.

Cryopreservation is critical for clinical translation of a TEPS, but recent studies with encapsulated beta cells or islets in particular have indicated impaired secretion post-

warming [22, 24, 25]. Although decreased cell viability may be an important factor in this reduced secretion, the state of the viable cells may also be impaired. In terms of cell function, however, previous studies on cryopreserved pancreatic substitutes have only examined insulin secretion post-warming [25, 29, 30]. Investigating fundamental processes in glucose-stimulated insulin secretion is important for gaining an in-depth understanding of the sublethal effects of cryopreservation on encapsulated beta cells or islets, as well as understanding possible cryopreservation-induced secretion defects. Studying intermediary metabolism is particularly important, as it is key to glucose-stimulated insulin secretion in beta cells [31-33]. One powerful method that has been employed to study intermediary metabolism in beta cells is ^{13}C nuclear magnetic resonance (NMR) and isotopomer analysis [34-36]. However, various parameters or procedures must be determined or optimized prior to using the ^{13}C NMR and isotopomer analysis method on the particular cells or tissue of interest. CHAPTER 4 addresses these issues, describing the development and optimization of parameters for ^{13}C labeling, extraction, and NMR isotopomer analysis for both Fresh and Cryopreserved encapsulated cells. In particular, the development of the perchloric acid extraction procedure, determination of isotopomer steady state, test of incubation medium on cryopreserved encapsulated cells, as well as determination of the appropriate model of glucose metabolism to use with tcaCALC are discussed. Using the optimized parameters and procedures developed in CHAPTER 4, the effects of cryopreservation on intermediary metabolism in encapsulated βTC-tet cells were investigated and are discussed in CHAPTER 5. In addition, insulin secretory response to both glucose stimulation and K^+-

induced depolarization after cryopreservation were studied and discussed in CHAPTER 5.

Although cryopreservation effects on viability and/or function of cells encapsulated in non-adhesive hydrogels have been studied [24, 25, 30, 37-44], not many studies have focused on similar effects on cells encapsulated in adhesive hydrogels [16, 45-47]. Studying cellular response after cryopreservation in an adhesive environment is especially important with respect to a TEPS, as studies have indicated the importance of adhesion in 3-D for encapsulated beta cells or islets [10-12]. Additionally, as different cell types, such as genetically engineered non-beta cells [48] and stem cells [48, 49] are being investigated for cell-based therapies for IDD, such cells may have different requirements for anchorage dependence in 3-D. The few studies on cells encapsulated in adhesive hydrogels have examined cryopreservation response after either conventional freezing [16, 45] or vitrification [50, 51], and have not compared the two. In CHAPTER 6 of this thesis, Stable C2C12 cells encapsulated in RGD and RGE-alginate hydrogels were cryopreserved and directly compared up to one day post-warming in order to investigate the effect of cell-matrix interactions on cryopreservation response in terms of metabolic activity and insulin secretion. Additionally, to address the longer-term response post-warming of Stable C2C12 cells encapsulated in an adhesive 3-D environment, Stable C2C12 cells were encapsulated in RGD-alginate hydrogels, cultured either 1 or 4 days post-encapsulation, cryopreserved, and assessed up to 3 days post-warming. As myoblast spreading in partially oxidized, RGD-modified hydrogels has been associated with myoblast differentiation and fusion into myotubes [20], and myoblast differentiation would be optimal for a pancreatic substitute prior to *in vivo* implantation, cell circularity

in beads was also assessed after cryopreservation. Additionally, intermediary metabolism was not studied from cryopreserved encapsulated Stable C2C12 cells as these cells do not possess the tight glucose stimulus-secretion coupling, of which intermediary metabolism is a key component, that is present in beta cells.

Finally, the conclusions and future directions from these studies are discussed in CHAPTER 7.

CHAPTER 2

SIGNIFICANCE

This thesis presents a systematic comparison of the *in vitro* effects of the two main cryopreservation methods that may be applied when preserving a tissue engineered construct. This is ***significant*** as cryopreservation studies in the literature often vary between cryopreservation method used, type of cell or construct cryopreserved, and method of analysis to evaluate cell function. Thus, it is often difficult to gain a fundamental understanding of the effects of different cryopreservation treatments on a particular system.

Specifically, work in this thesis investigates the effects of both conventional freezing and vitrification on different cellular aspects of pancreatic substitutes consisting of insulin-secreting cells encapsulated in adhesive and non-adhesive alginate matrices. With respect to a pancreatic substitute consisting of βTC-tet cells encapsulated in alginate hydrogels, our findings offer new insight into the effects of the two cryopreservation methods on cellular bioenergetics, with respect to TCA cycle pathways that have been shown to be key to insulin secretion [34-36]. Specifically, work in this thesis offers insight into understanding components of the insulin secretory pathway that are maintained after cryopreservation as well as those that should be investigated further to better understand compromised secretion from encapsulated beta cells post-warming. This work is ***novel***, as past studies have examined viability and/or insulin secretion post-warming in cryopreserved pancreatic substitutes [24, 25, 29, 30, 37, 52, 53] but none have evaluated fundamental aspects of glucose-stimulated insulin secretion in the

remaining viable cells, which are critical for proper construct function post-warming. In a broader sense, this work is ***significant*** as it offers insight into the effects of different cryopreservation procedures (i.e. conventional freezing vs. vitrification) on detailed cellular bioenergetics in a cryopreserved tissue engineered construct, for which information is current lacking in the scientific literature. By elucidating metabolic pathways that are affected by cryopreservation, and how they relate to cell function, cryopreservation protocols can be tailored to better maintain cell function in constructs post-warming.

With respect to a pancreatic substitute containing insulin-secreting cells in an adhesive matrix, this work is ***novel***, as there exist no reported studies on the effects of both vitrification and freezing on cells encapsulated in a 3-D adhesive alginate environment. In addition, the studies in this thesis are unique as they address the effects of cell-matrix interactions on cryopreservation response by encapsulating stably transfected, insulin-secreting myoblasts in adhesive, RGD-alginate vs. cells encapsulated in non-adhesive, RGE-alginate, which has also not been studied previously using both cryopreservation methods. Also, no studies have addressed the longer-term cellular response to both methods of cryopreservation in an adhesive alginate hydrogel environment up to a few days post-warming. This particular work is ***significant***, as it adds to the fundamental knowledge of the effects of different cryopreservation methods on cell viability and function in an adhesive hydrogel environment, which is particularly important as more studies in the literature are utilizing biomimetic hydrogels with the addition of adhesive motifs. Overall, studying the effects of cryopreservation on cells

with the added complexity of adhesion in 3-D provides a means to examine how attachment affects cell response to cryopreservation in this system.

CHAPTER 3

BACKGROUND

3.1 Diabetes

3.1.1 Type I and Type II Diabetes

Diabetes mellitus is a serious disease that results in elevated blood glucose levels. According to the Centers for Disease Control and Prevention, approximately 18.8 million people in the United States have been diagnosed with diabetes, with approximately 5-10% of diagnosed adults suffering from Type 1 diabetes [54]. Patients with Type I diabetes as well as some with Type 2 diabetes are insulin-dependent. Type 1 diabetes is caused by an autoimmune attack which destroys the insulin-producing beta cells of the islets of Langerhans in the pancreas. Type II diabetes is characterized by insulin resistance and a reduction in insulin production by beta cells in the pancreas. Although Type II diabetes can be initially controlled with proper diet and exercise [55] as well as by taking oral medications, some patients do become insulin-dependent over time.

3.1.2 Secondary Complications of Diabetes

Current treatments for insulin-dependent diabetes (IDD), including daily glucose monitoring and insulin delivery via daily injections or insulin pumps, do not provide tight glycemic control. This inability to tightly control blood glucose levels often leads to various secondary complications, such as kidney disease, blindness, heart disease, and stroke [54]. The secondary complications associated with diabetes are often caused by chronic hyperglycemia that can lead to tissue damage [56]. Specifically, microvascular

complications are one of the major causes of morbidity and mortality in patients with IDD [57]. One of the mechanisms of vascular damage is proposed to be through the production of advanced glycated end products (AGEs), which form due to reducing sugars binding to amine groups on proteins, lipids, or nucleic acids. Since advanced glycation of molecules occurs over a prolonged period of time, proteins with a low turnover rate, such as extracellular matrix molecules, are quite susceptible to advanced glycation [56]. In particular, collagen and elastin in blood vessels become increasingly cross-linked due to AGE formation, leading to an increase in blood vessel stiffness [58, 59]. This change in blood vessel compliance can lead to vascular dysfunction [60].

3.1.3 Current Treatments for Diabetes

3.1.3.1 Exogenous Insulin Therapy

Exogenous insulin therapy involves monitoring blood glucose levels daily with insulin delivery via either insulin injections or pumps. Insulin pumps are currently used by approximately 20-25% of patients in the United States that suffer from Type 1 Diabetes [61], with studies indicating better and less variable control of blood glucose levels compared to daily insulin injections [62, 63]. However, insulin pumps can be cumbersome and lead to possible infections at the insertion site in the skin [64]. Another major disadvantage of current insulin pumps is that they operate on an "open-loop" system, where there is no automatic feedback control to deliver the appropriate amount of insulin based on monitoring of real-time blood glucose levels.

The Diabetes Control and Complications Trial indicated that intensive insulin therapy via injections or pumps can delay the onset and progression of secondary

complications associated with diabetes [57]. However, intensive insulin therapy was found to increase the likelihood of hypoglycemic episodes in patients [57]. Although intense exogenous insulin therapy may reduce the progression of secondary complications of diabetes, it does not necessarily lead to their prevention. Thus, a more physiologic treatment is desired to better control blood glucose levels.

3.1.3.2 Whole Pancreas and Islet Transplantation

Current clinical cell-based therapies provide more physiologic glycemic control compared to exogenous insulin therapy. Whole pancreas transplantation leads to the reduction or elimination of the progression of secondary complications, and decrease in hypoglycemic episodes compared to exogenous insulin therapy [65]. However, issues persist with the requirement of immunosuppression, greater surgical complications compared with other organ transplant procedures [65], and increased risk of cardiac morbidity [66]. Islet transplantation represents a less invasive endocrine cell therapy compared to whole pancreas transplantation, and has been associated with less severe complications compared to whole pancreas transplantation [67]. Researchers at the University of Alberta at Edmonton found that hepatic portal vein transplantation of islets in combination with a glucocorticoid-free immunosuppressive regime led to insulin independence in all patients that received treatment [68]. However, after five years only 10% of patients remained insulin-independent [69], and issues remain with islet survival after engraftment and side effects of the immunosuppressive regime on the patient.

3.2 Tissue Engineered Pancreatic Substitutes

Tissue engineered pancreatic substitutes have the potential to provide more physiologic and less invasive blood glucose control than current treatments for IDD [3, 70]. Additionally, tissue engineering approaches have the potential to overcome the limitations of the Edmonton protocol in terms of islet availability by using non-human tissue and immune rejection by encapsulation. Various tissue-engineered pancreatic substitutes have been studied, with most involving encapsulation of pancreatic beta cells or islets in an immunoprotective barrier. Microencapsulation of cells in particular is advantageous because it creates constructs with a high surface-to-volume ratio and thus good mass transfer properties [71-73]. In addition, microcapsules are often only a few hundred microns to 1 mm in diameter, and thus easier to handle as well as implant *in vivo* [72].

One of the most common encapsulation systems consists of encapsulating cells in calcium alginate-poly-L-lysine-alginate (APA) beads [74]. Encapsulating cells in a hydrogel with a semi-permeable membrane may reduce the need for immunosuppressive therapy [73].The poly-L-lysine layer serves as a semipermeable membrane to prevent the entry of large molecules, such as antibodies, while allowing for the diffusion of nutrients and metabolites such as glucose and insulin [75]. In diabetic small animal studies, implantation of islets [75-78] or beta cells [79, 80] encapsulated in APA beads has led to restoration of normoglycemia. However, the poly-L-lysine layer may contribute to fibrotic overgrowth [81, 82] and an increase in cytokine expression [81-83] upon implantation of APA beads *in vivo*. Thus, studies of alginate encapsulation systems without the use of the poly-L-lysine layer have also been conducted. In particular, alginate-only beads crosslinked

with barium ions and containing islets have also been used to successfully treat the diabetic state in animal models [84-87].

3.3 Alginate

3.3.1 Alginate Material Properties

Hydrogels are ideal for cell encapsulation, as they are hydrophilic and have minimal protein adsorption and cell adhesion, leading to greater biocompatibility. In addition, they are permeable to nutrients and metabolites [71]. Alginates are the most often used hydrogels for cell encapsulation, as they are readily available, gel easily, and are biocompatible [74]. Alginates are natural polysaccharides derived from seaweed or bacteria and consist of block copolymers of 1-4-linked β-D mannuronic acid (M) and α-L-guluronic acid (G) in the form of M, G or MG blocks [88]. Divalent cations, such as Ca^{2+}, Ba^{2+} and Sr^{2+}, bind to the G residues via ionic interactions to crosslink the alginate in a 3-D conformation described by the "egg box model" (Figure 3.1). In this model, the chains of guluronic acid residues represent the corrugated cardboard in an egg box, and the divalent cations represent the eggs in the box [89].

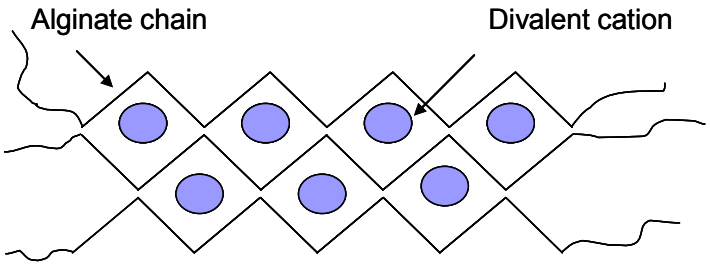

Figure 3.1 The "egg box model." Adapted from Grant et al. [89]

Alginate gels high in guluronic acid content tend to form gels with higher mechanical strength, porosity, and greater resistance to shrinking or swelling [88]. In addition, the alginate gel strength increases with the length of the G blocks and the concentration of the alginate [90].

The chemical composition (i.e. ratio of guluronic to mannuronic acid) of the alginate itself can affect the growth and functional characteristics of the cells encapsulated within it. βTC3 cells encapsulated in high mannuronic acid alginate have been shown to have greater proliferative capacity than cells encapsulated in high guluronic acid alginate. Specifically, βTC3 cells encapsulated in APA beads using high G alginate were shown to have an initial decline in growth, metabolic, and secretory activities, which reversed and started to increase after a few weeks in culture [91, 92]. Cells encapsulated in high M alginate, however, showed an increase in these properties from the beginning of the culture period [91, 92]. This has been attributed to a weaker alginate gel network in the lower G alginates [92]. Interestingly, βTC3 cells encapsulated in high G alginate without the poly-L-lysine layer did not experience any decline in growth unless regular $CaCl_2$ washes were performed to maintain the integrity of the calcium alginate crosslinking [93]. This discrepancy between APA beads and alginate-only beads may be due to the poly-L-lysine layer serving as a barrier to slow down the diffusion of calcium ions from the alginate, thus maintaining the integrity of the alginate gel network longer [94].

3.3.2 RGD-Alginate

Although alginates are widely used in encapsulation, they lack intrinsic cell-binding motifs. Even though some cell types are able to function in unmodified alginate hydrogels, other cells may require adhesion for better survival and proliferation [95]. In the context of a tissue engineered pancreatic substitute, it has been shown that some cell types benefit from adhesion to their matrix for cell survival and function [11, 12, 96]. Specifically, when cultured in PEG hydrogels with extracellular matrix (ECM) molecules such as collagen, fibrinogen, or laminin, encapsulated MIN6 cells exhibited higher viability than cells encapsulated in hydrogels without ECM proteins. Culturing in hydrogels containing collagen Type IV or laminin in particular resulted in higher insulin secretion compared to culturing in hydrogels with other ECM molecules or no ECM molecules [11]. Similarly, murine islets encapsulated in PEG hydrogels containing collagen type IV, laminin, or the laminin peptide IKVAV exhibited higher insulin secretion compared to islets encapsulated in gels without any additional ECM proteins or peptides, respectively [10]. MIN6 cells were shown to better maintain viability, exhibit a lower level of apoptosis, and secrete more insulin when encapsulated in laminin-peptide (i.e. IKLLI and IKVAV) functionalized as opposed to unmodified PEG hydrogels [12].

One way to allow for cell adhesion in an alginate matrix is to chemically modify the alginate chains with adhesive motifs. In particular, alginates have been covalently modified with the arginine-glycine-aspartic acid (RGD) peptide using aqueous carbodiimide chemistry to promote cell adhesion [97-102]. In this procedure, an amide bond is formed between the N-terminal amine on the RGD peptide and the carboxyl group on the uronate residue in the alginate chain (Figure 3.2) [98]. Hydrogels containing

the RGD adhesive peptide motif in particular have been used for encapsulation of a variety of cell types, including myoblasts [20, 103], bone marrow stromal cells [101], pre-osteoblasts [103], and human embryonic stem cells [104]. The RGD peptide, originally discovered in fibronectin [105], and found in other extracellular matrix (ECM) molecules, including vitronectin and laminin, has been widely used as an adhesive motif for cells [106]. Integrins containing the α_4, α_5, α_8, α_{IIb}, and α_v subunits bind to the RGD sequence in ECM molecules [107]. In particular, the C2C12 murine myoblast cell line has been well characterized in RGD-alginate, displaying the ability to survive, proliferate, and differentiate on 2-D [99] as well as in 3-D hydrogel systems [20].

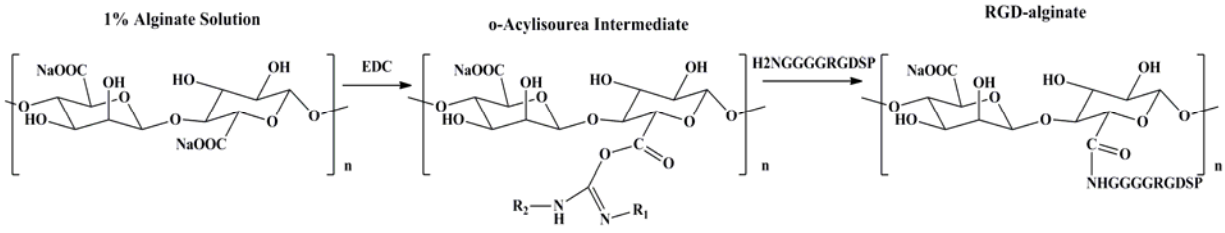

Figure 3.2 RGD conjugation to alginate via carbodiimide chemistry. Adapted from [98, 108]. The 1-Ethyl-3-[3-dimethylaminopropyl] carbodiimide hydrochloride (EDC) forms an O-acylisourea intermediate which is stabilized by *N*-hydroxysulfosuccinimide (sulfo-NHS). An amide bond is then formed between the N-terminal amine on the RGD peptide and the carboxyl group on the alginate chain.

3.3.3 Oxidized Alginate

Controlling the mechanical environment of encapsulated cells in alginate is important, as cellular behavior, such as proliferation and differentiation, can change with different mechanical properties of the 3-D environment [100, 109]. Specifically, a weaker and and/or degradable gel may be desirable for the spreading of adherent cells in 3-D, as they are more likely to migrate or spread if they have less resistance from the matrix [110]. Spread cells in hydrogels also mimic the tissue environment found *in vivo*.

However, since alginate is a natural polymer, the ability to fine tune its mechanical properties is limited. In addition, alginate hydrogels naturally degrade by a slow and poorly controlled process, occurring via loss of divalent cations to chelating compounds such as lactate and phosphate [88]. Degradable alginates created via sodium periodate oxidation can address the above issues by creating weaker alginate gels with more controlled degradation kinetics compared to native alginates. In these oxidized alginates, the carbon-carbon bond of the *cis*-diol group on the uronate residue is cleaved, converting the chair conformation to an open-chain adduct, with the formation of aldehyde groups at the oxidized carbon residues (Figure 3.3) [111]. The aldehyde groups then react with the hydroxyl groups on the two adjacent uronate residues to spontaneously form a six-membered hemiacetal ring [112].The open adduct formation allows for new rotation around 3 bonds (between carbon 4 (C4), C5, the original ring-oxygen atom, and C1 of the oxidized residue) [113]. This creates bonds that are susceptible to hydrolysis. The open-chain adduct can no longer participate well in crosslinking with divalent cations, so the extent of crosslinking in the oxidized alginates is lower compared to non-oxidized alginates. These weaker alginate gels also degrade over time, with the rate of degradation being controlled by percent oxidation of the alginate [111, 114] as well as pH and temperature [114, 115] .

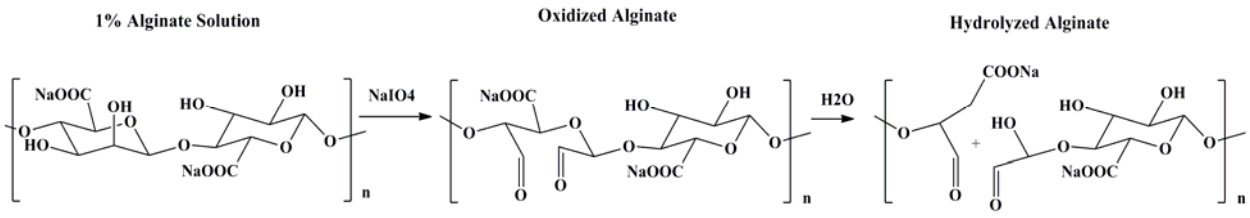

Figure 3.3 Sodium periodate oxidation of alginate. Figure adapted from [111]. During the oxidation procedure, the *cis*-diol group on the uronate residue is cleaved to form an open-chain adduct. The resulting alginate is susceptible to hydrolysis.

Oxidized alginates have been used in a variety of applications, including tissue engineering and delivery of growth factors [114, 116, 117]. With respect to cell delivery and tissue engineering, the oxidized alginate serves as a carrier to keep the cells in place while allowing for natural production of extracellular matrix and tissue formation from the encapsulated cells with degradation of the alginate hydrogel over time [114, 116]. In particular, oxidized alginates were first reported to be used to deliver encapsulated chondrocytes *in vivo*, and were shown to degrade *in vivo* with concurrent replacement of the alginate matrix with cell-derived matrix to help promote cartilage formation [114]. Additionally, oxidized alginates have been used as cell carriers to deliver human adipose stem cells *in vivo* to help promote new adipose tissue formation [116]. With respect to growth factor delivery, oxidized alginate gels have been used to successfully release VEGF in a hind limb ischemia model to promote angiogenesis [117].

3.4 Cell Sources for Pancreatic Substitutes

3.4.1 Islets

Although human islets represent an appropriate cell source for an encapsulated cell therapy, donor islet supply is limited. Thus, studies have looked into using xenogeneic islets, in particular porcine islets, as a cell source for treatment of IDD [48]. Porcine islets are advantageous as porcine insulin is similar to human insulin, and high yields of porcine islets can be obtained after isolation [48]. Indeed, studies have successfully shown reversal of hyperglycemia by implantation of encapsulated adult porcine islets in diabetic mouse models [118, 119]. Although reversal of diabetes in monkeys after implantation of porcine islets encapsulated in alginate-poly-L-lysine was reported [120], these results have not been reported to be reproduced. Additionally,

concerns persist regarding transfer of porcine endogenous retrovirus (PERV) from porcine islets to humans, as PERV has been shown to infect human cells *in vitro* as well as mouse tissue *in vivo* [121]. However, a study with transplantation of porcine fetal islets into diabetic patients detected no PERV infection in any patient up to 4-7 years post-transplant [122].

3.4.2 Stem Cells

Although beta-like cells derived from the differentiation of embryonic stem cells represent a promising, renewable beta cell source, issues still exist with differentiation of embryonic stem cells towards a true beta cell phenotype [49]. In particular, for human embryonic stem cell differentiation, studies have indicated that the resulting cells lack glucose-responsiveness *in vitro* [123, 124], with *in vivo* culture required to produce glucose-responsive cells [124]. Additionally, concerns arise over the possibility of tumor formation after implantation of embryonic stem cells [125]. Studies examining the use of induced pluripotent stem (iPS) cells to create insulin-secreting cells are forthcoming, but have resulted in questionable findings [49, 126], and low efficiency of differentiation of iPS cells into pancreatic beta cells [127]. Studies are also investigating differentiation of pancreatic progenitor cells as well as other adult stem cells such as bone-marrow derived mesenchymal stem cells into pancreatic beta cells [125]. Overall, although studies with stem cells differentiated towards a beta cell phenotype are forthcoming, issues still remain with determining the appropriate conditions for and creating cells that exhibit the necessary characteristics of a differentiated beta cell.

3.4.3 Transdifferentiation of Non-Beta Cells

Another area that has been examined for cell-based therapy for IDD is the transdifferentiation of non-beta cells into beta-like insulin-producing cells. Specifically, liver cells have been transdifferentiated towards a beta cell phenotype [128, 129]. In particular, Sapir et al. [128] transduced human and fetal liver cells with the PDX-1 gene and were able to obtain cells that were glucose responsive as well as had the ability to reverse hyperglycemia when implanted in diabetic mice, although blood glucose levels were higher than in healthy mice. This may have been caused by only a fraction of the implanted cells actually containing proinsulin [128]. Similarly, Zalzman et al. [129] were able to restore noromoglycemia in diabetic mice by implanting liver cells that had been incubated in serum-free medium with growth factors in order to differentiate cells into a more beta cell-like phenotype. However the cells had an insulin content of only 60% that of human pancreatic islets [129]. Thus, work still remains on obtaining transdifferentiated cells that exhibit beta cell-like phenotypes.

3.4.4 Cell Lines

3.4.4.1 Beta Cell lines

A promising alternative cell source for a pancreatic substitute, especially for use with animal models of diabetes, is cultured beta cells that have been immortalized via oncogene expression [130]. Using these cell lines allows for large amounts of cells to be grown in culture prior to incorporation into a construct and *in vitro* or *in vivo* study [130]. Human beta cell lines, however, generally tend to lose their differentiated function over time due to loss of expression of transcription factors for the insulin gene[130]. Mouse

beta cell lines are better to use for long-term culture because they retain telomerase activity and differentiated functions longer than human beta cell lines [130].

In order for a cell line to possibly be used *in vivo*, it is important that its growth be regulated so as to not form tumors once implanted. Although the βTC3 mouse insulinoma cell line has been used for various studies on a bioartificial pancreas [91-93, 131-136], its potential use *in vivo* is limited as its growth cannot be regulated [137]. The βTC-tet murine insulinoma line, derived from tumors of double transgenic C3HeB/FeJ mice, has been genetically engineered to express the simian virus 40 (SV40) large tumor antigen (TAg) oncoprotein under the control of the bacterial tetracycline (tet) operon. These cells have been genetically engineered to respond to the "tet off" system, whereby proliferation is stopped in the presence of tetracycline [138]. This growth arrest is reversible, as removal of tetracycline leads to continuation of proliferation. Encapsulated βTC-tet cells have also shown growth regulation *in vitro* [139] and *in vivo* [79] in the presence of tetracycline.

3.4.4.2 Myoblast Cell Lines

Autologous, non-beta cells offer an option for cell sourcing without the issue of immune rejection, as with allogeneic or xenogeneic cells. This would entail removing cells from the patient and genetically engineering them *ex vivo* before re-implantation, or delivering the gene *in vivo*. Various non-beta cells have been genetically engineered to express insulin, including hepatocytes [140, 141], intestinal endocrine cells [142-144], myoblasts [21, 145-147], and adipocytes [148]. Although studies with primary cells may be more appropriate than cell lines in terms of mimicking a potential autologous cell

therapy, cell lines can still be used to gain important fundamental information from *in vitro* as well as *in vivo* studies with animal models.

In particular, myoblasts are promising to use, as they can proliferate in culture and also exit the cell cycle to terminally differentiate and form myotubes [149]. This is important in the context of a tissue engineered construct, as differentiation of myoblasts into myotubes would prevent excessive, uncontrolled cell growth *in vivo*. Unfortunately, since myoblasts are non-neuroendocrine cells, they lack the prohormone convertases PC1/3 and PC2, and cannot process proinsulin to insulin [147]. However, by genetically engineering the proinsulin at the A-chain C-peptide and B-chain C-peptide junctions with furin-cleavable basic sequences, the proinsulin can be processed in these cells to insulin via the constitutive pathway of secretion by the ubiquitous protease furin [150]. One cell line in particular, the murine C2C12 adult skeletal muscle myoblast cell line, has been successfully genetically engineered to secrete furin-cleavable insulin [21, 145, 146].

Although insulin-secreting C2C12 cells have been genetically engineered further to exhibit tetracycline-controlled [146] and differentiation-dependent [145] insulin production, increasing the level of insulin secretion/accumulation is still desirable. In order to produce a more stable form of insulin [151] that accumulates to a greater extent [150], primary myoblasts [147] and C2C12 cells [21] have been genetically engineered with furin-cleavable B10 mutated human insulin. Insulin with the histidine-to-aspartic acid mutation at the tenth position in the B chain has also been shown to be more active than native insulin and has a higher affinity for the insulin receptor [152]. Specifically, when transfected with a furin-cleavable B10 human proinsulin construct vs. a furin-cleavable human proinsulin construct alone, primary rat myoblasts transfected with the

former were shown to secrete more proinsulin [147]. Additionally, encapsulated myoblasts, genetically engineered to constitutively secrete insulin, would likely serve as a basal source of insulin for patients with IDD.

Based on the characteristics described above, βTC-tet cells and C2C12 cells, stably transfected to secrete insulin in our laboratory [21], were chosen to address the objectives in this thesis.

3.5 Cryopreservation

3.5.1 Cryoprotectants

One of the first uses of cryoprotectants during cryopreservation was described by Polge et al., who discovered the benefit of using glycerol in cryopreserving fowl sperm [153]. Cryoprotectant (CPAs) are used to decrease the concentration of water inside the cell, thereby reducing the likelihood of intracellular ice formation. There are two main types of cryoprotectants: permeating and non-permeating. Permeating cryoprotectants can enter the cell and include dimethylsulfoxide (DMSO), ethylene glycerol, and 1,2-propanediol [154]. In addition to reducing the concentration of intracellular water, permeating cryoprotectants are also important in decreasing the intracellular concentration of solutes, reducing the likelihood of cell injury due to solution effects (discussed below). Non-permeating cryoprotectants cannot enter the cell, and include sugars such as trehalose and polyvinyl pyrollidone [154]. Non-permeating cryoprotectants are important osmotic buffers that prevent the cell from swelling, especially during cryoprotectant removal post-thaw [155]. Additionally, trehalose in particular is thought to stabilize plasma membranes during cryopreservation of cells [156].

3.5.2 Conventional Freezing

Conventional freezing has been used to successfully cryopreserve cells in suspension with high recovery post-thaw [155, 157]. Important variables in conventional freezing include the concentration of the cryoprotectant, temperature of CPA addition, rate of cooling and warming, as well as the temperature of CPA removal [155]. There are two major modes of cell freezing injury during slow freezing that can be described by the two factor hypothesis [158]. According to this hypothesis of cell damage, cooling cells at too high of a cooling rate leads to intracellular ice formation, which can damage the intracellular components of the cell [159]. On the other hand, if cells are cooled too slowly, damage by "solution effects" occurs whereby the cell may become dehydrated or damaged by the high concentration of intra and extracellular electrolytes. The optimal slow cooling rate is dependent on cell type, and is represented by an inverted "U" curve, where cooling too fast or too slow leads to low cell viability post-thaw. If conventional freezing is done properly, ice will form only in the extracellular milieu with the intracellular environment forming a vitreous state [160]. Rapid thawing (e.g. 200^{o}C/min) is usually used with slow freezing processes to prevent the growth of any intracellular nuclei that may have formed during the cooling process and to prevent a large extent of recrystallization of extracellular ice [157].

Although extracellular ice is not damaging to cells in suspension, it can be damaging to more complex systems, such as tissues. Ice formation can damage the 3-D architecture of the tissue and is thought to be the most serious obstacle when cryopreserving more complex multicellular systems [155]. Specifically, conventional

freezing has been shown to be unsuccessful for the cryopreservation of various tissues such as blood vessels, corneas, and cartilage due to ice formation [161].

3.5.3 Vitrification

Since ice formation may damage tissue engineered constructs, an alternative "ice-free" method of cryopreservation is desirable. Vitrification has shown promise in preserving various tissue engineered constructs, including encapsulated hepatocytes [51], tissue engineered blood vessels [162], and tissue engineered pancreatic substitutes [24, 29, 30]. Vitrification is the process by which a glassy state is formed when a liquid becomes too viscous to flow and becomes a solid without crystallization, or ice formation. As the temperature in the system is lowered, molecular motion decreases, translational and rotational molecular motion are stopped, and the system is trapped in a high energy state [160]. Two important issues related to the cryoprotectants used in the vitrification process include the cytotoxicity and potential osmotic excursions that may occur due to the high concentration of CPAs necessary to vitrify [5, 6] (usually above 5.5 M). In addition, osmotic excursions caused by the high concentration of CPAs used can be reduced by using multi-step addition and removal protocols [28] as well as osmotic buffers to reduce cell swelling [155]. Recently, a model for CPA addition/removal at concentrations relevant for vitrification has been developed for beta cells in order to reduce osmotic excursions [28]. Temperature is also important when dealing with CPAs, as cytotoxicity decreases as the temperature is reduced [155, 163, 164].

All liquids have the potential to vitrify, given that they are cooled sufficiently quickly and that the sample volume is low [165]. The critical cooling rate is defined as

the rate of cooling at which the volume fraction in the sample that is crystallized is less than 10^{-6} [166]. A solution will vitrify if it is cooled at or above its critical cooling rate. Once vitrified, the solution exhibits structural properties of a liquid and mechanical properties of a solid. The temperature at which this liquid to glass transition occurs is known as the glass transition temperature or T_g [165]. During warming, however, if the warming rate is not fast enough, existing crystals may grow or new ice nucleation may occur. This transition from a glassy to a crystalline state is known as devitrification and the growth of existing ice nuclei is called recrystallization [160]. Thus, the critical warming rate, above which ice formation will not occur during the warming process, is also very crucial to a successful vitrification procedure. Although it may be possible to vitrify tissue systems, achieving the warming rates necessary to avoid ice formation upon warming has been quite challenging [160].

3.5.4 Cryopreservation of Microencapsulated Insulin-Secreting Cells

Studies examining cryopreservation of encapsulated islets or beta cells vary based on cryopreservation method used, species, and type of encapsulation matrix. Currently, no studies in the literature have examined cryopreservation of encapsulated insulin-secreting cells other than encapsulated beta cells or islets. A few studies in particular have examined cryopreservation effects on encapsulated beta cell lines [22, 39]. Mukherjee et al. reported impaired viability and insulin secretory function after conventional freezing of APA encapsulated murine βTC3 cells, with freezing-associated damage to the alginate matrix [22]. Another study examining cryopreservation of sodium cellulose-sulfate encapsulated hamster HIT-T15 cells found that freezing constructs using

a solution containing 1 M glycerol resulted in little cell loss post-warming with recovery over a week post-warming [39].

With respect to cryopreservation of alginate-encapsulated islets, studies have examined conventional freezing of encapsulated rat [37, 52, 167], porcine [53], and canine islets [168]. In particular, a study examining freezing of APA encapsulated rat islets, found that glucose-stimulated insulin secretion in Frozen constructs was similar post-warming to Fresh controls, and *in vivo* transplantation of Cryopreserved encapsulated islets successfully restored normoglycemia in all implanted diabetic mice for up to 90 days [37]. The study found similar insulin secretion function *in vitro* and *in vivo* using two methods of conventional freezing: 1). cooling from 4^{o}C to -70^{o}C in an isopropyl alcohol bath, followed by plunging into liquid nitrogen [169], and 2). Rajotte's protocol [170], cooling from 4^{o}C to -45^{o}C at 0.2^{o}C/min with ice nucleation at -7.5^{o}C [37]. However, another study by the same group examining the effects of conventional freezing on APA encapsulated porcine islets, found that the two conventional freezing methods gave different results in terms of insulin secretory function post-warming [53], indicating species-specific responses to freezing of alginate-encapsulated islets. Rajotte's protocol worked best for encapsulated porcine islets compared to using linear cooling with an isopropyl alcohol bath; however, only 70% of islet batches were glucose responsive post-warming, and after transplantation into diabetic mice, only 60% of mice became normoglycemic for 90 days [53]. A more recent study of cryopreservation of rat islets encapsulated in barium alginate hydrogels reported success in maintaining glucose-stimulated insulin secretion post-warming and 80% graft function after transplantation into diabetic rats for up to 4 weeks [38]. A longer-term follow-up study with

Cryopreserved barium-alginate encapsulated rat islets found maintenance of normoglycemia in diabetic rats for greater than 360 days post- transplantation, with studies still ongoing [167]. With respect to Cryopreserved encapsulated canine islets, Rajotte et al. [168] found that transplantation resulted in restoration of normoglycemia in diabetic nude mice.

Studies by Iwata's group have explored cryopreservation of hamster islets encapsulated in agarose [24, 25]. An *in vitro* study reported a 45% decrease in insulin secretion, with respect to non-preserved controls, after both freezing and vitrification of agarose-encapsulated rat islets, with capsule damage after freezing [25]. A follow-up *in vivo* study with vitrified encapsulated islets indicated impairment in insulin secretion post-warming, with a requirement of twice the number of Vitrified encapsulated islets to maintain normoglycemia for a similar time period to non-preserved controls in addition to the use of immunosuppression [24].

3.6 Glucose-Stimulated Insulin Secretion (GSIS) and Mitochondrial Metabolism

In the consensus model for GSIS, an increase in extracellular glucose concentration leads to an increase in glucose consumption, which results in an increase in the ATP/ADP ratio, closure of ATP-sensitive K^+ (K_{ATP}) channels, plasma membrane depolarization, opening of voltage-gated Ca^{2+} channels, increase in intracellular Ca^{2+}, and exocytosis of insulin [171-173]. Although this pathway, sometimes referred to as the K_{ATP} channel-dependent or 'triggering' pathway, is widely accepted, it does not explain all aspects of GSIS, and evidence has indicated that a K_{ATP} channel-independent or "amplifying" pathway is also important [172, 174-176] . In order to better understand the

amplifying pathway of secretion, some studies have focused on the roles of metabolic coupling factors generated from the mitochondria on GSIS [32]. Indeed, it has been shown that mitochondrial metabolism is important not only for ATP generation, but also for the generation of metabolites via anaplerotic pathways for stimulus-secretion coupling in the beta cell [33, 177]. Overall, as intermediary metabolism is critical in GSIS, it is important to study it after cryopreservation of a pancreatic substitute.

3.7 ^{13}C NMR and Isotopomer Analysis

^{13}C nuclear magnetic resonance (NMR) is a powerful tool to study metabolism. It is advantageous for studying metabolism as multiple labeled metabolites can be seen in one spectrum, and more information can be gained than with ^{14}C radioisotopic techniques [178, 179]. Since the natural abundance of ^{13}C is only 1.1%, it can be introduced into the cell as an isotopic tracer, with its path being traced by the labeling patterns found in enriched metabolites (Figure 3.4).

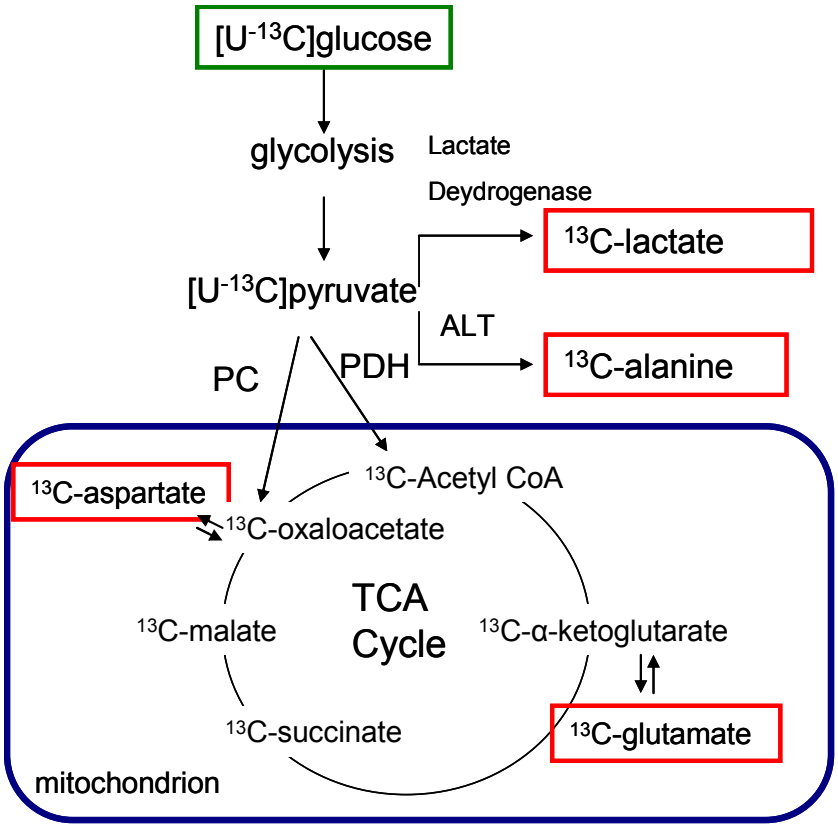

Figure 3.4 Labeling of metabolites in the cell after introduction of U-^{13}C (uniformly labeled-^{13}C) glucose. Metabolites in red have high enough intracellular concentrations to be detected by NMR. PC (pyruvate carboxylase); PDH (pyruvate dehydrogenase); ALT (alanine aminotransferase) (Adapted from Papas et al.[180]).

^{13}C NMR and isotopomer analysis have been used to study specific metabolic fluxes in the tricarboxylic acid (TCA) cycle [35, 36, 178, 181-185]. The labeled molecule analyzed is often glutamate, as it is found in relatively high concentrations in the cell and is considered to be in fast exchange with the TCA cycle intermediate α-ketoglutarate [179, 186]. The presence of ^{13}C-^{13}C spin-spin coupling between adjacently labeled carbons in the glutamate molecule allows for the detection of isotope isomers, called isotopomers, in the NMR spectrum [178]. In terms of glutamate labeling, C4 and C5 are derived from acetyl-CoA, and C1, C2, and C3 are derived from oxaloacetate from each turn of the TCA cycle. Relative areas of the isotopomer patterns of glutamate in the ^{13}C

spectrum are analyzed with the tcaCALC modeling program to obtain relative metabolic fluxes through specific TCA cycle pathways [179].

Although early studies using ^{13}C NMR and isotopomer analysis often centered on metabolism in the perfused heart [181, 184, 185], more recently, one of the main focuses of ^{13}C NMR and isotopomer analysis has been studying glucose metabolism in beta cells [35, 36, 182, 183]. Recent studies utilizing ^{13}C NMR and isotopomer analysis have specifically highlighted the importance of mitochondrial metabolism in GSIS, by correlating certain metabolic fluxes with insulin secretion using specific models in the tcaCALC modeling program [32, 35, 36, 182, 187]. In particular, one study using the INS-1 cell line described the dual-pyruvate pool model (Figure 3.5A), where there were two independent pyruvate pools present in the cell that did not mix and that pyruvate cycling correlated with glucose responsiveness more than oxidation of pyruvate to acetyl-CoA [182]. Another study examining the role of anaplerotic substrates in the TCA cycle of INS-1 cells also found a strong correlation between insulin secretion and flux through pyruvate carboxylase (PC), with the addition of anaplerotic substrates leading to an increase in pyruvate carboxylase flux [35]. However, more recently, in a study looking at four different beta cell lines (INS-1, R7T1, βTC3, and βTC-tet) it has been suggested that a modified single pyruvate pool model of mitochondrial metabolism with a second non-PC anaplerotic entrance (Figure 3.5B) may be more appropriate and better reflect the bioenergetics of the beta cell [36, 187]. In particular, a modified single pyruvate pool model was used to show that encapsulation of beta cells leads to a decrease in flux through glycolysis and pyruvate carboxylase with an increase in flux through a second non-PC anaplerotic entrance [183]. These ^{13}C NMR studies form a basis for evaluating

the effects of different cryopreservation methods on the intermediary metabolism of insulin-secreting cells.

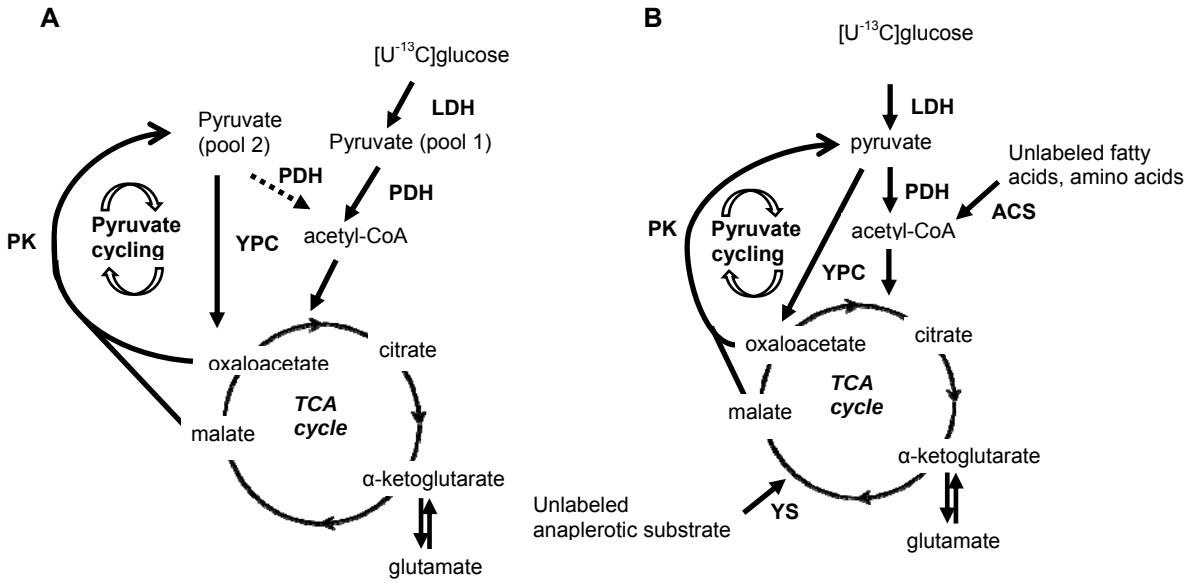

Figure 3.5 Two models of mitochondrial metabolism in the beta cell that have been applied in the tcaCALC modeling program to calculate metabolic fluxes, adapted from Simpson et al. [36]. A).a dual pyruvate pool model, B). a modified single pool model with a second non-pyruvate carboxylase anaplerotic substrate entrance to the TCA cycle.

CHAPTER 4

DEVELOPMENT OF OPTIMIZED PARAMETERS AND PROCEDURES FOR ^{13}C LABELING, EXTRACTION, AND ISOTOPOMER ANALYSIS OF FRESH AND CRYOPRESERVED ENCAPSULATED βTC-TET CELLS

4.1 Introduction

^{13}C NMR and isotopomer analysis is a powerful method that can be used to measure relative carbon flow into the tricarboxylic acid (TCA) cycle by using metabolic models to analyze isotopomer patterns in the ^{13}C NMR spectrum [179, 188, 189]. In particular, this method has been applied in as diverse situations as investigating substrate selection in the heart [181] and preferred metabolic pathways in the pancreatic beta cell [34-36]. Applying the method of ^{13}C NMR and isotopomer analysis to cultured cells or tissues, however, involves various key steps, including choosing and/or designing an appropriate metabolite extraction procedure that leads to sufficient signal-to-noise ratio (SNR) in the NMR spectrum; determining isotopomer steady state [179, 188]; and determining the appropriate model of metabolism to use to interpret the ^{13}C NMR-derived data [187]. In particular, obtaining sufficient SNR in ^{13}C NMR spectra derived from cellular extracts can be challenging, as the ^{13}C nucleus is inherently insensitive [188, 190]. Therefore, a carefully designed procedure is necessary and must be followed closely to reproducibly obtain sufficient SNR. This chapter details the development of the methodology for ^{13}C NMR and isotopomer analysis for Fresh and Cryopreserved encapsulated βTC-tet cells. First, important steps in the extraction procedure itself are

discussed, followed by the determination of isotopomer steady state from Fresh encapsulated cells, and verification of maintenance of metabolic activity after incubation in basal and high glucose medium for both Fresh and Cryopreserved cells. ^{13}C NMR spectra were also obtained from Frozen and DPS-vitrified beads to ensure sufficient SNR was obtainable with the parameters used. Finally, two models of glucose metabolism are compared in order to determine the appropriate model to use with tcaCALC to determine relative metabolic fluxes.

4.2 Materials and Methods

4.2.1 Cell Culture and Encapsulation

All chemicals and reagents were obtained from Sigma (St. Louis, MO) unless otherwise noted. βTC-tet cells were obtained from the laboratory of Dr. Shimon Efrat (Albert Einstein College of Medicine, Bronx, NY) [191]. Cells were cultured as monolayers in T-175 flasks in fully supplemented, 25 mM glucose DMEM, referred to as complete DMEM, containing 4 mM L-glutamine, supplemented with 10% (v/v) FBS (Gemini Bioproducts, West Sacramento, CA, USA), 1% (v/v) penicillin (10,000 U/ml)-streptomycin (10,000 μg/ml) (Mediatech, Manassas, VA), and 1% L-glutamine (Mediatech). Medium was changed every 2-3 days, and cultures were split at ratios of 1:5 to 1:7 when confluent. Cells were cultured in a humidified incubator at 37^{o}C with 5% CO_2/95% air.

At the time of encapsulation, cells were detached from monolayers using 0.25% trypsin (Mediatech) and resuspended in 2% PRONOVA Ultrapure LVM alginate (FMC Biopolymer, Philadelphia, PA) in order to achieve an encapsulation density of $7x10^7$

cells/ml. Cells were encapsulated using an electrostatic bead generator (Nisco Engineering AG, Zurich, Switzerland), with alginate cross linked in a 1.1% (w/v) $CaCl_2$ bath , as described previously [30], but without the poly-L-lysine and alginate coating process. This high cell density was used in order to obtain good SNR in the NMR spectrum. Beads formed were approximately 500-600 μm in diameter and were incubated overnight on a platform rocker (Stovall, Greensboro, NC) in complete DMEM prior to performing experiments.

4.2.2 Vitrification

Encapsulated βTC-tet cells were vitrified using the cryoprotectant (CPA) cocktail DPS, containing 3 M dimethylsulfoxide (DMSO), 3 M 1,2 propanediol (PD), and 0.5 M Sucrose (Fisher Chemical, Fisher Scientific, Pittsburgh, PA). For the CPA addition procedure, CPAs were added to beads on ice in a stepwise fashion according to the protocol in Table 4.1. This protocol was developed with the aid of a mathematical model that minimized cell osmotic excursions while ensuring CPA equilibration at each step [192]. One ml of beads was placed in a 100 μm cell strainer (BD Biosciences, Bedford, MA) and sequentially transferred through CPA solutions of increasing concentration (Table 4.1) at 4^oC in a six-well plate (BD Biosciences). After CPA addition, the beads in each strainer plus CPA (total volume 1.5 ml) were transferred to each of 3 pre-siliconized 20 ml borosilicate glass scintillation vials (Fisherbrand/Fisher Scientific), and 700 μl of isopentane (EMD Chemicals, Gibbstown, NJ, USA) was added on top of the CPA/bead mixture in each vial. Vials were transferred to a pre-chilled rack and the rack was placed in an isopentane bath in a mechanical freezer (Sanyo North

America, San Diego, CA) set at -135°C for fast cooling to ~ -100°C (~64°C/min). The rack was then transferred to a shelf in the freezer for slow cooling (~2°C/min) to -130°C. During cooling, temperature was tracked with a thermocouple in a dummy sample containing only CPA and isopentane. After overnight storage in the freezer, one ml of beads was warmed at a time by agitating vials in a room temperature 30% (v/v) DMSO bath. CPAs were then removed stepwise at room temperature in a similar fashion as CPA addition (Table 4.1). After CPA removal, beads were aliquoted out for immediate assay for the medium incubation test.

For obtaining ^{13}C NMR spectra from Vitrified encapsulated cells, vitrification was performed 13 separate times. Beads were warmed 1 ml at a time, and incubated at 37°C until all beads were warmed. A volume of 12 ml beads was then aliquoted out for the extraction experiments. Details on the scale-up procedure are also described in CHAPTER 5.

Table 4.1 Cryoprotectant addition/removal protocol for DPS vitrification. A: addition; R: removal; RT: room temperature (22°C); PD: 1,2 propanediol

Step	*DMSO (M)*	*PD (M)*	*Sucrose (M)*	*Time (min)*	*Temperature (°C)*
A1	1	1	0.15	2	4
A2	2	2	0.3	2	4
A3	3	3	0.5	2	4
R1	2.25	2.25	0.3	2	RT
R2	1.5	1.5	0.2	2	RT
R3	0.75	0.75	0.1	2	RT
R4	0	0	0	4	RT

4.2.3 Conventional Freezing

For freezing for the medium incubation test, complete DMEM at 4°C, containing 10% (v/v) DMSO, was added to 1 ml of beads. Beads were incubated in this solution for

10 minutes, and then transferred to 2.0 ml cryogenic vials (Corning Inc., Corning, NY) and placed in a Mr. Frosty isopropyl alcohol bath (Nalgene/Thermo Fisher Scientific, Rochester, NY) in a -80^{o}C freezer (VWR International Inc., Radnor, PA) for 1.5 hours. Subsequently, vials were plunged into liquid nitrogen. After overnight storage, 1 ml of beads at a time was warmed rapidly by agitating vials in a 37^{o}C water bath until no ice was visible in the vials. Beads were next placed in complete DMEM at 37^{o}C for 10 minutes. After a subsequent wash with complete DMEM, beads were aliquoted out for immediate assay.

For obtaining ^{13}C NMR spectra from Frozen encapsulated cells, beads were frozen 8 times in 1 ml batches. Beads were warmed 1 ml at a time, and incubated at 37^{o}C until all beads were warmed. A volume of 7 ml of beads was then aliquoted out for the extraction experiments. Details on the scale-up are also described in CHAPTER 5.

4.2.4 ^{13}C Labeling and Extraction of Fresh Encapsulated βTC-tet Cells for the Isotopomer Steady-State Study

^{13}C labeling and extraction were performed one day post-encapsulation on a volume of 6 ml of Fresh beads (approximately 200x10^{6} cells). This bead volume was used because it gave sufficient SNR in NMR spectra (Figure 4.1). Beads were washed 4 times with glucose and glutamine-free basal DMEM supplemented with 1.31 g/l BSA (Sigma). Next, beads were incubated in the same type of medium at a 1:10 bead: medium volume ratio for 1 hour at 37^{o}C. Beads were subsequently washed once with basal medium and once with labeling medium, containing 15 mM uniformly labeled ^{13}C (U-^{13}C) glucose (Cambridge Isotope Laboratories, Andover, MA) in glucose-free DMEM

(pH 7.4) plus 10% (v/v) FBS (Gemini), 1% (v/v) L-glutamine (Mediatech), and 1% (v/v) penicillin-streptomycin (Mediatech). Next, beads were incubated in the same type of medium, at a 1:10 bead: medium volume ratio, for 3-15 hours. Subsequently, perchloric acid extraction was performed based on the protocol in Simpson et al. [183], with modifications. The extraction procedure was performed on ice with ice-cold reagents. Beads were washed with glucose-free and glutamine-free DMEM and alginate was dissolved in 110 mM sodium citrate (Fisher Chemical/Fisher Scientific). Cells were pelleted at 200xg at 4^{o}C for 10 minutes, and the pellet was washed with 0.85% (w/v) NaCl. Cells were then extracted twice in 0.5 M perchloric acid using an Omni GLH homogenizer (Omni International, Marietta, GA) with an Omni Tip™ plastic generator probe (for hard tissues) to prevent paramagnetic ion contamination. Supernatants were pooled and neutralized with 0.01-5 M KOH to pH 7.0 using an InLab® Cool (Metler Toledo, Columbus, OH) low temperature pH electrode. This solution was then centrifuged at 10,000xg to remove precipitated salts and Chelex-100® resin (2g/10 ml extract volume) was added to the supernatant to remove paramagnetic ions. After stirring the solution containing Chelex resin for one hour on ice, the resin was removed by filtration through Whatman Grade 540 quantitative ashless filter paper (Whatman Inc., Piscataway, NJ) in a Nalgene® polysulfone filter holder (Thermo Fisher Scientific). Subsequently, the resin was chased with ultrapure water. The pH of the filtrate was adjusted to approximately 7.4 with 0.01-1 M HCl. The final extract was placed in 50 ml centrifuge tubes (with 15-20 ml extract per tube), covered with two lab wipes, and frozen at -80^{o}C. The frozen extract was placed in a lyophilizer (Labconco Corporation, Kansas

City, MO) for two days prior to reconstitution. Special care was taken to avoid contact with metal whenever possible, to reduce potential paramagnetic ion contamination.

4.2.5 ^{13}C Extract Reconstitution and NMR Spectroscopy

After lyophilization, dried extracts were transferred from 50 ml centrifuge tubes to 2.0 ml microcentrifuge tubes with plastic disposable spatulas (VWR) and reconstituted in 200 µl of 99.99% D_2O. Subsequently the extract was spun at 18,300xg at room temperature for 10 minutes. The supernatant was removed after centrifugation, transferred to a new 1.7 ml microcentrifuge tube, and placed on ice for 30 minutes to precipitate out $KClO_4$ salts. The extract was then centrifuged at 18,000xg for 10 minutes at 0^oC to pellet out additional precipitated salts. The supernatant was then removed, transferred to a new 1.7 ml microcentrifuge tube, and allowed to warm to room temperature. Subsequently, an NMR long tip transfer pipette (Wilmad-LabGlass, Vineland, NJ) was used to transfer the sample to a 5 mm symmetrical NMR microtube (Shigemi Inc., Allison Park, PA) that was magnetic susceptibility-matched to D_2O. The glass insert was then placed into the tube in such a way as to prevent air bubbles in the sample. NMR data were acquired with a 5 mm broadband probe in an 11.7 T vertical bore Bruker DRX 500 magnet with an Avance Console (Bruker, Billerica, MA) with previously described parameters [36, 183].

New and re-used NMR tubes were thoroughly cleaned prior to use to help reduce potential paramagnetic ion contamination. All reagents, except for ethanol, were 0.2 µm filtered prior to use to remove possible particulates. New NMR tubes and inserts were soaked overnight in 10 mM EDTA in ultrapure water, and subsequently rinsed

thoroughly with ultrapure water. Additional rinses in 1M HCl as well as ultrapure water were also performed. Re-used NMR tubes and inserts were first rinsed with ultrapure water, followed by 1M HCl and ultrapure water rinses prior to overnight incubation in 10 mM EDTA. Tubes and inserts were finally rinsed with ultrapure water and 100% ethanol and air dried overnight on an NMR tube rack.

4.2.6 ^{13}C NMR Spectra Analysis and tcaCALC Modeling

^{13}C NMR spectra were processed using NUTS NMR software (Acorn NMR, Fremont, CA). Prior to relative peak area determination, a 1 Hz line broadening factor and polynomial baseline correction were applied to all spectra. Peaks were referenced to the lactate C3 peak at 21.0 ppm. Relative multiplet peak areas of isotopomer patterns of glutamate C2, C3, and C4 were determined using a line-fitting routine in NUTS as described previously [36]. Subsequently, relative multiplet peak areas were analyzed using the tcaCALC modeling program in order to determine relative metabolic fluxes [179, 181, 188]. In order to get a visual representation of how well the models represented the experimental data, tcaCALC-derived metabolic fluxes were input to tcaSIM to generate simulated spectra. In addition, %C3/C4 error [36, 183, 187] as well as residual sum of square values [183] were determined to examine how well model-derived results fit the experimental data.

4.2.7 Medium Incubation Test

Fresh and Cryopreserved beads were split into two subgroups, and subsequently exposed to two different medium incubation schemes. Under “condition 1,” a 0.1 ml

volume of beads from each treatment (Fresh, Frozen, Vitrified) was incubated in complete DMEM for 6 hours. Subsequently, beads were washed 3 times with 1 ml of complete DMEM, followed by exposure to complete DMEM for 6 hours. Under "condition 2," a 0.1 ml volume of beads from each group was incubated in 0 mM glucose DMEM + 1.31 g/l BSA for one hour. Subsequently, beads were washed 3 times with 1 ml of 0 mM glucose DMEM + 1.31 g/l BSA. Next, beads were exposed to 15 mM glucose DMEM, supplemented with 10% FBS (Gemini Bioproducts, West Sacramento, CA), 1% P/S, and 1% L-glutamine for 6 hours. This last solution is henceforth referred to as "15 mM FS."

4.2.8 Metabolic Activity of Beads after Medium Incubation Test

After the medium incubation test, beads from Fresh, Frozen, and DPS-vitrified groups were transferred to 12-well plates and incubated with 1 ml complete DMEM and 100 µl of alamarBlue® stock solution (Life Technologies, Carlsbad, CA) for 1.5 hours at 37^{o}C. Subsequently, three 100 µl aliquots from each sample were placed into separate wells of a black 96-well microplate (Nalgene/Nunc) and fluorescence was read using a SpectraMax Gemini plate reader (Molecular Devices, Sunnyvale, CA) with excitation and emission wavelengths of 544 and 590 nm, respectively.

4.2.9 Statistical Analysis

Data are presented as mean ± standard deviation. Statistics were performed using either a one-way ANOVA using the General Linear Model or a two-tailed t-test in

Minitab (Minitab Inc., State College, PA). Pairwise comparisons were performed using Tukey's test. Values of $p<0.05$ were considered statistically significant.

4.3 Results and Discussion

4.3.1 Summary of Important Conditions for Perchloric Acid Extraction of Encapsulated Cells and Reconstitution of Extracts

Perchloric acid extraction was used to extract metabolites from encapsulated cells, as in a previous study with encapsulated βTC3 cells [183]. Important additional modifications were made in order to ensure good signal-to-noise ratio (SNR) in the NMR spectrum. First, as opposed to extraction of metabolites form intact beads, beads were solubilized and cells pelleted to get better SNR. For the homogenization procedure, a special OmniTip™ plastic probe (Omni International) was used in order to reduce potential paramagnetic ion contamination. A special low temperature InLab® Cool pH electrode (Metler Toledo, Columbus, OH) was used to measure the pH of samples at 4°C.

With respect to reconstitution of the metabolite extract, in order to increase the concentration of metabolites in the reconstituted sample, a volume of only 200 µl of D_2O was added to the lyophilized extract. After addition of D_2O, multiple centrifugations and incubation on ice were used to help precipitate out salts to reduce sample conductivity and help increase SNR [193]. In addition, a symmetrical NMR microtube and glass insert (Shigemi NMR), magnetic susceptibility matched to D_2O, were used to allow for a small sample volume without a decrease in spectral resolution. This was used as an alternative to using a standard 5 mm NMR tube which would normally require larger volumes of

around 500-600 µl of sample. All NMR tubes were soaked in 10 mM EDTA overnight and rinsed in ultrapure water prior to use in order to help remove potential paramagnetic ions. In general, extra precaution was taken during extraction and reconstitution procedures to avoid contact with metal to minimize potential paramagnetic ion contamination. Using this extraction and reconstitution method, NMR spectra with SNR sufficient for isotopomer analysis were obtained. A representative ^{13}C NMR spectrum obtained from an extraction of Fresh beads is shown in Figure 4.1.

Additionally, methanol/chloroform dual-phase extractions [194] were attempted on pelleted cells from solubilized beads to see if ^{31}P NMR spectra could also be obtained from extracts to assess ATP/ADP levels in the sample. However, this extraction method was found to be undesirable as a viscous supernatant was present even after several washes, possibly due to the presence of remaining alginate.

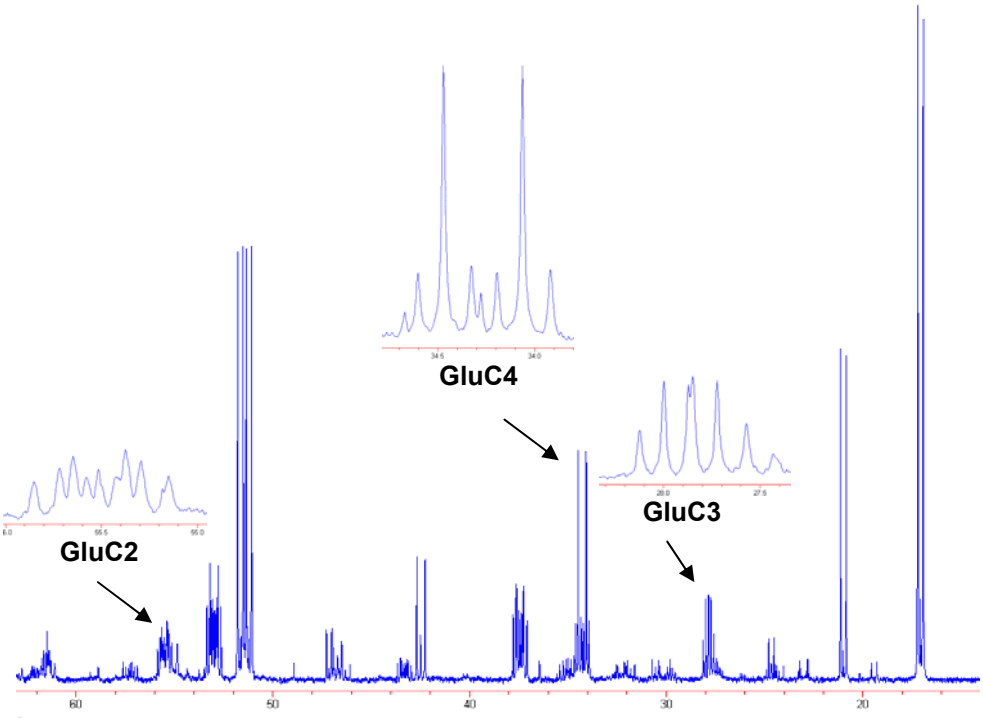

Figure 4.1 Representative ^{13}C NMR spectrum obtained after ^{13}C labeling and extraction on 6 ml of Fresh beads incubated in labeling medium for 6 hours.

4.3.2 Isotopomer Steady State Study

Establishing isotopomer steady state, where isotopomer patterns are not changing with time, is especially important for determining relative metabolic fluxes using the modeling program tcaCALC [179, 188]. With respect to ^{13}C NMR and isotopomer analysis studies examining metabolic fluxes in relation to insulin secretion in beta cells [34-36], when switching to the labeling medium, cells are exposed to the labeled substrate (i.e. ^{13}C-glucose) as well as possibly different concentrations of nutrients in medium. Thus, it is important to ensure that enough time has been given after introduction of ^{13}C-enriched substrates to cells to allow for the number of turns of the TCA cycle necessary for the replacement of endogenous ^{12}C-labeled metabolites with ^{13}C-labeled metabolites as well as to ensure that metabolism and isotopomer patterns are not changing with time. However, as the previously mentioned studies are often performed in batch culture systems, where there is not continuous replenishment of the external medium, it is important to not wait an extended period of time after addition of the labeling medium in order to prevent the associated changes in metabolism that may occur due to changes in metabolite concentrations in the incubation medium over time. Thus, performing a study where the relative multiplet peak areas of the glutamate resonances of interest, specifically glutamate carbons C2, C3, and C4, are examined over time is necessary.

Fresh beads were incubated in medium containing 15 mM U-^{13}C glucose for 3-15 hours. The glutamate carbon resonances analyzed included the following types of multiplets: doublet (D), triplet (T), quartet (Q), and singlet (S). As indicated in Figure 4.2A, for glutamate C2 (GluC2), the relative peak areas did not change with time, except

for C2Q, which was higher at the 12 hour time point compared to the 3 hour time point ($p<0.05$). For glutamate C3 (GluC3) (Figure 4.3A), the relative multiplet peak areas changed with time, with an overall increase in the C3 triplet and a decrease in the singlet peak. There was no difference between relative peak areas from 3 to 6 or 6 to 9 hours except for the GluC3 triplet, which was greater at 6 hours than at 3 hours ($p<0.05$). For glutamate C4 (GluC4) (Figure 4.4A), there was an overall decrease in the D45 resonance and an increase in the C4Q with time. No difference was found between the 6 and 9 hour time points or 3 and 6 hour time points for glutamate C4.

Overall, for most of the multiplets, there was no difference in relative multiplet peak areas between 3 and 6 and 6 and 9 hours. Therefore, although the isotopomer patterns overall changed with time, around the 6 hour timeframe, most of the multiplet peak areas remained constant. Thus, a "pseudo" isotopomer steady state was approximated at the 6 hour period. The precise reason for the continued changes in isotopomer patterns is unclear; however, one possibility is that this is caused by changes in the concentration of nutrients and metabolites in the medium as a result of cellular metabolic activity. Avoiding these changes, for example, by implementing a single-pass perfusion system, is not desirable due to the high cost of the labeled glucose necessary for the duration of the experiment. Additionally, the changes in isotopomer patterns present in the batch culture system used here do not preclude the use of the analysis, especially as most patterns were not changing around the chosen incubation time frame.

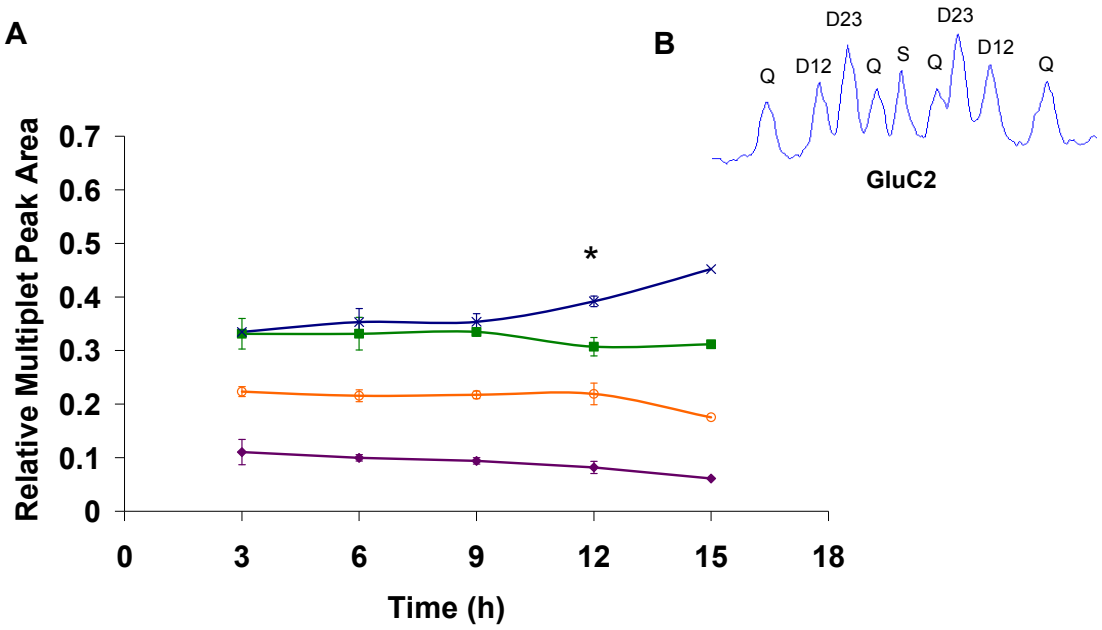

Figure 4.2 A). Relative multiplet peak areas of the glutamate C2 (GluC2) resonance during incubation in 15 mM U-^{13}Cglucose DMEM for 3-15 hours. The quartet (Q) multiplet is represented by the blue line, doublet 23 (D23) by the green line, doublet 12 (D12) by the orange line, and the singlet (S) by the purple line. B). Representative glutamate C2 resonance with multiplets labeled. *indicates $p<0.05$ compared to 3 hour time point. *n=3* for 3-12 hours and *n=1* for 15 hours.

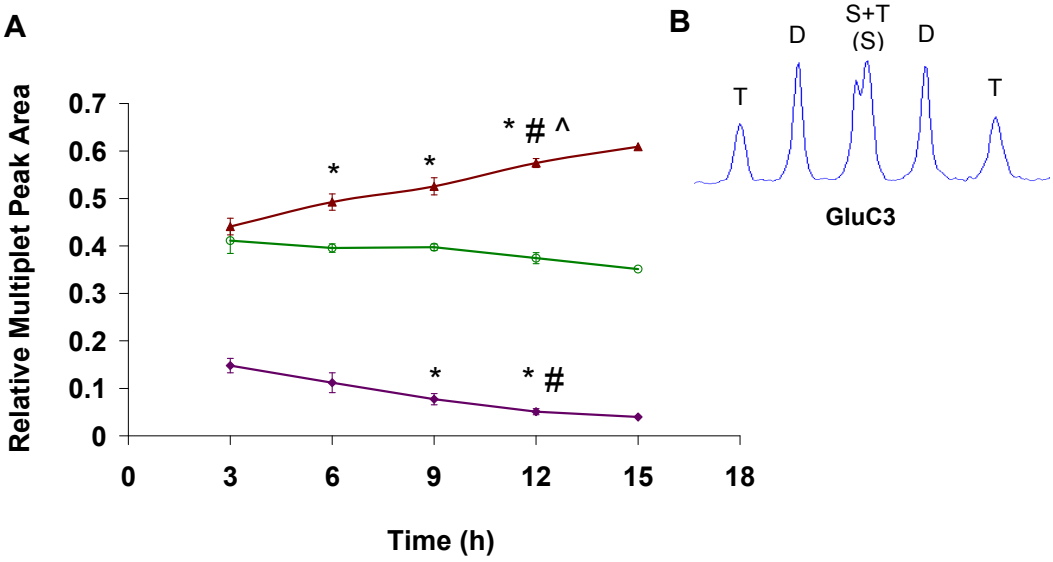

Figure 4.3 A)**.** Relative multiplet peak areas of the glutamate C3 (GluC3) resonance during incubation in 15 mM U-^{13}Cglucose DMEM for 3-15 hours. The singlet (S) multiplet is represented by the purple line, doublet (D) by the green line, and the triplet (T) by the red line. B). Representative glutamate C3 resonance with multiplets labeled. *$p<0.05$ compared to 3 hour time point, $^{\#}p<0.05$ compared to 6 hour time point, ^$p<0.05$ compared to 9 hour time point. *n=3* for 3-12 hour incubations and *n=1* for 15 hour incubation.

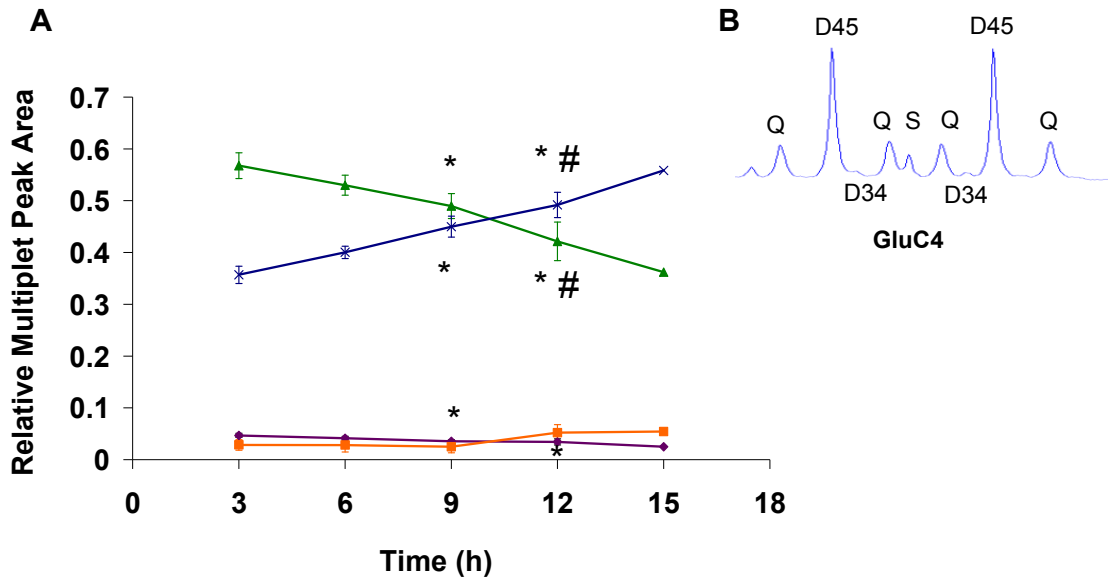

Figure 4.4 A). Relative multiplet peak areas of the glutamate C4 (GluC4) resonance during incubation in 15 mM U-^{13}Cglucose DMEM for 3-15 hours. The singlet (S) multiplet is represented by the purple line, doublet 45 (D45) by the green line, quartet (Q) by the blue line, and doublet 34 (D34) by the orange line. B). Representative GluC4 resonance with multiplets labeled. *$p<0.05$ compared to the 3 hour time point, $^{\#}p<0.05$ compared to 6 hour time point. *n=3* for 3-12 hour incubations and *n=1* for 15 hour incubation

4.3.3 Medium Incubation Test

After establishing the appropriate incubation time in the labeling medium from the isotopomer steady state study, it was necessary to ensure that metabolic activity was maintained in the Cryopreserved beads after the basal and labeling medium incubation scheme imposed upon the encapsulated cells. For ^{13}C NMR and isotopomer analysis studies specifically looking at metabolism in βTC cell lines, the cells are exposed to glucose-free and serum-free solutions prior to high glucose exposure to mimic glucose-stimulated insulin secretion conditions [36, 183]. Although this incubation scheme is likely not a concern for Fresh encapsulated cells, the additional stress of nutrient deprivation immediately post-warming may have adverse effects on the Cryopreserved encapsulated cells. Thus, it was important to ensure that incubation of the Cryopreserved

beads in glucose and serum-free medium followed by incubation in fully supplemented 15 mM glucose DMEM did not lead to a significant decrease in metabolic activity compared to incubation in complete DMEM post-warming. This test was also important in evaluating the approximate bead volume necessary to obtain sufficient SNR in the NMR spectra from the Cryopreserved groups, based on the 6 ml volume used for Fresh beads.

As indicated by Figure 4.5, there was no difference in metabolic activity (when normalized to the Fresh group cultured in complete DMEM) between the Frozen "condition 1" and Frozen "condition 2" groups or the DPS-vitrified "condition 1" and DPS-vitrified "condition 2" groups ($p>0.05$). It was therefore determined that the basal and labeling incubation scheme applied did not affect the metabolic activity of the cells in the DPS-vitrified or Frozen beads compared to Cryopreserved beads incubated in complete DMEM for the same period. Thus, the incubation scheme was deemed appropriate for use with DPS-vitrified and Frozen beads for subsequent ^{13}C labeling and extraction experiments. In addition, the metabolic activity in the DPS-vitrified beads under incubation condition 2 was approximately 50-60% that of the Fresh control cultured under the same conditions. Thus, as a volume of 6 ml of Fresh beads was deemed sufficient to obtain a good SNR in the NMR spectra, a 12 ml bead volume of DPS-vitrified beads was chosen for the ^{13}C labeling and extraction experiments. Similarly, as the metabolic activity of the Frozen beads was approximately 90-100% that of the Fresh group under the same incubation condition, a 7 ml volume of Frozen beads was chosen for the subsequent ^{13}C labeling and extraction experiments. Although the chosen bead volume for the DPS-vitrified and Frozen beads was such to allow for a

similar metabolic activity compared to the Fresh control, it is important to note that isotopomer analysis is cell-number independent.

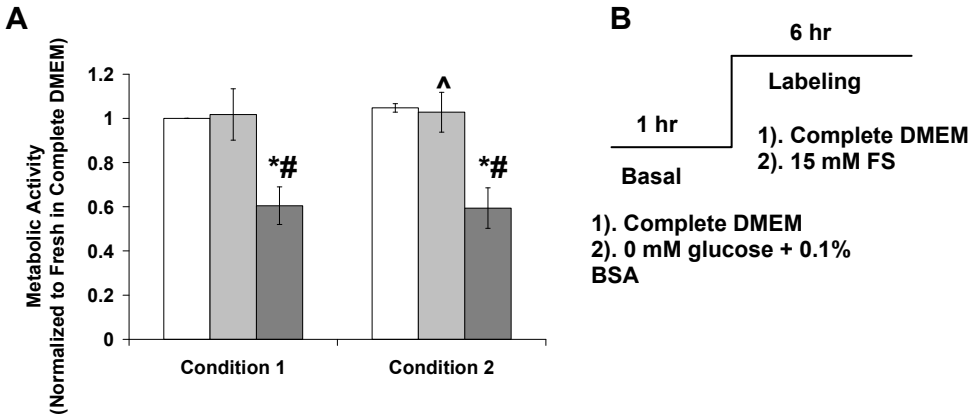

Figure 4.5 A). Metabolic activity of Fresh (white bars), Frozen (light gray bars), and DPS-vitrified (dark gray bars) beads after medium incubation test. B).Medium incubation scheme used in current experiment. Beads cultured under "condition 1" were exposed to fully supplemented, 25 mM glucose DMEM (complete DMEM) for one hour, followed by another 6 hours in complete DMEM. Beads cultured under "condition 2" were incubated in 0 mM glucose DMEM + 1.31 g/l BSA for one hour followed by a six-hour incubation in fully supplemented, 15 mM glucose DMEM (15 mM FS). Metabolic activity was assessed with alamarBlue®. *indicates $p<0.05$ compared to Fresh within same incubation condition, #indicates $p<0.05$ compared to Frozen within same medium incubation condition, ^indicates $p<0.05$ compared to incubation in complete DMEM within same cryopreservation treatment group. *n=3*

4.3.4 ^{13}C NMR Spectra From Frozen and DPS-Vitrified Encapsulated βTC-tet Cells

As the appropriate extraction procedure and isotopomer steady state period were determined for Fresh beads, and the medium incubation scheme deemed appropriate for the Cryopreserved groups, it was important to ensure that good quality ^{13}C NMR spectra could be obtained from the Frozen and DPS-vitrified beads. As indicated in Figures 4.6 and 4.7, high quality ^{13}C NMR spectra were obtained for both groups. The scale-up procedure used for cryopreservation is also described in CHAPTER 5.

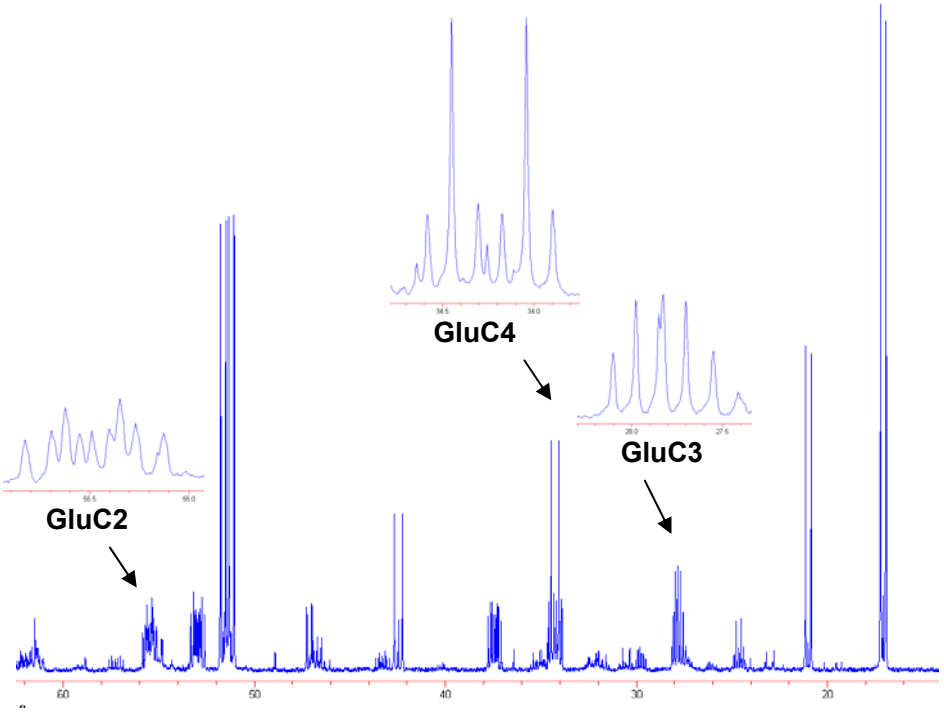

Figure 4.6 Representative ^{13}C NMR spectrum obtained after ^{13}C labeling and extraction of 7 ml of Frozen beads incubated in basal medium for 1 hour followed by labeling medium for 6 hours.

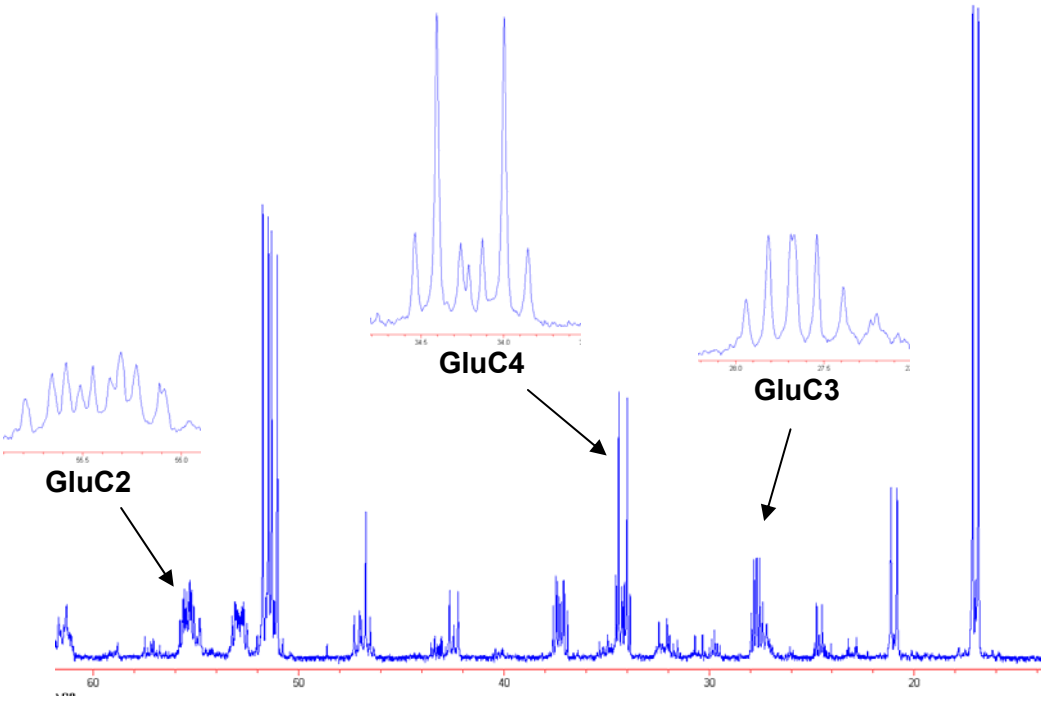

Figure 4.7 Representative ^{13}C NMR spectrum obtained after ^{13}C labeling and extraction of 12 ml of DPS-vitrified beads incubated in basal medium for 1 hour followed by labeling medium for 6 hours.

4.3.5 Determination of Appropriate Model of Glucose Metabolism for Use with tcaCALC

Choosing the appropriate model of glucose metabolism to use with tcaCALC is important, as different models used on the same experimental data can lead to different results in relative metabolic fluxes [187]. Thus, it was important in the current study to ensure that the model chosen represented the experimental data well. Two models of glucose metabolism, a "standard" model (Figure 4.8A) as well as a previously published modified model (Figure 4.8B), referred to as the "modified" model, containing a second non-pyruvate carboxylase (PC) entrance to the TCA cycle [36, 183, 187], were compared with NMR-derived data in order to determine which model better represented the experimental data. The modified model has been used previously with encapsulated βTC3 cells [183] as well as βTC-tet cells cultured in monolayers [36]. For this, tcaCALC-derived data were input into tcaSIM, a companion program to tcaCALC, to obtain simulated spectra to assess how well the models visually represented the experimental data. In terms of simulated spectra, the modified model better represented the experimental data, which was especially evident when examining the C4 quartets, which were overestimated by the standard model (Figure 4.9). To more quantitatively compare the two models with the experimental data, the percent C3/C4 error as well as the residual sum of square values between model-predicted values and experimental data were evaluated. As indicated in Table 4.2, the modified model had lower percent C3/C4 error and residual sum of square values ($p<0.05$) than the standard model, indicating again that the modified model better represented the experimental data. The modified model also fit experimental data from DPS-vitrified and Frozen bead spectra better than

the standard model (data not shown). Thus, the modified single pyruvate pool model was chosen to use with tcaCALC to determine relative metabolic fluxes for the subsequent studies.

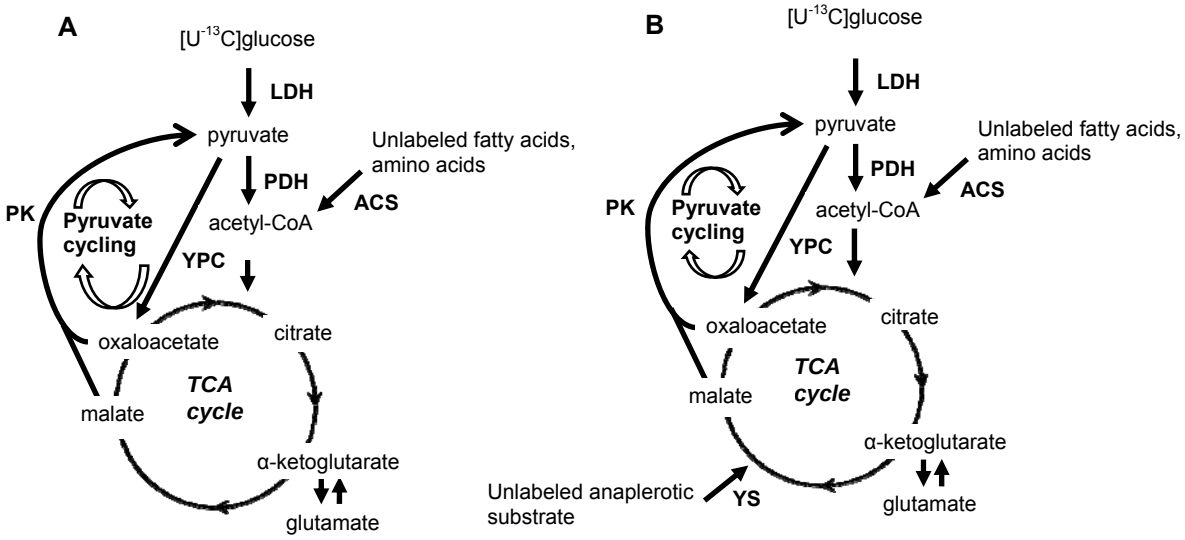

Figure 4.8 A). Standard model and B). a previously published modified model of glucose metabolism containing a second non-pyruvate carboxylase entrance to the TCA cycle applied in tcaCALC [36]. Adapted from Simpson et al [36]. The tcaCALC fluxes represented above are PK (phosphoenol-pyruvate carboxykinase/pyurvate kinase or malic enzyme); LDH (glycolysis); PDH (pyruvate dehydrogenase); YPC (pyruvate carboxylase); ACS (acetyl-CoA synthetase); and YS (non-pyruvate carboxylase anaplerosis).

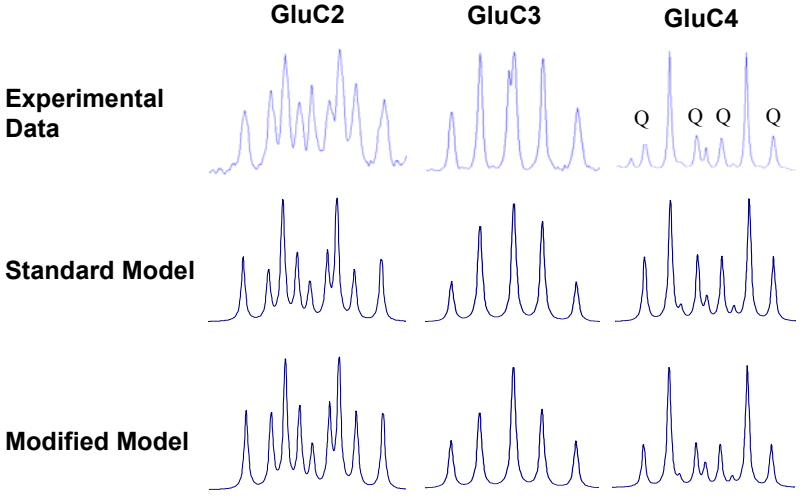

Figure 4.9 Representative experimental and tcaSIM-derived simulated spectra from Fresh beads. Simulated spectra were obtained by inputing tcaCALC-derived metabolic fluxes into tcaSIM. Q represents the quartet multiplet.

Table 4.2 Comparison of model-derived parameters and experimental data for a standard model and modified model of glucose metabolism from Fresh encapsulated βTC-tet cells. * $p<0.05$ compared to standard model. *n=3*

	Standard	**Modified**
%C3/C4 Error	71.79 ± 17.90	3.21 ± 3.46*
Sum of Squares	0.2112 ± 0.0590	0.0064 ± 0.0038*

4.4 Conclusions

In this study, we established parameters and procedures necessary for ^{13}C NMR and isotopomer analysis from Fresh and Cryopreserved encapsulated βTC-tet cells. This involved a) establishing an extraction protocol that allowed for sufficient SNR in the NMR spectrum from Fresh and Cryopreserved encapsulated βTC-tet cells; b) determining the appropriate incubation time in the high glucose labeling medium to achieve isotopomer steady state; c) verifying that metabolic activity of Cryopreserved encapsulated cells did not decrease when incubated according to the necessary incubation scheme; and d) determining the appropriate model of glucose metabolism to use in interpreting the ^{13}C-NMR-derived isotopomer data. Relative metabolic fluxes obtained using the optimized parameters and procedures developed in this chapter from Fresh and Cryopreserved groups will be discussed in CHAPTER 5.

CHAPTER 5

CRYOPRESERVATION EFFECTS ON INTERMEDIARY METABOLISM IN A PANCREATIC SUBSTITUTE: A ^{13}C NUCLEAR MAGNETIC RESONANCE STUDY*

5.1 Abstract

Cryopreservation is important for clinical translation of tissue engineered constructs. With respect to a pancreatic substitute, encapsulated islets or beta cells have been widely studied for the treatment of insulin-dependent diabetes mellitus. Besides cell viability loss, cryopreservation may affect the function of the remaining viable cells in a pancreatic substitute by altering fundamental processes in glucose-stimulated insulin secretion, such as pathways associated with intermediary metabolism, potentially leading to insulin secretion defects. In this study, we used ^{13}C nuclear magnetic resonance (NMR) spectroscopy and isotopomer analysis to determine the effects of conventional freezing and ice-free cryopreservation (vitrification) on carbon flow through tricarboxylic acid (TCA) cycle-associated pathways in encapsulated murine insulinoma βTC-tet cells; the secretory function of the encapsulated cells post-preservation was also evaluated. Specifically, calcium alginate-encapsulated βTC-tet cells were frozen or vitrified with a cryoprotectant cocktail. Beads were warmed and ^{13}C labeling and extraction performed. Insulin secretion rates were determined during basal and labeling periods and during

*Adapted from Ahmad et al., Cryopreservation Effects on Intermediary Metabolism in a Pancreatic Substitute: A ^{13}C Nuclear Magnetic Resonance Study. *Tissue Engineering* (Accepted)

small-scale glucose stimulation and K^+-induced depolarization. Relative metabolic fluxes were determined from ^{13}C NMR spectra using a modified single pyruvate pool model with the tcaCALC modeling program. Treatments were compared to non-preserved controls. Results showed that relative carbon flow through TCA cycle-associated pathways was not affected by conventional freezing or vitrification. However, vitrification, but not freezing, led to impaired insulin secretion on a per viable cell basis. The reduced secretion from the vitrified group occurred irrespective of scale and was present whether secretion was stimulated by glucose or K^+-induced depolarization, indicating that it might be due to a defect in late-stage secretion events.

5.2 Introduction

Encapsulated islets or beta cells have been studied extensively as tissue-engineered pancreatic substitutes, as they may provide more physiologic control of blood glucose levels compared to exogenous insulin therapy [79, 131, 195-202]. For future clinical translation, long-term storage of encapsulated cells for off-the-shelf availability is essential, and cryopreservation is a promising means towards achieving this objective. The two main methods of cryopreservation, vitrification, or ice-free cryopreservation, and conventional freezing, have both been studied in preserving encapsulated islets [24, 25, 37, 38, 40] or beta cells [30, 39]. Vitrification is promising since it may maintain biomaterial integrity better than conventional freezing, as indicated in previous studies with encapsulated islets [25] and insulinoma cells [30].

In terms of construct function post-preservation, recent studies have indicated that insulin secretion is often impaired after cryopreservation, specifically after conventional

freezing of encapsulated insulinoma cells [30] and conventional freezing [25] or vitrification [24, 25] of encapsulated islets. Although a reduction in cell viability may be an important component of this decreased secretion, the function of the remaining viable cells may also be compromised. Thus, an understanding of cryopreservation effects on fundamental aspects of beta cell function is critical for elucidating cryopreservation-induced secretion anomalies; however, no studies have addressed the quality of the remaining viable cells in cryopreserved encapsulated islets or beta cells, besides their ability to secrete insulin [24, 25, 30, 37, 38, 40]. Evaluating intermediary metabolism after cryopreservation is especially important, as it is key to glucose-stimulated insulin secretion (GSIS) in beta cells [31-33, 171], and cryopreservation has been shown to affect aspects of intermediary metabolism in other systems [203, 204]. Recently, ^{13}C nuclear magnetic resonance (NMR) spectroscopy and isotopomer analysis were used to study mitochondrial metabolism in GSIS, by correlating certain metabolic fluxes with insulin secretion using specific models applied in the tcaCALC modeling program [32, 34, 36, 183, 187, 205]. Since the natural abundance of ^{13}C is only 1.1%, it can be introduced into cells as an isotopic tracer, with its path being followed by the labeling patterns found in enriched metabolites [178]. Adjacently labeled ^{13}C carbons lead to the formation of isotopomer patterns, and analysis of steady-state glutamate isotopomer patterns with models of metabolism can estimate relative carbon flow through tricarboxylic acid (TCA) cycle-associated pathways, thus allowing for a quantitative assessment of intermediary metabolism [179].

In this work, we applied ^{13}C NMR and isotopomer analysis to elucidate the intermediary metabolism of calcium alginate-encapsulated murine insulinoma βTC-tet

cells post-cryopreservation by conventional freezing and vitrification. The secretory function of the encapsulated cells was also characterized. Cell-derived ^{13}C-glutamate isotopomers were analyzed using a previously published model of glucose metabolism [36, 183, 187] with tcaCALC to determine relative metabolic fluxes through TCA cycle-associated pathways, and the corresponding insulin secretion was measured post-preservation. To gain further insight into effects on secretion, the latter was measured in response to both glucose and high K^+ exposure. The ramifications of our findings towards identifying specific cellular processes affected by cryopreservation are discussed.

5.3 Materials and Methods

5.3.1 Cell Culture and Encapsulation

All chemicals were from Sigma (St. Louis, MO) unless otherwise noted. The βTC-tet cell line was obtained from S. Efrat (Albert Einstein College of Medicine, Bronx, NY).[191] Cells were cultured as monolayers in DMEM (pH 7.4) containing 25 mM glucose and 4 mM L-glutamine, supplemented with 10% (v/v) fetal bovine serum (FBS) (Gemini Bioproducts, West Sacramento, CA), 1% (v/v) penicillin (10,000 U/ml)-streptomycin (10,000 μg/ml) (Mediatech, Manassas, VA), and 1% L-glutamine (Mediatech) to a final concentration of 6 mM. This medium is henceforth referred to as complete DMEM. Cells were cultured in a humidified incubator at 37^{o}C with 5% CO_2/95% air, and used between passages 37 and 42.

Cells were detached from monolayers using 0.25% trypsin (Mediatech) and encapsulated at $7x10^7$ cells/ml alginate in 2% PRONOVA ultrapure LVM sodium alginate (FMC Biopolymer, Philadelphia, PA), with droplets crosslinked in 1.1% (w/v)

$CaCl_2$, as described previously [30] but without poly-L-lysine coating. Beads were 500-600 μm in diameter and were incubated overnight on a platform rocker (Stovall, Greensboro, NC) in complete DMEM. All salt solutions used in the encapsulation and subsequent procedures were adjusted to 300 mOsm to ensure isotonicity.

5.3.2 Vitrification

Cryopreservation was performed one day post-encapsulation. Beads were vitrified using the cryoprotectant (CPA) cocktail DPS comprised of 3 M dimethylsulfoxide (DMSO), 3 M 1,2 propanediol (PD), and 0.5 M sucrose (Fisher Chemical, Fisher Scientific, Pittsburgh, PA) in a modified version of the EuroCollins carrier solution. The EuroCollins component of the CPA solution contained 34.95 g/l glucose, 0.84 g/l $NaHCO_3$ (Fisher Chemical), 1.12 g/l KCl, and 1.68 g/l NaCl. Initial studies indicated that a volume of 6 ml Fresh beads was adequate to obtain sufficient signal-to-noise ratio in the ^{13}C NMR spectra. As vitrified/warmed beads had a minimum metabolically active cell number of 50% that of fresh beads, a 13 ml bead volume was vitrified to obtain a sufficient signal-to-noise ratio. Although similar metabolically active cell numbers were used for all groups to obtain sufficient signal-to-noise ratios, at isotopomeric steady state, isotopomer analysis is cell-number independent. CPAs were added to beads on ice stepwise according to the protocol in Table 5.1. This protocol was developed using a mathematical model that minimized cell osmotic excursions while ensuring CPA equilibration at each step [192]. One ml of beads was placed in a 100 μm cell strainer (BD Biosciences, Bedford, MA) and sequentially transferred through CPA solutions of increasing concentration (Table 5.1) at 4^oC in a six-well plate (BD

Biosciences). Following CPA addition, beads plus CPA were transferred to 20 ml glass scintillation vials (Fisherbrand/Fisher Scientific), and isopentane (EMD Chemicals, Gibbstown, NJ) was added on top of the CPA/bead mixture. Vials were transferred to a rack and the rack placed in an isopentane bath in a mechanical freezer (Sanyo North America, San Diego, CA) set at -135^{o}C for fast cooling to approximately -100^{o}C at a rate of ~64^{o}C/min. Vials were then transferred to a shelf in the freezer for slow cooling at ~2^{o}C/min to -130^{o}C, after which they were transferred to freezer storage boxes. During cooling, temperature was tracked with a thermocouple in a sample containing only CPA and isopentane. For each ^{13}C extraction, vitrification was performed on 1 ml bead aliquots 13 separate times. Vials were kept in the freezer overnight, and the next day 1 ml of beads was warmed at a time by agitating vials in a room temperature 30% (v/v) DMSO bath. Vitrification in each vial was verified by visual observation after cooling and immediately prior to warming [206]. Additionally, no crystallization/devitrification was visible upon warming. CPAs were then removed stepwise at room temperature in a similar fashion as CPA addition (Table 5.1). After CPA removal, beads were incubated in complete DMEM at 37^{o}C until all 13 ml of beads were warmed and CPA removed. Beads were then combined and a 12 ml volume withdrawn for labeling and extraction.

Table 5.1 Cryoprotectant addition/removal protocol for DPS vitrification.

Step	DMSO (M)	PD (M)	Sucrose (M)	Time (min)	Temperature (^{o}C)
A1	1	1	0.15	2	4
A2	2	2	0.3	2	4
A3	3	3	0.5	2	4
R1	2.25	2.25	0.3	2	RT
R2	1.5	1.5	0.2	2	RT
R3	0.75	0.75	0.1	2	RT
R4	0	0	0	4	RT

A: addition; R: removal; RT: room temperature; PD: 1,2 propanediol

5.3.3 Conventional Freezing

Beads were frozen in complete DMEM containing 10% (v/v) DMSO. After incubation in this solution at 4°C for 10 minutes, beads were transferred to 2.0 ml cryogenic vials (Corning Inc., Corning, NY) and placed in a Mr. Frosty isopropyl alcohol bath (Nalgene/Thermo Fisher Scientific, Rochester, NY) in a -80°C freezer (VWR International Inc., Radnor, PA) for 1.5 hours, followed by plunging into liquid nitrogen. As previous studies indicated a minimum metabolically active cell number of approximately 90% that of Fresh beads post-warming, 8 ml of beads were frozen (in 1 ml batches) to obtain a sufficient signal-to-noise ratio in the NMR spectra. After overnight storage, 1 ml of beads at a time was warmed rapidly by agitating vials in a 37°C water bath until no ice was visible. Beads were next placed in complete DMEM at 37°C for 10 minutes. After a subsequent wash with complete DMEM, beads were incubated in complete DMEM at 37°C until all batches were warmed. Beads were then combined and a 7 ml volume withdrawn for labeling and extraction.

5.3.4 ^{13}C Labeling and Perchloric Acid Extraction of Encapsulated Cells

Figure 5.1 shows the experimental procedure for ^{13}C labeling and extraction. ^{13}C labeling and extraction was performed one day post-encapsulation for Fresh and two days post-encapsulation for cryopreserved beads. A 6 ml bead volume was used for the Fresh control. After washing beads 4 times with basal medium consisting of glutamine-free and glucose-free DMEM supplemented with 1.31 g/l bovine serum albumin (BSA) (Sigma) at pH 7.4, beads were incubated in the same type of medium for 1 hour at 37°C. Beads were subsequently washed once with basal medium and once with labeling

medium, containing 15 mM uniformly labeled ^{13}C glucose (Cambridge Isotope Laboratories, Andover, MA) in glucose-free DMEM (pH 7.4) plus 10% (v/v) FBS (Gemini), 1% (v/v) L-glutamine (Mediatech), and 1% (v/v) penicillin-streptomycin (Mediatech), and incubated in the same type of medium for 6 hours. This labeling period was determined in a previous isotopomeric steady-state study (data not shown). Subsequently, perchloric acid extraction was performed based on the protocol in Simpson et al. [183], with modifications. Beads were washed with glucose-free and glutamine-free DMEM and alginate was dissolved in 110 mM sodium citrate (Fisher Chemical/Fisher Scientific). Cells were pelleted at 200xg at 4^{o}C for 10 minutes, and the pellet was washed with 0.85% (w/v) NaCl. Cells were then extracted twice in 0.5 M perchloric acid using an Omni GLH homogenizer (Omni International, Marietta, GA) with an Omni Tip™ plastic generator probe to prevent paramagnetic ion contamination. Supernatants were pooled and neutralized with 0.01-5 M KOH. This solution was then centrifuged at 10,000xg to remove precipitated salts and Chelex-100® resin (Sigma) was added to the supernatant to remove paramagnetic ions. After stirring the solution containing chelex resin for one hour on ice, the resin was removed by filtration through ashless filter paper (Whatman Inc., Piscataway, NJ) in a Nalgene® polysulfone filter holder (Thermo Fisher Scientific). Subsequently, the resin was chased with ultrapure water. The pH of the filtrate was adjusted to approximately 7.4 with 0.01-1 M HCl. The final extract was frozen at -80^{o}C and subsequently placed in a lyophilizer (Labconco Corporation, Kansas City, MO) for two days prior to reconstitution.

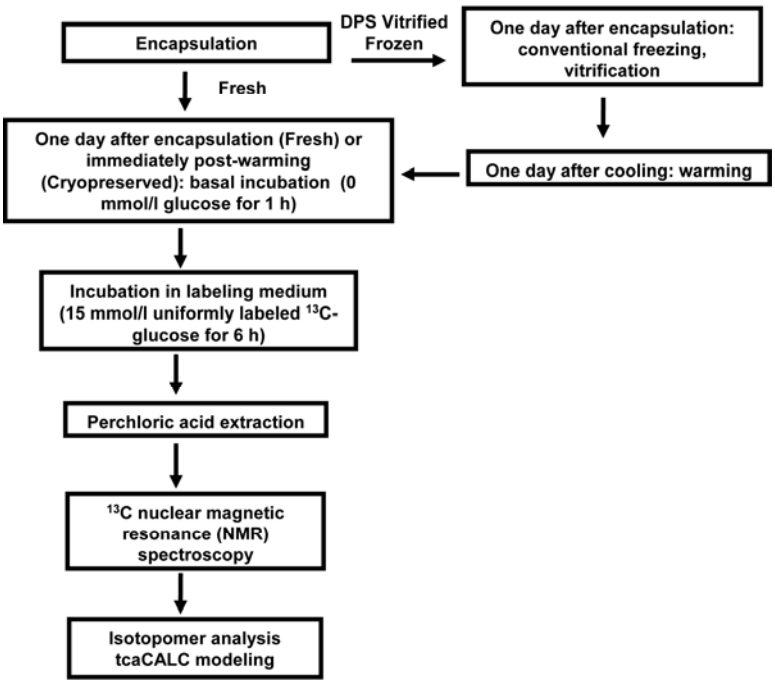

Figure 5.1 Overall experimental procedure for ^{13}C labeling and extraction experiments of Fresh and Cryopreserved encapsulated βTC-tet cells.

5.3.5 ^{13}C Extract Reconstitution and NMR Spectroscopy

Lyophilized extracts were reconstituted in 200 µl of 99.99% D_2O and subsequently spun at 18,300xg at room temperature for 10 minutes. The supernatant was placed on ice for 30 minutes to precipitate out $KClO_4$ salts prior to being centrifuged at 18,000xg for 10 minutes at 0^oC to pellet out additional precipitated salts. The supernatant was allowed to warm to room temperature before being placed in a 5 mm symmetrical NMR microtube (Shigemi Inc., Allison Park, PA) that was magnetic susceptibility-matched to D_2O. NMR data were acquired with a 5 mm broadband probe in an 11.7 T vertical bore Bruker DRX 500 magnet with an Avance Console (Bruker, Billerica, MA) with previously described parameters [36, 183].

5.3.6 ^{13}C NMR Spectra Analysis and tcaCALC Modeling

^{13}C NMR spectra were processed using NUTS NMR software (Acorn NMR, Fremont, CA). A 1 Hz line broadening factor and polynomial baseline correction were applied to spectra prior to relative peak area determination. Peaks were referenced to the lactate C3 peak at 21.0 ppm. Relative multiplet peak areas of isotopomer patterns of glutamate C2, C3, and C4 were determined using a line-fitting routine in NUTS as described previously [36]. Relative multiplet peak areas were input into tcaCALC [179, 181, 207] to determine metabolic fluxes relative to the flux through citrate synthase, defined as 1.

To determine the appropriate model of glucose metabolism to use with tcaCALC, %C3/C4 error [36, 183, 187] and the residual sum of squares [183] were determined for a standard model of metabolism and a previously published modified single pyruvate pool model containing a second non-pyruvate carboxylase anaplerotic entrance to the TCA cycle [36, 183, 187]. Parameters examined in tcaCALC included relative fluxes through glycolysis (LDH), pyruvate dehydrogenase (PDH), pyruvate carboxylase (YPC), phosphoenolpyruvate carboxykinase/pyruvate kinase or malic enzyme (PK), acetyl-CoA synthetase (ACS), non-pyruvate carboxylase anaplerosis (YS), and the average relative flux of pyruvate carboxylase and pyruvate kinase-pyruvate cycling [(YPC+PK)/2] [34, 205]. To ensure local minima were not reached during modeling, convergence to the same output was confirmed using multiple initial parameter estimates, and simulated spectra were generated based on the tcaCALC output using tcaSIM. Conditions of complete scrambling between oxaloacetate and fumarate and no conserved orientation transfer between succinyl-CoA and malate were assumed. Relative metabolic fluxes

were converted to percent carbon entry into the TCA cycle from different metabolic pathways relative to the total carbon entry into the TCA cycle, defined as follows:

Total carbon entry to the TCA cycle = PDH + ACS + YS + YPC (Eq. 1)

Similarly, relative fluxes were converted to percent carbon entering and leaving the pyruvate pool using the following equations:

Total carbon flow into the pyruvate pool = PK + LDH (Eq. 2)

Total carbon flow out of the pyruvate pool = PDH + YPC (Eq. 3)

5.3.7 Insulin Secretion during ^{13}C Labeling and Extraction Experiments

The average insulin secretion rate (ISR), calculated as (total insulin accumulation up to a given time point)/(time of incubation), was measured during basal and labeling periods and normalized to the viable cell number determined at the end of the six-hour labeling period. Medium samples were taken at the following times, where t=0 hour represents the beginning of the basal incubation period: 0 hour, 1 hour, 1.5 hours, 4 hours, and 7 hours (end of labeling period).

5.3.8 Small-Scale Glucose-Stimulated Insulin Secretion Experiment

Fresh, Frozen, and DPS-vitrified beads were exposed to the same basal and high glucose incubation conditions as during the ^{13}C labeling and extraction experiments, except on a smaller scale, with 0.3 ml beads per group in duplicate wells. At this scale, cryopreservation was performed in a single batch, as opposed to the multiple batches used in the scaled-up experiments. Stimulation index was determined by dividing the high glucose ISR measured during the initial 0.5 hours by the basal ISR. Medium

samples were removed at the same time points as the scaled-up ^{13}C experiments for later assay of insulin, and the viable cell number was measured at the end of the experiment.

5.3.9 K^+ Depolarization Experiment

Fresh, Frozen, and DPS vitrified beads were exposed to high K^+ to induce insulin secretion by membrane depolarization using a protocol adapted from Fleischer et al.[208] Cryopreservation was performed on a small scale in a single batch. Briefly, 0.3 ml of encapsulated cells from each group in duplicate wells were exposed for 1 hour to HEPES buffered Krebs-Ringer buffer (KRB) containing 4.7 mM KCl (pH 7.4) supplemented with 1.31 g/l BSA (basal incubation), followed by 1 hour in HEPES buffered KRB containing 47 mM KCl (pH 7.4) also supplemented with 1.31 g/l BSA (high K^+ incubation). The NaCl concentration in the high K^+ KRB was reduced to maintain isotonicity. Medium samples were taken at the beginning and end of the basal incubation, and at the beginning, 0.5 hours, and end of the high K^+ incubation period. Samples were stored at -80^{o}C for later assay for insulin. At the end of the basal period, beads from a parallel well containing 0.2 ml beads were solubilized, and cells were pelleted and extracted to measure intracellular insulin. Intracellular and secreted insulin was normalized to the viable cell number measured at the end of the experiment.

5.3.10 Assays

Insulin concentrations in medium samples were determined using a mouse insulin ELISA kit (Mercodia, Uppsala, Sweden) according to manufacturer's instructions. Absorbance was read at 450 nm on a SpectraMax Plus microplate reader (Molecular

Devices, Sunnyvale, CA). Intracellular insulin was extracted using a mammalian cell lysis kit (Sigma). Viable cell numbers were measured by solubilizing beads with sodium citrate and using trypan blue dye exclusion.

5.3.11 Statistical Analysis

Data are reported as mean ± standard deviation. Values were obtained from three independent experiments (n=3). Statistical analyses were performed with a two-tailed t-test or a one-way ANOVA using the General Linear Model in Minitab® (Minitab Inc., State College, PA). Multiple pairwise comparisons were performed using Tukey's post-hoc analysis. Values of $p<0.05$ were considered to be statistically significant.

5.4 Results

5.4.1 Metabolic Fluxes from Fresh and Cryopreserved Encapsulated Cells

Metabolic fluxes were determined using a modified single pyruvate pool model [36, 183, 187] (Figure 5.2), as it was shown to have lower %C3/C4 error and lower residual sum of square values compared to a standard model of metabolism without a second non-pyuruvate carboxylase anaplerotic entrance to the TCA cycle (data not shown).

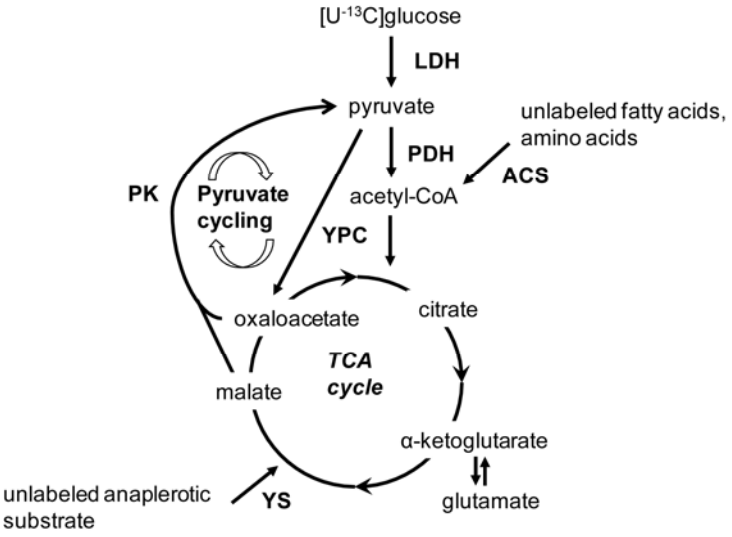

Figure 5.2 A previously published modified single pyruvate pool model of glucose metabolism applied in tcaCALC to determine metabolic fluxes. Figure adapted from Simpson et al. [36] The tcaCALC fluxes represented above are PK (phosphoenol-pyruvate carboxykinase/pyurvate kinase or malic enzyme); LDH (glycolysis); PDH (pyruvate dehydrogenase); YPC (pyruvate carboxylase); ACS (acetyl-CoA synthetase); and YS (non-pyruvate carboxylase anaplerosis).

The similarity of the simulated and experimental glutamate spectra (Figure 5.3) indicates that the metabolic model and parameters used provided a good representation of experimental results. As indicated in Figure 5.4A, there were no differences in the raw relative metabolic fluxes among the different treatment groups and the Fresh, non-cryopreserved control group ($p>0.05$). Figure 5.4B indicates that when converting raw metabolic flux data into percent carbon flow into the TCA cycle, there were also no differences among groups for any of the pathways examined ($p>0.05$). Percent carbon entry via non-pyruvate carboxylase anaplerosis, pyruvate carboxylase anaplerosis, and pyruvate dehydrogenase was similar among groups, with 28-36% of carbon entry via each pathway. In addition, there was negligible entry to the TCA cycle via the acetyl-CoA synthetase pathway, with less than 1% entry in all groups. To gain a snapshot of metabolism upstream of the TCA cycle, flow into and out of the pyruvate pool was also

examined. Figure 5.4C shows that no differences among the treatments and the Fresh non-cryopreserved group were identified. More pyruvate entered the pyruvate pool through malic enzyme or phosphoenolpyruvate carboxykinase/pyruvate kinase than through glycolysis for all groups ($p<0.05$).

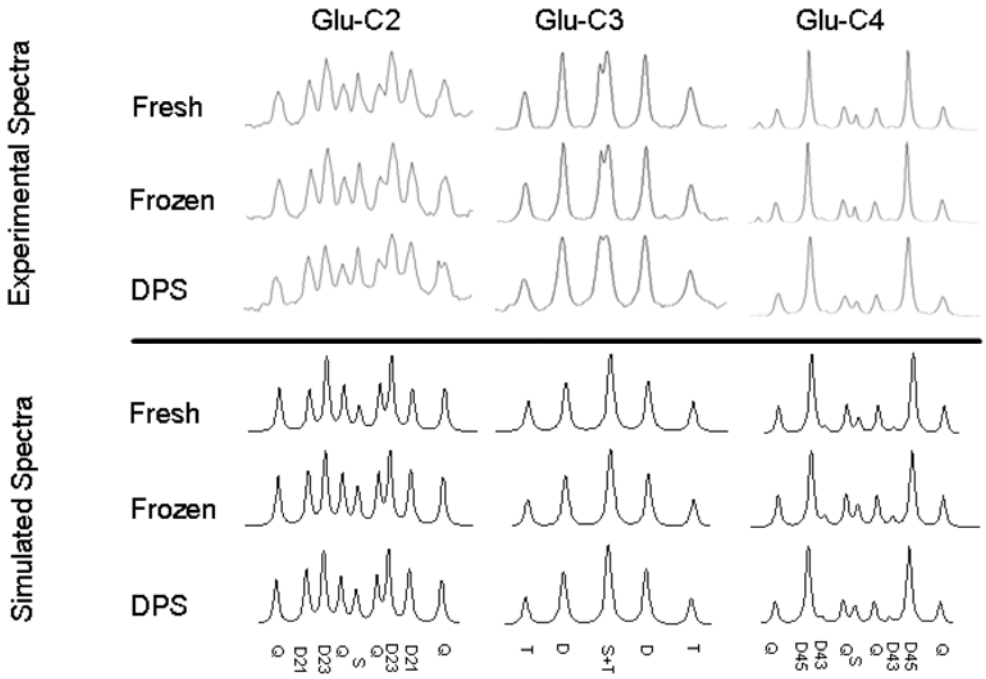

Figure 5.3 Representative isotopomer patterns from glutamate C2, C3, and C4 resonances from experimental spectra obtained from extracts of Fresh, Frozen, and DPS-vitrified encapsulated βTC-tet cells and simulated spectra obtained from tcaSIM based on tcaCALC output. A modified single pyruvate pool model was used to determine the tcaCALC output. The different multiplet components are represented by Q (quartet), D (doublet), S (singlet), and T (triplet).

A

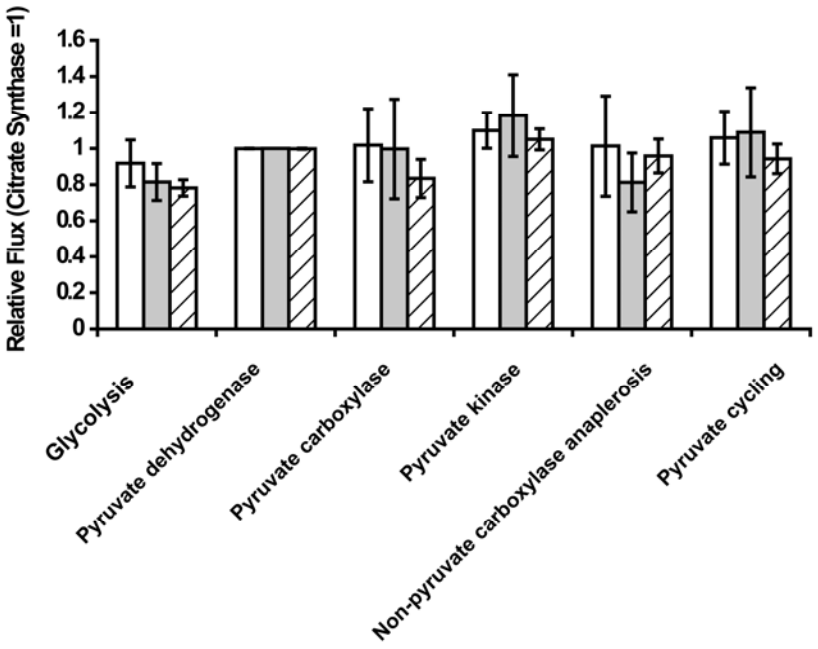
Relative Flux (Citrate Synthase =1)
1.6
1.4
1.2
1
0.8
0.6
0.4
0.2
0
Glycolysis
Pyruvate dehydrogenase
Pyruvate carboxylase
Pyruvate kinase
Non-pyruvate carboxylase anaplerosis
Pyruvate cycling

B

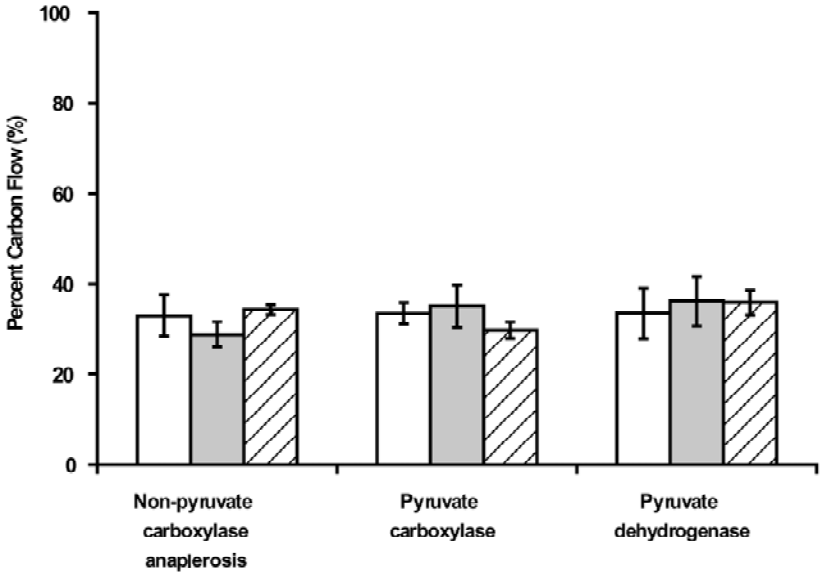
Percent Carbon Flow (%)
100
80
60
40
20
0
Non-pyruvate carboxylase anaplerosis
Pyruvate carboxylase
Pyruvate dehydrogenase

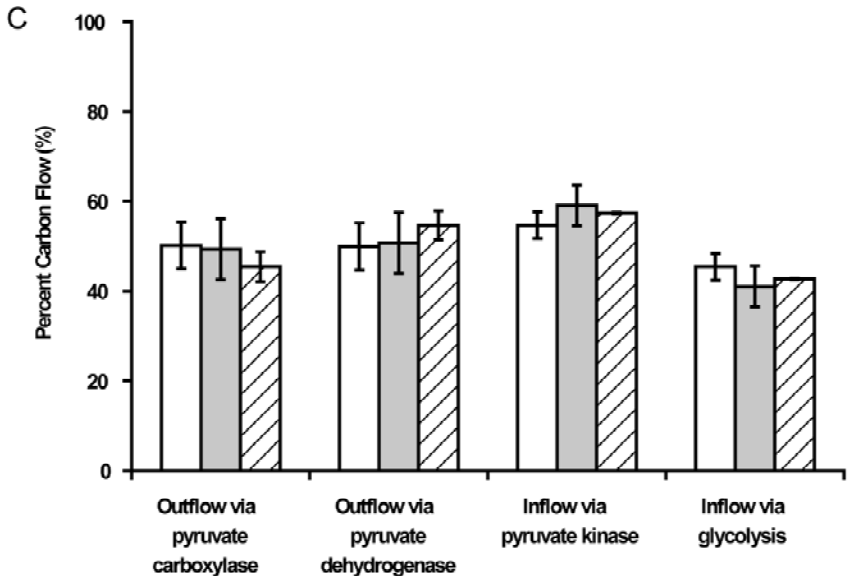

Figure 5.4 Cryopreservation effects on metabolism of encapsulated βTC-tet cells determined using a modified single pyruvate pool model applied in tcaCALC. A). Relative metabolic fluxes, B). Percent carbon flow into the tricarboxylic acid (TCA) cycle, C). Percent carbon flow into and out of the pyruvate pool. Data obtained from Fresh (white bars), Frozen (gray bars), and DPS-vitrified (striped bars) groups. Data are presented as mean ± standard deviation. *n=3*

5.4.2 Insulin Secretion during ^{13}C Labeling and Extraction Studies

Figure 5.5 shows that on a per viable cell basis, there was no difference in insulin secretion rate (ISR) between Fresh and Frozen groups during the basal period and at all time points assayed in the high glucose labeling period. However, ISR per viable cell was significantly lower for the DPS group compared to the Fresh or Frozen groups at all time points during the high glucose labeling period ($p<0.05$).

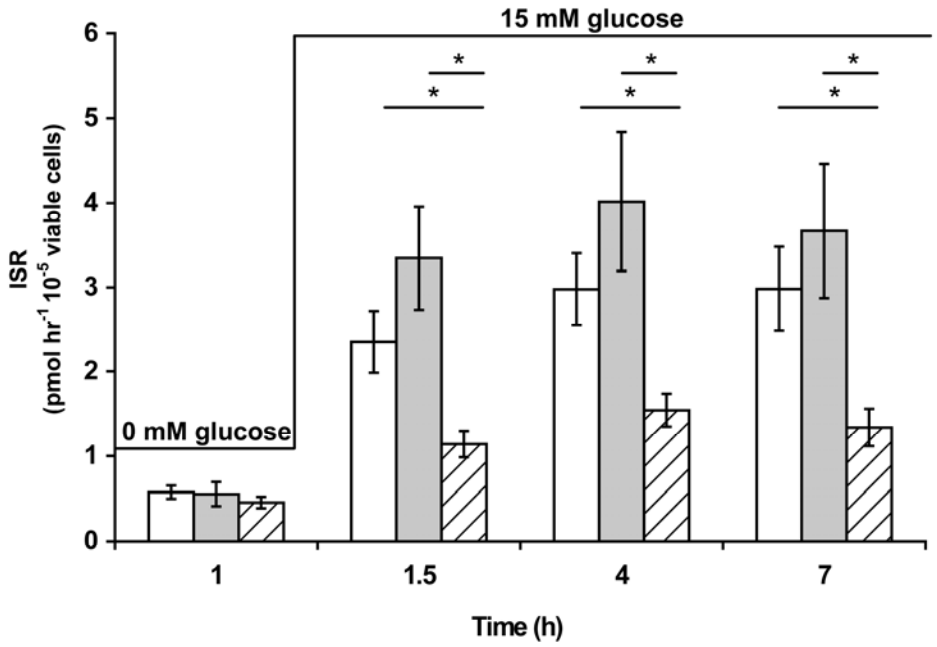

Figure 5.5 Insulin secretion rate (ISR) measured during basal and high glucose ^{13}C-labeling periods for Fresh (white bars), Frozen (gray bars), and DPS-vitrified encapsulated βTC-tet cells (striped bars). *indicates statistical significance ($p<0.05$). Data are presented as mean ± standard deviation. *n=3*

5.4.3 Insulin Secretion during Small-Scale GSIS Experiment

To investigate if the decreased ISR from the DPS group was due to the required scale-up of the vitrification process for the extraction procedure, insulin secretion was also tested on a smaller scale. Insulin secretion during the smaller scale GSIS experiment resulted in trends similar to those seen in the large-scale extraction experiments (Figure 5.6A). Specifically, there was no difference in ISR per viable cell among the three groups during the basal period and between the Fresh and Frozen groups during the high glucose period. At the 4 and 7 hour time points during the high glucose period, however, ISR was lower for DPS compared to Fresh and Frozen groups.

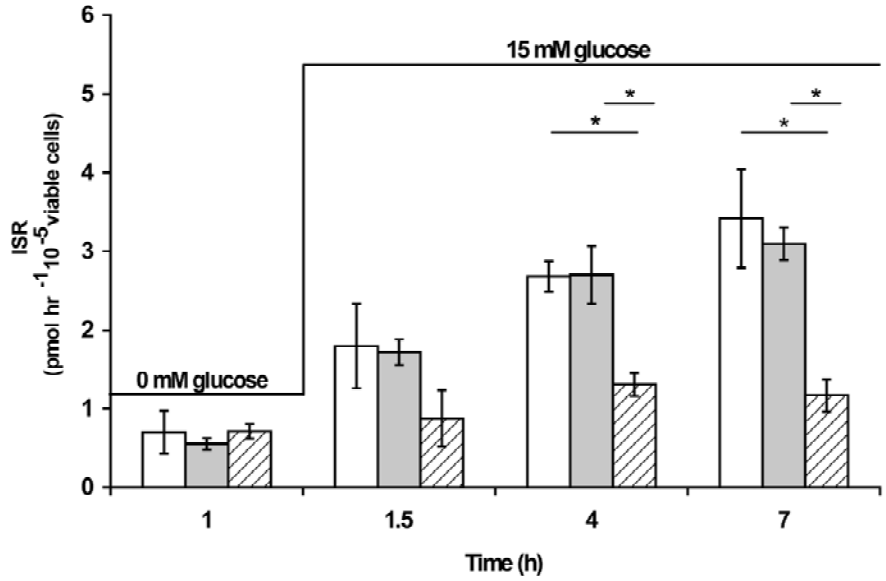

Figure 5.6 Insulin secretion rate (ISR) from encapsulated βTC-tet cells during small-scale glucose-stimulated insulin secretion (GSIS) experiment for Fresh (white bars), Frozen (gray bars), and DPS-vitrified groups (striped bars). *indicates statistical significance ($p<0.05$). Data are presented as mean ± standard deviation. *n=3*

5.4.4 Insulin Secretion during K^+-Induced Depolarization

To investigate if the depolarization/exocytosis response was affected by vitrification with DPS, encapsulated cells were exposed to a high extracellular [KCl]. As indicated in Figure 5.7A, ISR measured during exposure to 47 mM KCl was much lower for DPS compared to the Fresh group at both the 1.5 and 2 hour time points ($p<0.05$), and there was no difference between the Fresh and Frozen groups. In addition, there was no difference in ISR between the Fresh and DPS groups during the basal period. For the Fresh and Frozen groups, the stimulation index with high K^+ was higher than that with glucose (Figure 5.7B). However, there was no difference between the two indices for the DPS group. Importantly, there were no differences in intracellular insulin content measured at the end of the basal period among the three groups, with 23.79 ± 3.53, 24.85

± 5.75, and 19.09 ± 3.39 pmol/10^5 viable cells for Fresh, Frozen, and DPS vitrified groups, respectively.

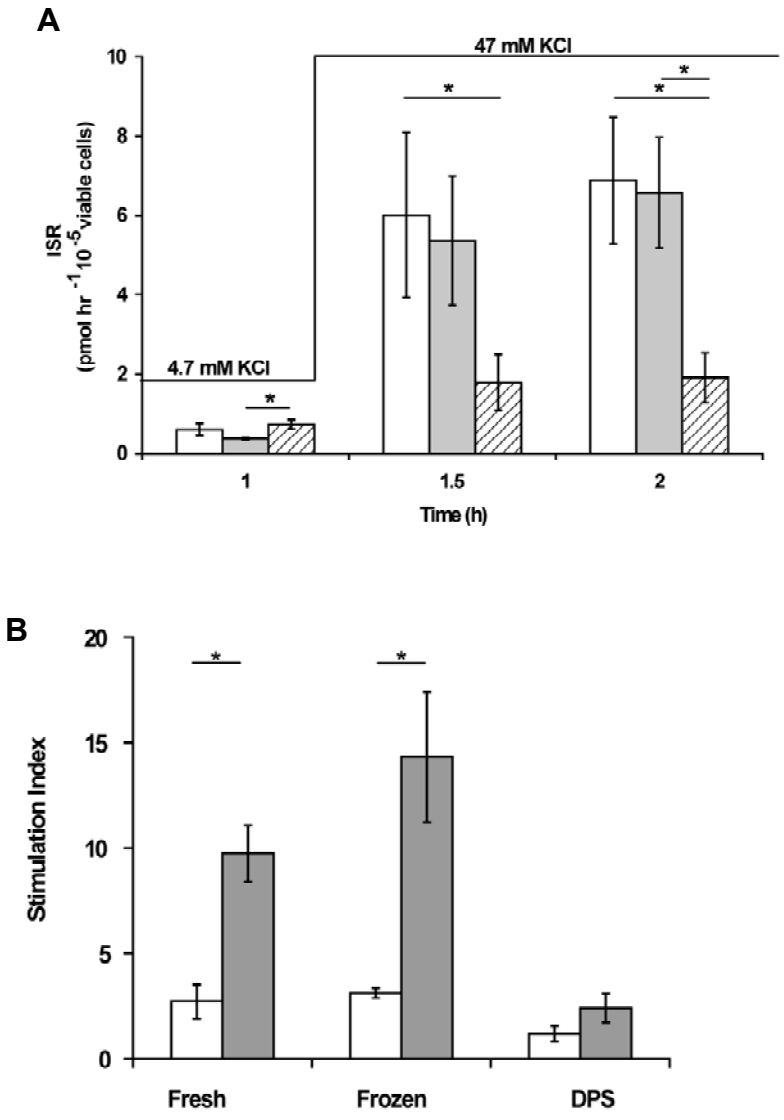

Figure 5.7 Insulin secretion rate (ISR) from encapsulated βTC-tet cells during A). small –scale K^+-induced depolarization experiment for Fresh (white bars), Frozen (gray bars), and DPS-vitrified groups (striped bars). B). Stimulation indices from GSIS (white bars) and K^+-induced depolarization (gray bars) for Fresh, Frozen, and DPS-vitrified groups. *indicates statistical significance ($p<0.05$). Data are presented as mean ± standard deviation. *n=3*

5.5 Discussion

Cryopreservation is important for clinical translation of pancreatic substitutes, but recent studies have often shown impaired insulin secretion post-cryopreservation in encapsulated islets or insulinoma cells [24, 25, 30]. Although an overall reduction in viable cell number is likely a significant contributor to the impaired secretion, cryopreservation stresses may also affect the function of the remaining viable cells. In this study, we applied ^{13}C NMR and isotopomer analysis to evaluate the effects of two cryopreservation methods on the intermediary metabolism of encapsulated βTC-tet cells and examined secretory function both after glucose and non-nutrient secretagogue stimulation. Using a modified, single pyruvate pool model of metabolism [36, 183, 187], we found that relative carbon flow through the TCA cycle-associated pathways examined was not significantly affected by either conventional freezing or vitrification. Furthermore, insulin secretion per viable cell was not affected by conventional freezing. However, the glucose-stimulated and depolarization-induced insulin secretion responses were significantly compromised by vitrification.

It is well established that intermediary metabolism is a crucial component in the glucose-stimulated insulin secretion response in beta cells [31-33, 171]. Understanding how metabolic pathways are affected by cryopreservation is important in better evaluating impaired insulin secretion and in designing optimal cryopreservation protocols. Specifically, the use of ^{13}C NMR and isotopomer analysis allows for a comprehensive view of mitochondrial metabolism [178], by examining carbon flow through various metabolic pathways at once, which has not been done previously for cryopreserved encapsulated islets or beta cells. Although this method alone does not

determine absolute metabolic fluxes, it does allow for the evaluation of relative metabolic fluxes and preferred metabolic pathways, which have shown significant correlations with insulin secretion [34, 36].

Reports in the literature are conflicting with respect to secretory function after cryopreservation in encapsulated islets [24, 25, 37, 38, 40] or beta cells [30] and also vary with species, type of cryopreservation method, and insulin secretion protocol used. Additionally, few studies have directly compared conventional freezing to vitrification [25, 30]. Studies on cryopreservation of encapsulated hamster islets have indicated impaired insulin secretion from Vitrified [24, 25] and Frozen [25] constructs *in vitro*, with freezing leading to capsule breakage. On the other hand, Vitrified encapsulated βTC3 cells reportedly exhibited similar insulin secretion to nontreated controls, although Frozen encapsulated cells exhibited lower secretion [30]. However, the particular cell line, freezing protocol, and vitrification solutions used were different than those used in the current study.

Although secretion from the Frozen group appeared slightly elevated compared to Fresh in the large-scale ^{13}C NMR experiments, the increase was not statistically significant. More importantly, insulin secretory function was significantly lower in the DPS vitrified group relative to Fresh (Figure 5.5). This decreased secretion is likely not due to the large-scale of the ^{13}C experiments, as a similar trend was observed in the small-scale secretion study (Figure 5.6).

Although studies using ^{13}C NMR and isotopomer analysis typically do not show correlations between all metabolic fluxes and insulin secretion, the significant decrease in insulin secretion in the DPS group without any corresponding changes in metabolic

fluxes is noteworthy and unprecedented. This maintenance of carbon flow through TCA cycle pathways suggests that insulin secretion may be compromised downstream of the TCA cycle in the DPS-vitrified group.

Various steps downstream of the TCA cycle may be potentially affected by DPS-vitrification, with one possible area being depolarization/exocytosis. In particular, studies have examined the K^+-induced depolarization responses from various cryopreserved cells and tissues [209-211]. One study on cryopreservation of boar spermatozoa indicated impaired response to depolarization after high K^+ exposure in Frozen cells, where the rise in intracellular calcium was three times lower compared to that in Fresh cells [209]. Additionally, studies on Conventionally Frozen blood vessels have indicated impairment in contractility response after exposure to high K^+ compared to unfrozen controls [210, 211]. Specifically, the reduced contractility response from Frozen human internal mammary arteries has been associated with enhanced basal intracellular calcium concentration in smooth muscle cells post-warming due to possible enhancement in calcium flux through voltage-gated calcium channels and activation of protein kinase C after cryopreservation [210]. A subsequent study, also indicating impairment in contractility response after freezing, suggests that freezing-induced membrane depolarization and activation of the Rho/Rho kinase pathway are important factors in the increased basal intracellular calcium concentration after Conventional Freezing of human saphenous veins [211]. With respect to Vitrified blood vessels, Song et al. examined the effects of drug agonist-induced contractility in Vitrified and Frozen rabbit veins, and found similar responses to most agonists from Vitrified veins relative to Fresh controls [212]. Overall, studies have reported on the effects of freezing on K^+ induced

depolarization response from Frozen cells [209] or tissues [210, 211], but the effects of vitrification on K^+ induced depolarization responses remain less known.

It has been previously shown that βTC-tet cells stimulated by high K^+ had a higher fold induction in insulin secretion compared to cells stimulated by glucose [208]. Similarly, in our study, significantly higher stimulation indices were found for high K^+ stimulation compared to high glucose stimulation for the Fresh and Frozen groups, but not the DPS group. The blunted insulin secretion from the DPS group after high K^+ exposure and the similar stimulation indices between high K^+ and high glucose exposure for DPS may indicate a defect in depolarization/exocytosis. Importantly, this is corroborated by the similar intracellular insulin content among the three groups at the end of the basal period, which indicates that the lower induced secretion from the DPS group was not due to insufficient intracellular insulin. Although the reason for the reduced secretion is unclear, defects in the membrane depolarization mechanism itself or in subsequent steps, such as the opening of voltage-gated calcium channels and the rise in intracellular calcium, are possibilities.

5.6 Conclusions

Using ^{13}C NMR and isotopomer analysis, we found that intermediary metabolism was maintained in encapsulated βTC-tet cells cryopreserved by either vitrification or conventional freezing. Additionally, insulin secretion was maintained post-warming in Conventionally Frozen constructs. Although vitrification may be advantageous due to better maintenance of biomaterial integrity in some systems, our study indicates compromised insulin secretion, possibly due to defects in late-stage secretion events.

Overall, our results offer new insight into understanding insulin secretion pathways that are maintained after cryopreservation as well as those that should be investigated further to better understand compromised secretion from encapsulated beta cells post-warming.

CHAPTER 6

CRYOPRESERVATION EFFECTS ON RECOMBINANT MYOBLASTS ENCAPSULATED IN ADHESIVE ALGINATE HYDROGELS

6.1 Abstract

Cryopreservation is critical for long-term storage of microencapsulated cells. Although many studies have examined cryopreservation of cells encapsulated in non-adhesive hydrogels, as bio-functionalized hydrogels, such as those with adhesive motifs, are increasingly being used, it is important to understand how the additional complexity of 3-D adhesion affects cryopreservation outcome. Indeed, evidence suggests that adhesion plays an important role in cell response to cryopreservation. With respect to a pancreatic substitute, studies have indicated benefits with adhesion in 3-D. Thus, the main objectives of this study were 1). to assess the effect of cell-matrix interactions on cryopreservation response in terms of metabolic activity and insulin secretion from encapsulated, stably transfected murine C2C12 myoblasts and 2). to determine the longer-term cryopreservation response of the cells encapsulated in a 3-D adhesive hydrogel matrix. ***Materials/Methods:*** To determine the effect of cell-matrix interactions on Cryopreserved encapsulated cell response, stably transfected C2C12 cells, encapsulated in partially oxidized RGE and RGD-alginate hydrogels, were compared and assessed for metabolic activity and insulin secretion after freezing and vitrification. To assess the longer-term response of cells encapsulated in RGD-alginate hydrogels, encapsulated cells were cultured either 1 or 4 days post-encapsulation, cryopreserved,

and assessed up to 3 days post-warming for metabolic activity and insulin secretion. Cell morphology was assessed one day post-warming via circularity measurements. ***Results:*** Cells encapsulated in RGE or RGD-modified alginate responded similarly after vitrification and conventional freezing in terms of metabolic activity and insulin secretion up to one day post-warming. Frozen RGD-alginate encapsulated cells responded similarly to Fresh controls in terms of metabolic activity and insulin secretion over 3 days post-warming. However, DPS-vitrified beads exhibited lower metabolic activity one day post-warming. Cell circularity was also similar between Fresh and Cryopreserved groups. ***Conclusions:*** The presence of cell-matrix interactions did not affect cell response to cryopreservation in terms of metabolic activity and insulin secretion up to one day post-warming. In spite of initial differences in metabolic activity and insulin secretion rate relative to Fresh controls for the DPS-vitrified group, overall, conventional freezing and DPS-vitrification maintain metabolic activity, insulin secretion rate, and cell morphology for Stable C2C12 cells encapsulated in partially oxidized, RGD-alginate hydrogels.

6.2 Introduction

Cryopreservation is critical for long-term storage of tissue engineered constructs [4, 5, 213, 214]. The two main methods of cryopreservation are conventional freezing and vitrification (ice-free cryopreservation). Although extracellular ice formation is not necessarily detrimental to single cells in suspension, ice formation during freezing presents a significant challenge in cryopreserving multicellular systems and tissues [4, 5]. Thus, vitrification, or ice-free cryopreservation, has been investigated for preservation of various natural tissues [5, 215, 216] as well as tissue engineered constructs [24, 25, 30,

50, 51, 162, 214]. However, vitrification may potentially lead to cell osmotic excursions as well as cytotoxicity due to the high concentration of cryoprotectants used in the procedure [5, 6]. Thus, it is important to study both vitrification and freezing methods in order to determine the best method of preservation for a given 3-D construct.

Cell microencapsulation within 3-D hydrogels has been widely studied for various tissue engineered constructs, with alginate commonly being used as the encapsulation polymer [74, 217, 218]. With respect to cryopreservation of encapsulated cells, most studies have examined cellular response in non-adhesive hydrogel systems [24, 25, 30, 37-44]. However, to better control cell fate in 3-D, bio-functionalized hydrogels are increasingly being studied, with additions of bioactive motifs to help control cellular processes such as cell adhesion [219, 220]. Adhesion in 3-D is especially important, as cell-matrix interactions have been shown to be important for cell survival, proliferation, and differentiation among other cell processes [221].

With respect to a pancreatic substitute, unmodified alginate has been commonly used for cell encapsulation [8, 71]. However, as various cells types are being explored for use in cell-based therapies for insulin-dependent diabetes [48], different degrees of anchorage dependence may become necessary upon their encapsulation in a 3-D hydrogel environment. In addition, recent evidence suggests that cell-matrix interactions in 3-D are beneficial for encapsulated beta cells or islets [11, 12, 96]. Thus, adhesive hydrogels may be advantageous for certain pancreatic substitutes. In particular, alginate polymer chains have been coupled with the ubiquitous tripeptide RGD [222], in order to promote cell adhesion in 3-D [20, 101, 223]. Specifically, the C2C12 myoblast cell line has been well

characterized in RGD-alginate, displaying the ability to survive, proliferate, and differentiate on 2-D [99] as well as in 3-D hydrogel systems [20].

It is critical to study the viability and function of cells in an adhesive environment post-cryopreservation, as previous studies suggest that adhesion plays an important role in cell response to cryopreservation. Indeed, literature reports indicate that cells in suspension respond differently to cryopreservation than cells attached to a substrate [14, 15, 17, 224]. In addition, encapsulation underneath or within adhesive matrices has been suggested to improve cryopreservation response for certain cells compared to cells in suspension [16, 17, 225]. However, cryopreservation studies on cells in 3-D adhesive hydrogels have generally focused on either the effects of conventional freezing [16, 45] or vitrification [50, 51] and rarely compare or decouple the separate effects of encapsulation and adhesion [16]. Additionally, no study has directly examined cryopreservation response to both vitrification and freezing in 3-D adhesive vs. non-adhesive hydrogel matrices.

In this study, we used a model pancreatic substitute consisting of C2C12 cells, stably transfected to secrete insulin, encapsulated in partially oxidized, RGD-modified alginate hydrogels. To address the issue of the effects of cell-matrix interactions on cellular response to both vitrification and conventional freezing, we compared metabolic activity and insulin secretion up to one day post-warming for Cryopreserved Stable C2C12 cells encapsulated in RGD and RGE-modified, partially oxidized alginate hydrogels. As previous studies have indicated benefits of longer-term culture of encapsulated cells pre-preservation [17, 225], we cryopreserved beads 1 and 4 days after encapsulation, and assessed metabolic activity and insulin secretion up to 3 days post-

warming. Cell morphology after cryopreservation was also quantified and compared to that of Fresh controls, as cell spreading has been associated with myoblast differentiation and fusion to form myotubes in RGD-alginate hydrogels [20].

6.3 Materials and Methods

6.3.1 Alginate Modification

All chemicals were obtained from Sigma (St. Louis, MO), unless otherwise indicated. Alginate was partially oxidized with sodium periodate based on previously published protocols [20, 111, 226]. Briefly, 1% (w/v) Pronova UP LVM alginate (FMC Biopolymer, Philadelphia, PA) was dissolved in ultrapure water. Subsequently, sodium periodate (Acros Organics, Geel, Belgium) was added to the alginate solution at 21.6 mg/g alginate [20] and stirred in the dark at room temperature for 19 hours. Subsequently, a two-fold molar excess, compared to the sodium periodate used, of ethylene glycol was added to the alginate solution to quench the oxidation reaction and stirred for an additional 2 hours [226]. Alginate was then placed in 2000 MWCO dialysis cassettes (Thermo Fisher Scientific, Waltham, MA) and dialyzed against ultrapure water for 3 days prior to lyophilization.

Partially oxidized alginate was subsequently reconstituted and conjugated with either GGGGRGDSP [20] or GGGGRGESP peptides (Biomatik Corporation, Wilmington, DE) at 10mg/g alginate using aqueous carbodiimide chemistry [98, 99]. The incorporation efficiency of the RGD peptide into the alginate matrix was previously described [98]. Briefly, 1% (w/v) partially oxidized alginate was dissolved in 0.1 M MES buffer with 0.3 M NaCl (pH 6.5) for four hours at room temperature. Subsequently, 1-Ethyl-3-[3-dimethylaminopropyl] carbodiimide hydrochloride (EDC) (Thermo Fisher

Scientific) and N-hydroxysulfosuccinimide (sulfo-NHS) (Thermo Fisher Scientific) were dissolved in MES buffer immediately prior to the reaction and added to the alginate to obtain a 2:1 molar ratio. The alginate solution was then allowed to react for 5 minutes prior to addition of the respective peptides [101]. The resulting solution was continuously mixed at room temperature for 20 hours prior to being transferred to 3500 MWCO dialysis cassettes (Thermo Fisher Scientific) for three-day dialysis against ultrapure water to remove unbound peptide and reactants. The peptide-modified, partially oxidized alginate was subsequently lyophilized.

6.3.2 Cell Culture and Encapsulation/Coating

Stable C2C12 cells, previously transfected with furin-cleavable, B10-modified human insulin [21], were cultured in DMEM (Mediatech, Manassas, VA) with 10% FBS (Gemini Bioproducts, West Sacramento, CA), 1% penicillin/streptomycin (P/S) (Mediatech) and 1 μg/ml puromycin (Sigma) in order to maintain constant selective pressure on the cells. Cells were plated at approximately 300-350,000 cells per T-175 flask and cultured under subconfluent conditions in order to prevent cell differentiation [99] in a 37^{o}C humidified incubator with 95% air/5% CO_2. All salt solutions used for encapsulation/coating were adjusted to 300 mOsm by adjusting the amount of the major salt component in the solution. For encapsulation, cells were detached from flasks using 0.25% trypsin (Mediatech) and cell number determined using trypan blue dye exclusion. The cell suspension was then centrifuged, and 3.5 % oxidized RGD or RGE-modified LVM, reconstituted in 0.85% NaCl (w/v), was added to the cell pellet in order obtain an encapsulation density of $3x10^6$ cells/ml alginate. This low cell density was used to

promote cell-matrix interactions over cell-cell interactions. Beads of 300-600 μm diameter were formed using an electrostatic bead generator (Nisco Engineering AG, Zurich, Switzerland) and crosslinked in a 1.1% (w/v) $CaCl_2$ bath. Beads were immediately coated according to the procedure of Sun [227], with modifications. Briefly, beads were placed in 0.1% (w/v) CHES in 1.1% (w/v) $CaCl_2$ for 3 minutes, washed with 1.1% (w/v) $CaCl_2$, and then incubated in 0.1% poly-L-lysine (PLL) (MW 15,000-30,000, Sigma) in 0.85% (w/v) NaCl, with mixing, for 5 minutes. Beads were then exposed to successive washes in 0.1% (w/v) CHES in 1.1% (w/v) $CaCl_2$, 1.1% (w/v) $CaCl_2$, and 0.85% (w/v) NaCl (two washes). Beads were then incubated in 0.2% w/v Pronova UP LVM (unmodified) alginate in 0.85% (w/v) NaCl for 4 minutes. After one additional wash in 0.85% (w/v) NaCl, beads were washed with culture medium and then placed in T-25 flasks. Beads were not exposed to sodium citrate as the last step. Flasks were placed on a platform rocker (Stovall, Greensboro, NC) in an incubator at 37°C. Encapsulated cells were cultured in the same type of medium as monolayers.

6.3.3 Cryopreservation

6.3.3.1 Vitrification

For vitrification, the cryoprotectant (CPA) cocktail solution DPS, consisting of 3 M dimethylsulfoxide (DMSO), 3 M 1,2 propanediol, and 0.5 M sucrose in a modified version of the EuroCollins carrier solution, containing 34.95 g/l glucose, 0.84 g/l $NaHCO_3$ (Fisher Chemical, Fisher Scientific, Pittsburgh, PA), 1.12 g/l KCl and 1.68 g/l NaCl was used. For CPA addition, approximately 0.7 ml beads were placed in 40 μm cell strainers (BD Biosciences, Bedford, MA), and sequentially transferred through CPA

solutions of increasing concentration at 4°C in a six-well plate (BD Biosciences) (Table 5.1). After incubation in the last CPA addition solution, beads and solution were transferred to pre-siliconized 20 ml borosilicate glass vials (Fisherbrand/Fisher Scientific) and a layer of isopentane (EMD Chemicals, Gibbstown, NJ) was placed on top of the CPA and beads. Vials were then placed on ice until transferred to a pre-chilled rack. The rack was then placed in an isopentane bath in a -135°C freezer for fast cooling to approximately -100°C (~64°C/min) prior to transfer to a rack in the freezer for slow cooling (~2°C/min) to -130°C. Temperature was tracked during the cooling process using a thermocouple placed in a sample vial containing only CPA solution and isopentane. Vitrification was verified by visual observation after cooling and immediately prior to warming of vials [206]. After overnight storage, vials were warmed rapidly in a 30% (v/v) DMSO in water bath at room temperature. Additionally, there was no crystallization/devitrification visible upon warming in the DMSO/water bath. Subsequently, vials were placed on ice and transferred to cell strainers for subsequent CPA removal in a stepwise fashion of decreasing CPA concentration at room temperature. Beads were then placed in T-12.5 flasks in fully supplemented DMEM at 37°C or aliquoted out for immediate assay.

Table 6.1 Cryoprotectant addition/removal protocol for DPS vitrification. A: addition; R: removal; RT: room temperature; PD; 1,2 propanediol

Step	DMSO (M)	PD (M)	Sucrose (M)	Time (min)	Temperature (°C)
A1	1	1	0.15	2	4
A2	2	2	0.3	2	4
A3	3	3	0.5	2	4
R1	2.25	2.25	0.3	2	RT
R2	1.5	1.5	0.2	2	RT
R3	0.75	0.75	0.1	2	RT
R4	0	0	0	4	RT

6.3.3.2 Conventional Freezing

For conventional freezing, beads were added to 10% DMSO in fully supplemented DMEM at 4°C incubated for 10 minutes. Beads and solution were subsequently transferred to 2.0 ml cryogenic vials (Corning Inc., Corning, NY) which were placed in a Mr. Frosty isopropyl alcohol bath (Nalgene/Thermo Fisher Scientific, Rochester, NY) in a -80°C freezer (VWR International, Radnor, PA) for 1.5 hours. Subsequently, vials were plunged into liquid nitrogen. After overnight storage, beads were warmed rapidly in a 37°C water bath until no ice was visible. Beads were then placed in fully supplemented DMEM at 37°C for 10 minutes, followed by one wash in fully supplemented DMEM. Beads were subsequently transferred to T-12.5 flasks with fully supplemented DMEM and placed in the incubator at 37°C or aliquoted out for immediate assay.

6.3.4 Metabolic Activity and Insulin Secretion

Metabolic activity from encapsulated cells was measured using alamarBlue® (Life Technologies, Carlsbad, CA). For the study comparing metabolic activity for the Fresh RGD/RGE/No peptide alginate encapsulated cells, 0.1 ml beads were added to 1 ml DMEM and 100 µl alamarBlue stock solution in a 12-well plate. After incubation for four hours at 37°C, samples of supernatant from each well were placed in a black 96-well plate (Nalgene/Nunc) and fluorescence was measured using a Synergy H4 Multimode microplate reader (Biotek Instruments, Winooski, VT) using excitation and emission wavelengths of 544 nm and 590 nm, respectively. For cryopreservation studies, 50 µl of beads were placed in 1 ml DMEM and 100 µl alamarBlue® stock solution and incubated

at 37°C for 4 hours. Medium was sampled at the beginning and end of the alamarBlue® assay period for insulin as well as for measuring fluorescence, as mentioned above. Insulin concentrations in samples were measured using an ultrasensitive human insulin radioimmunoassay kit (Millipore, St. Louis, MO), according to manufacturer's instructions.

6.3.5 LIVE/DEAD® Staining of Beads and Image Analysis

At one day post-warming, beads were stained with the LIVE/DEAD® viability kit (Life Technologies). Briefly, beads were washed 3 times in 0 mM glucose, phenol-free DMEM and then incubated in the same type of DMEM for 30 minutes with 2 μM calcein AM and 4 μM ethidium homodimer. Subsequently, beads were imaged using an LSM 510 NLO confocal microscope with the following excitation/emission settings: calcein AM (excitation: 488 nm/emission: 500-530 nm) and ethidium homodimer (excitation: 543 nm/emission: 560 nm) (Carl Zeiss, Thornwood, NY). A number of 10-20 beads were imaged per group, with Z-stacks taken every 10-20 μm.

For image analysis, Image J (NIH) was used to determine circularity of the cells in the beads. One Z-stack was taken per bead. For each image in the Z-stack, the green channel was isolated, a channel intensity threshold value of 30 was chosen, and particles with a size greater than 30 pixels squared were analyzed. For each bead, the average circularity from each slice was calculated and circularity values from each slice were averaged to obtain the circularity per bead.

6.3.6 Actin/Nuclei Staining

Fresh RGE and RGD-modified beads were fixed and cells stained with rhodamine phalloidin (Life Technologies) and DAPI (Life Technologies) to qualitatively assess cell morphology on the day of cryopreservation. Beads were washed with phenol-free DMEM and fixed in 3.7% methanol-free formaldehyde (Thermofisher Scientific) for 20 minutes, followed by 2 washes in DMEM. Subsequently, beads were incubated in 0.5% triton-X 100 (Acros Organics, Geel, Belgium) for 15 minutes, rinsed twice with DMEM, and blocked with 1% BSA in DMEM for 20 minutes. Beads were then incubated in rhodamine phalloidin for 20 minutes, washed once in DMEM, and then stained with DAPI for 15 minutes. Subsequently, beads were washed twice in DMEM and mounted onto glass slides using Prolong Antifade Gold Reagent (Life Technologies) and a cover slip. Each cover slip was sealed at the edges with clear nail polish. Cells in beads were imaged using an LSM 510 NLO confocal microscope (Carl Zeiss) with a 63x objective and excitation and emission settings of 543 and 554-707 nm, respectively. DAPI was imaged using a multiphoton laser at 750 nm.

6.3.7 Statistical Analysis

Data are represented as mean ± standard deviation. If necessary, data were normalized using the Box-Cox transformation [228] prior to statistical analysis. Data were analyzed using a One-way ANOVA and Tukey's post-hoc analysis in the General Linear Model in Minitab (Minitab Inc., State College, PA). When comparing cell circularity per bead among different groups, individual beads were nested within encapsulations. Values of $p<0.05$ were considered statistically significant.

6.4 Results

6.4.1 Characterization of Stable C2C12 Cells Encapsulated in RGD and Non-Adhesive Alginate Hydrogels

In order to determine the appropriate RGD-alginate matrix to allow for cell spreading in 3-D while maintaining bead integrity during culture and post-preservation, various bead preparations were tested (refer to Appendix D). Following these tests, it was determined that 3.5% oxidized, RGD-modified LVM (cross-linked with calcium) coated with 0.1% PLL was the appropriate matrix. Encapsulated Stable C2C12 cells were then evaluated in adhesive (RGD) vs. non-adhesive matrices (RGE/no peptide) to establish the importance of cell-matrix interactions for these cells in alginate and to determine the appropriate non-adhesive matrix for subsequent studies. Stable C2C12 cells were encapsulated in beads containing RGD, RGE or no peptide alginate and assessed over 4 days for cell morphology, bead integrity, and metabolic activity. As indicated in Figure 6.1, bead integrity was maintained over 4 days in culture. In addition, spreading was apparent in RGD but not RGE/no peptide groups on Days 1 and 4. Viable cells were present in all beads on Days 1 and 4, as apparent from LIVE/DEAD® images (data not shown).

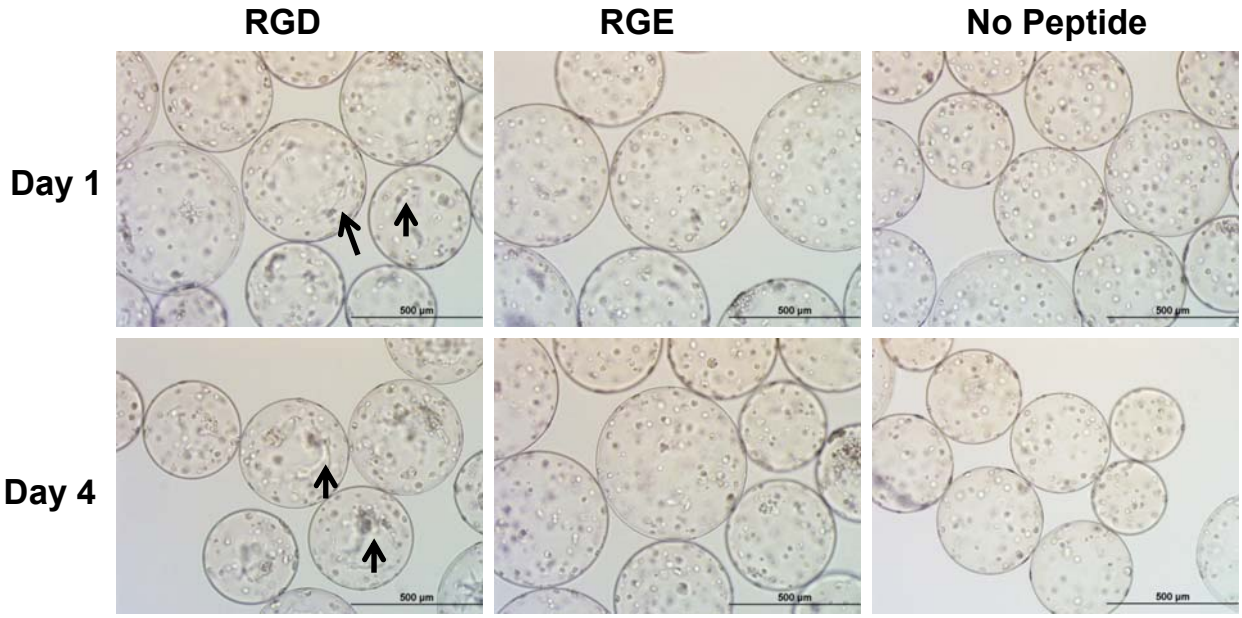

Figure 6.1 Representative light microscopy images (10x) of encapsulated Stable C2C12 cells cultured 1 and 4 days post-encapsulation in RGD/RGE/no peptide alginate hydrogels (10x). Arrows indicate spread cells. Scale bars represent 500 µm.

Figure 6.2 shows the metabolic activity over time for Stable C2C12 cells encapsulated in the different alginate hydrogels. Metabolic activity was maintained in cells encapsulated in RGD-modified alginate hydrogels from Day 1 to Day 4 ($p>0.05$), although there was a decline in metabolic activity for Stable C2C12 cells encapsulated in non-adhesive (RGE-modified and no peptide) alginates from Day 1 to Day 4 ($p<0.05$). Also, there was a decline in metabolic activity from Day 2 to Day 3 and from Day 2 to Day 4 for the RGE group ($p<0.05$). However, there was no difference between RGE and no peptide alginate groups at any given time point ($p>0.05$). On the basis of these results and the fact that an RGE-alginate matrix more closely resembles a RGD-matrix, RGE was selected as the appropriate non-adhesive control. The Stable C2C12 cells encapsulated in RGD-alginate had a higher metabolic activity compared to non-adhesive alginates from Day 2 onward ($p<0.05$).

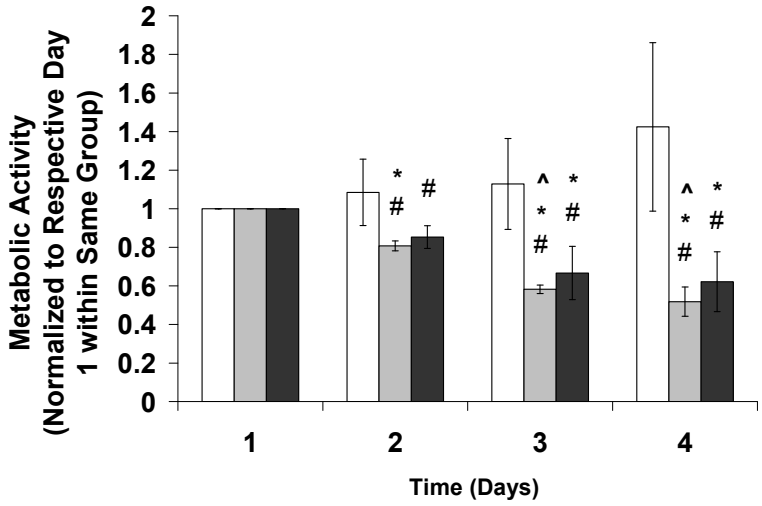

Figure 6.2 Metabolic activity over time for cells encapsulated in 3.5% RGD (white bars), RGE (light gray bars), and no peptide (dark gray bars) LVM alginate, and normalized to respective groups on Day 1. $^{\#}p<0.05$ compared to RGD group at same time point, *p<0.05 compared to Day 1 within same group. ^p<0.05 compared to same group on Day 2. *n=3-4*

6.4.2 Cryopreservation Effects on Stable C2C12 Cells Encapsulated in RGD vs. RGE-Alginate Hydrogels

In order to evaluate the effects of cell-matrix interactions on cellular response after cryopreservation, Stable C2C12 cells encapsulated in RGD and RGE-alginate, cryopreserved one day post-encapsulation, were compared up to one day post-warming. As shown in Figures 6.3A and 6.3B, there was no difference in metabolic activity (normalized to respective Fresh controls) for Stable C2C12 cells encapsulated in RGD or RGE-alginate hydrogels up to one day post-warming after either DPS-vitrification or conventional freezing, respectively. Similarly, Figures 6.3C and 6.3D indicate no difference in insulin secretion (normalized to Fresh controls) for Stable C2C12 cells encapsulated in RGD or RGE alginate-hydrogels, after cryopreservation. The average ISR values for the Fresh RGD group were 5.82 ±0.80 and 3.76 ±0.45 μU/(0.05 ml

beads*hr) at t0 and t1, respectively. The average ISR values for the Fresh RGE group were 4.79 ± 0.89 and 2.38 ± 0.67 μU/(0.05 ml beads*hr) at t0 and t1, respectively.

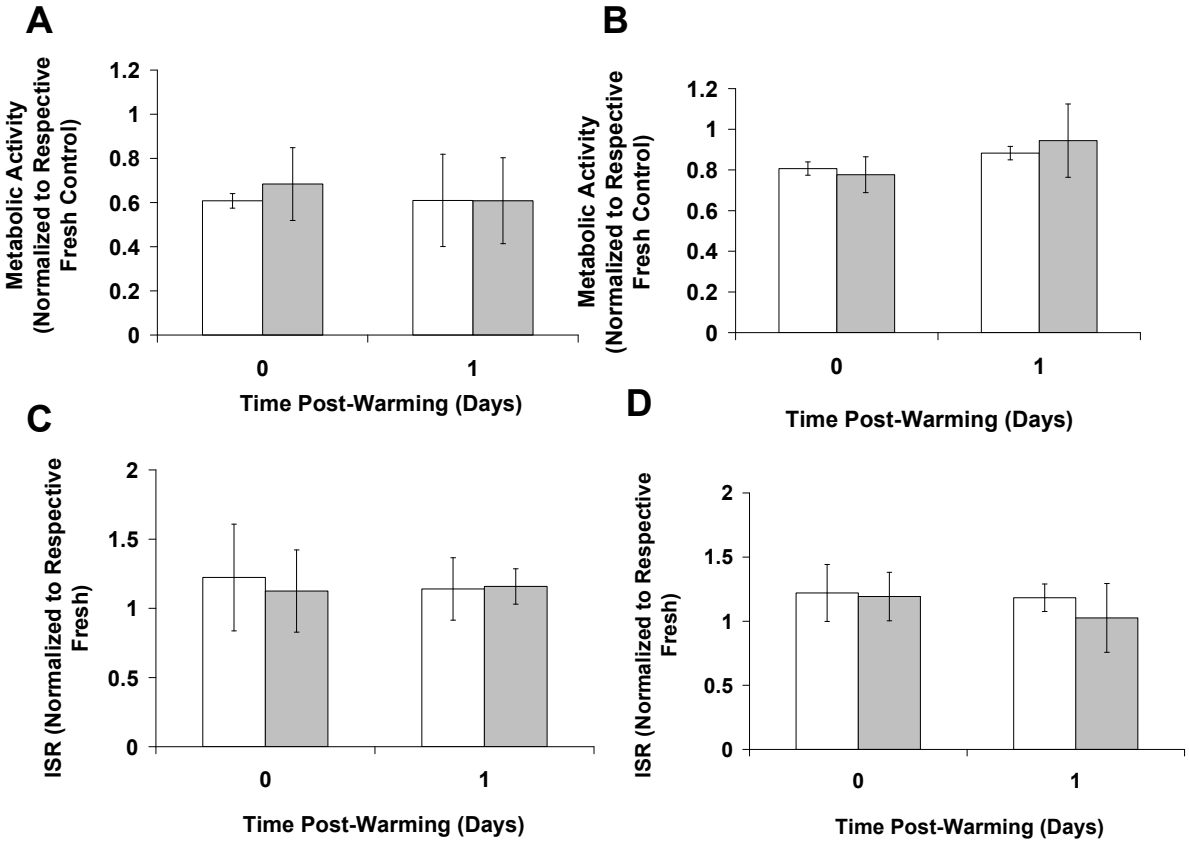

Figure 6.3 Cellular response to cryopreservation in adhesive (RGD, white bars) vs. non-adhesive (RGE, gray bars) alginate hydrogels in terms of A). metabolic activity-DPS-vitrified; B).metabolic activity-Frozen, C). insulin secretion rate (ISR)-DPS vitrified, and D). ISR-Frozen. Groups were normalized to their respective Fresh controls. *n=3-4*

6.4.3 Metabolic Activity in RGD-Alginate Hydrogels after 1 or 4 Days of Pre-Cryopreservation Culture

To determine the effect of cryopreservation and culture time pre-preservation on metabolic activity post-warming in RGD-alginate encapsulated Stable C2C12 cells, encapsulated cells were cryopreserved either 1 or 4 days post-encapsulation and assessed up to 3 days post-warming. Beads that were cultured for one day post-encapsulation and

subsequently cryopreserved are referred to as the "RGD C1" group, and beads cultured for 4 days prior to cryopreservation are referred to as the "RGD C4" group. As indicated in Figure 6.4A, there was no difference in metabolic activity between the Frozen group and the respective Fresh control at any time point assayed ($p>0.05$). However, the DPS-vitirifed group exhibited lower metabolic activity than the Fresh control immediately post-warming ($p<0.05$). Metabolic activity was maintained within the Cryopreserved groups and the Fresh control up to 3 days post-warming. With respect to the cells encapsulated and cultured 4 days prior to cryopreservation (RGD C4), Figure 6.4B indicates the DPS-vitrified group had lower metabolic activity compared to the respective Fresh control and the Frozen group immediately post-warming ($p<0.05$). There was no difference in metabolic activity between the Frozen and Fresh groups at any time point assayed for the RGD C4 group. Additionally, all groups exhibited an increase in metabolic activity from 0 to 3 days post-warming ($p<0.05$).

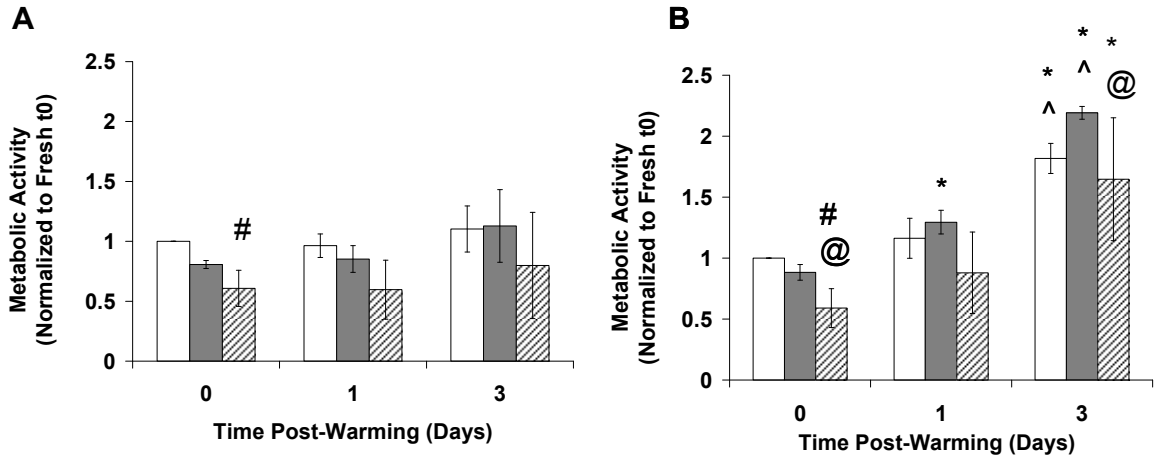

Figure 6.4 Metabolic activity in Fresh and Cryopreserved Stable C2C12 cells encapsulated in RGD-alginate hydrogels and cultured A).1 or B). 4 days post-encapsulation, prior to cryopreservation. All groups were normalized to the Fresh group at t0. The Fresh group is represented by the white bars, the Frozen group by the dark gray bars, and the DPS-vitrified group by the striped bars. *$p<0.05$ compared to same group at t0, ^$p<0.05$ compared to same group at one day post-warming, $^{\#}p<0.05$ compared to Fresh group at same time point, $^{@}p<0.05$ compared to Frozen group at same time point. *n=3*

6.4.4 Insulin Secretory Function Over Time After 1 or 4 Days of Pre-Cryopreservation Culture

To determine the effect of cryopreservation and culture time pre-preservation on insulin secretion post-warming in RGD-alginate encapsulated cells, encapsulated Stable C2C12 cells were cryopreserved either 1 (RGD C1) or 4 (RGD C4) days post-encapsulation and assessed up to 3 days post-warming. Figure 6.5A shows insulin secretory function from Fresh and Cryopreserved beads over time for the RGD C1 group (normalized to the Fresh t0 group) over time. There were no differences between the Fresh and Frozen group and Fresh and DPS-vitrified group at any time point assayed for the RGD C1 group ($p>0.05$). Additionally, insulin secretion decreased from immediately post-warming to one day post-warming for the Fresh control, with a slight increase from time 1 to 3 days post-warming ($p<0.05$). Figure 6.5B shows insulin secretion from the beads cryopreserved 4 days post-encapsulation (RGD C4), normalized to the Fresh t0 group. Overall, all groups exhibited an increase in normalized insulin secretion rate from immediately post-warming to 3 days post-warming and from one day post-warming to 3 days post-warming ($p<0.05$). The DPS group transiently had higher insulin secretion than the Fresh group immediately post-warming ($p<0.05$). Similar to the RGD C1 group, there were no differences in insulin secretion between the Fresh and Frozen groups at any time point analyzed. The average ISR values for the Fresh groups at t0 were 5.82 ± 0.80 and 4.26 ± 0.85 μU/(0.05 ml beads*hr) for RGD C1 and RGD C4, respectively.

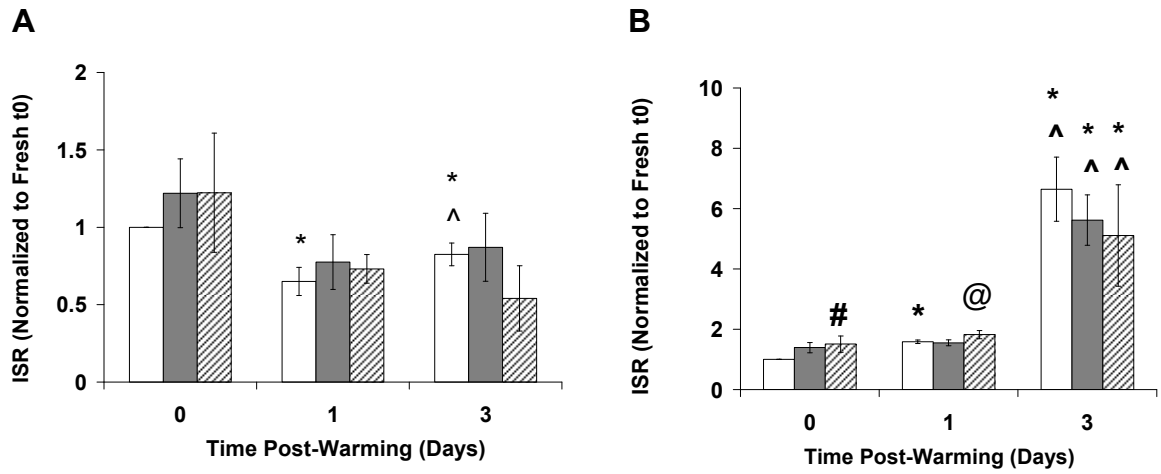

Figure 6.5 Cryopreservation effects on insulin secretory function of Stable C2C12 cells encapsulated in RGD-alginate hydrogels cultured A).1 or B). 4 days post-encapsulation, prior to cryopreservation. Cryopreserved groups and Fresh controls were assessed up to 3 days post-warming. All groups were normalized to the Fresh group at t0. The Fresh group is represented by the white bars, the Frozen group by the dark gray bars, and the DPS-vitrified group by the striped bars *$p<0.05$ compared to same group at t0, ^$p<0.05$ compared to same group at one day post-warming, $^{\#}p<0.05$ compared to Fresh group at same time point, $^{@}p<0.05$ compared to Frozen group at same time point. *n=3*

6.4.5 Direct Comparison of Pre-Cryopreservation Culture Time on Metabolic Activity and Insulin Secretion Post-Warming From RGD-Alginate Hydrogels

In order to more directly assess the effect of pre-culture time on cryopreservation response, the same data used in Figures 6.4 and 6.5 were re-analyzed with Cryopreserved groups normalized to the same day Fresh control, and cryopreservation responses from RGD C1 and RGD C4 groups at each respective time point were directly compared. Figures 6.6A and 6.6B show metabolic activity in DPS-vitrified and Frozen beads, respectively, up to three days post-warming (normalized to their respective, same day Fresh controls). Figures 6.6A and 6.6B show that there was no difference in cryopreservation response for the RGD C1 or RGD C4 group in terms of metabolic activity post-warming for the DPS-vitrified or Frozen beads, respectively. Figures 6.6C

and 6.6D show insulin secretory response post-warming for DPS-vitrified and Frozen beads cultured 1 day (RGD C1) or four days (RGD C4) prior to cryopreservation. Overall, beads cultured for 1 day or 4 days prior to cryopreservation had similar insulin secretion rates (normalized to respective Fresh controls). However, at one day post-warming, Frozen beads from the RGD C1 group exhibited higher normalized insulin secretion rates compared to the beads from the RGD C4 group ($p<0.05$).

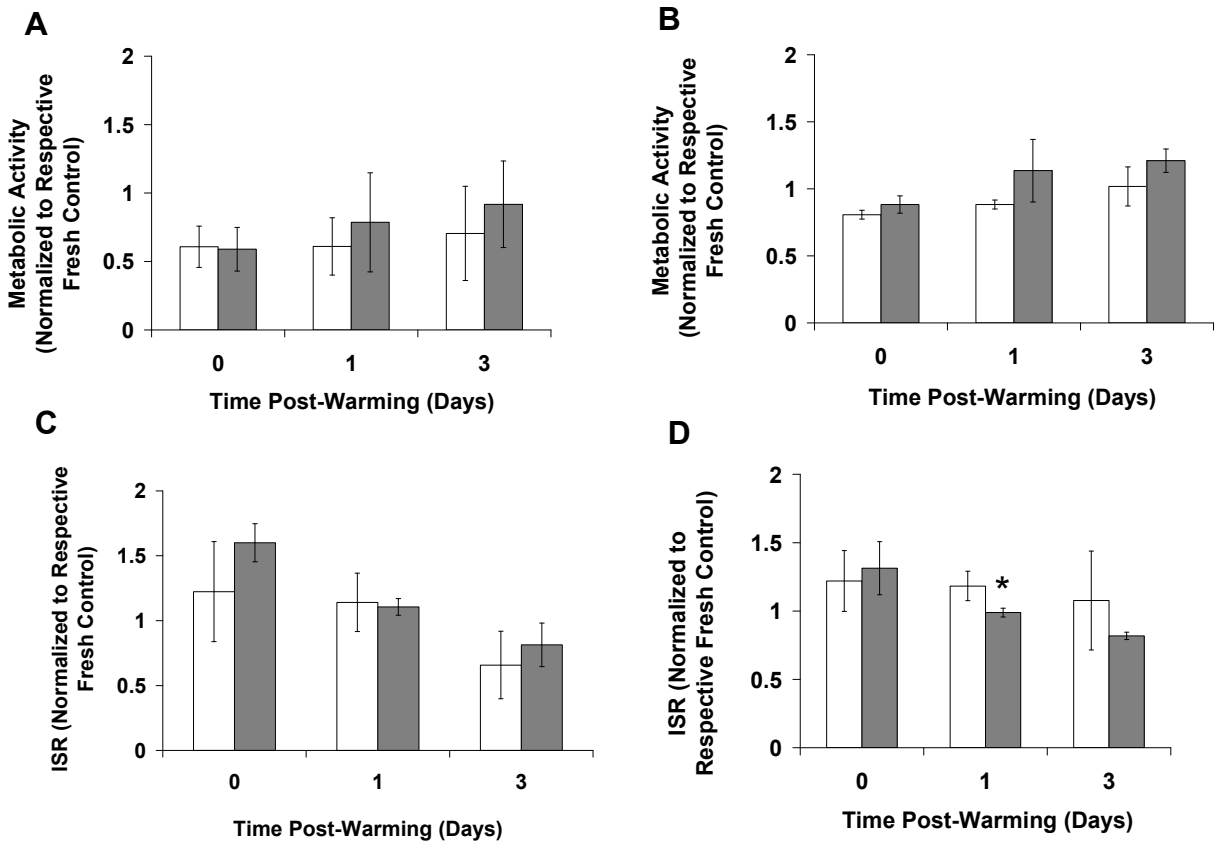

Figure 6.6 Effect of culture time prior to cryopreservation on Stable C2C12 cells encapsulated in RGD-alginate hydrogels and cultured for 1 (RGD C1-white bars) or 4 (RGD C4-gray bars) days prior to cryopreservation A). metabolic activity-DPS vitrified, B). metabolic activity-Frozen and C). ISR-DPS-vitrified and D). ISR-Frozen.*$p<0.05$ compared to the other group at same time point. *n=3*

6.4.6 LIVE/DEAD® Staining/Confocal Imaging and Image Analysis From Fresh and Cryopreserved Beads

To assess cell morphology and viability within the beads, LIVE/DEAD® staining and confocal imaging were performed one day post-warming for the RGD C1, RGD C4, and RGE groups. As indicated by representative images in Figure 6.7A, there was no extensive cell death present one day post-warming for the RGD C1 Cryopreserved beads when compared to the Fresh control. Additionally, some spreading was present in the beads. Figure 6.7B indicates that there was also no extensive cell death one day post-warming for the cryopreserved beads in the RGD C4 group. Although spreading was apparent in the RGD C4 group, there was some heterogeneity in cell morphology among beads. Figure 6.7C indicates that viable cells were present one day post-warming for all RGE groups. Overall, the cell morphology appeared rounded in the RGE-alginate beads.

Figure 6.8A shows the average and distribution of circularity values per bead from Fresh RGE, RGD C1, and RGD C4 beads. Cells encapsulated in the non-adhesive matrix, RGE, exhibited a higher cell circularity per bead (more rounded shape) compared to the cells in both RGD groups (RGD C1 and RGD C4) ($p<0.05$). In addition, cells in the RGD C4 beads exhibited a lower cell circularity per bead (more elongated shape) compared to both the RGE and the RGD C1 beads.

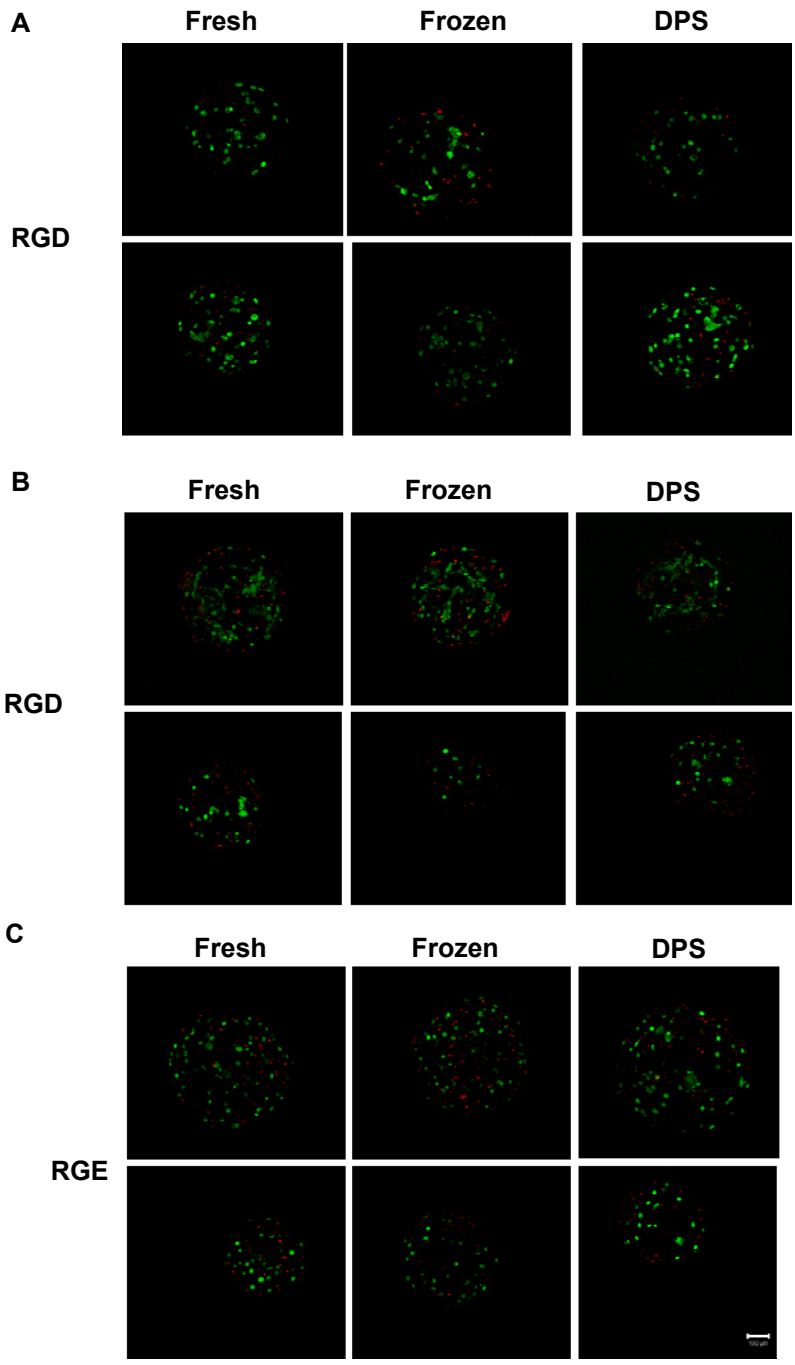

Figure 6.7 Representative LIVE/DEAD® images (10x) from 3-D projections of beads one day post-warming for Cryopreserved groups and respective Fresh controls for A). RGD C1, B). RGD C4, and C). RGE groups. Scale bar represents 100 µm.

Figures 6.8B and 6.8C indicate that for each of the RGD C1 and RGD C4 groups there was no difference in cell circularity per bead between the Cryopreserved groups and the Fresh controls. Figure 6.8D indicates that in the non-adhesive matrix, RGE, there was

no difference between the cell circularity per bead in the Fresh control and either Frozen or Vitrified groups ($p>0.05$). However, the DPS-vitrified group exhibited a higher cell circularity per bead compared to the Frozen group ($p<0.05$). In addition, when directly comparing cell circularity per bead in the Cryopreserved RGD C1 or RGD C4 groups, the beads in the RGD C4 group exhibited lower cell circularity per bead ($p<0.05$), indicating cells in those beads were more spread than cells in the cryopreserved beads from the RGD C1 group one day post-warming (data not shown).

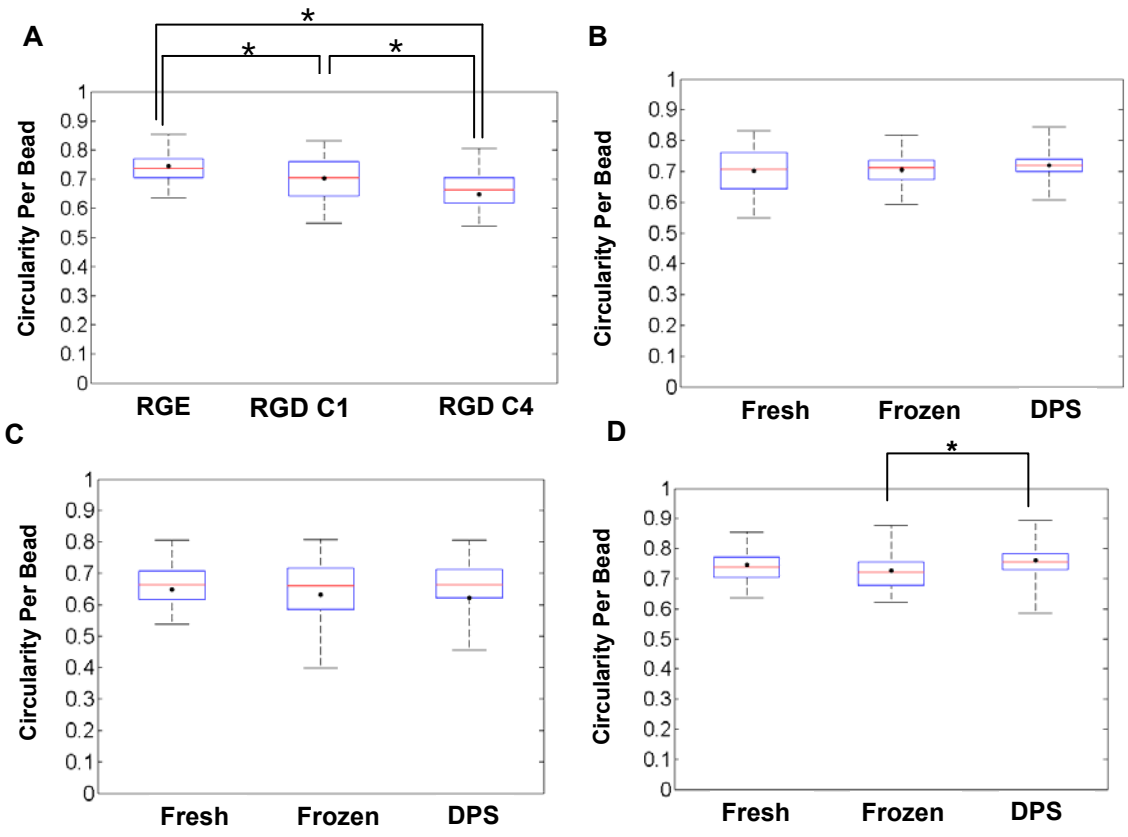

Figure 6.8 Box plots displaying circularity per bead for A). Fresh RGE, RGD C1 and RGD C4, B). RGD C1 Fresh and Cryopreserved, C). RGD C4 Fresh and Cryopreserved, and D). RGE Fresh and Cryopreserved groups. •average bead circularity for each group, and whiskers on each plot extend from minimum to maximum values of bead circularity within a given group. The red line represents the median and the bottom and top of each box represent the 25th and 75th percentile, respectively. *n=3* for 3 independent encapsulations/cryopreservations.Ten-20 beads per treatment were analyzed.

6.4.7 Bead Integrity Immediately Post-Warming

In order to assess bead integrity after cryopreservation, phase contrast light microscopy images were taken of Fresh and Cryopreserved beads. As indicated in Figure 6.9, overall bead integrity was maintained immediately post-warming in the Cryopreserved groups with respect to the Fresh controls. On average, fewer than 10% of the beads were broken for RGD C1, RGD C4, and RGE groups for both cryopreservation treatments and the Fresh control immediately post-warming. The percentage of broken beads was determined by counting beads in 6 independent fields of view for each group, and averages were taken from 2-3 independent experiments.

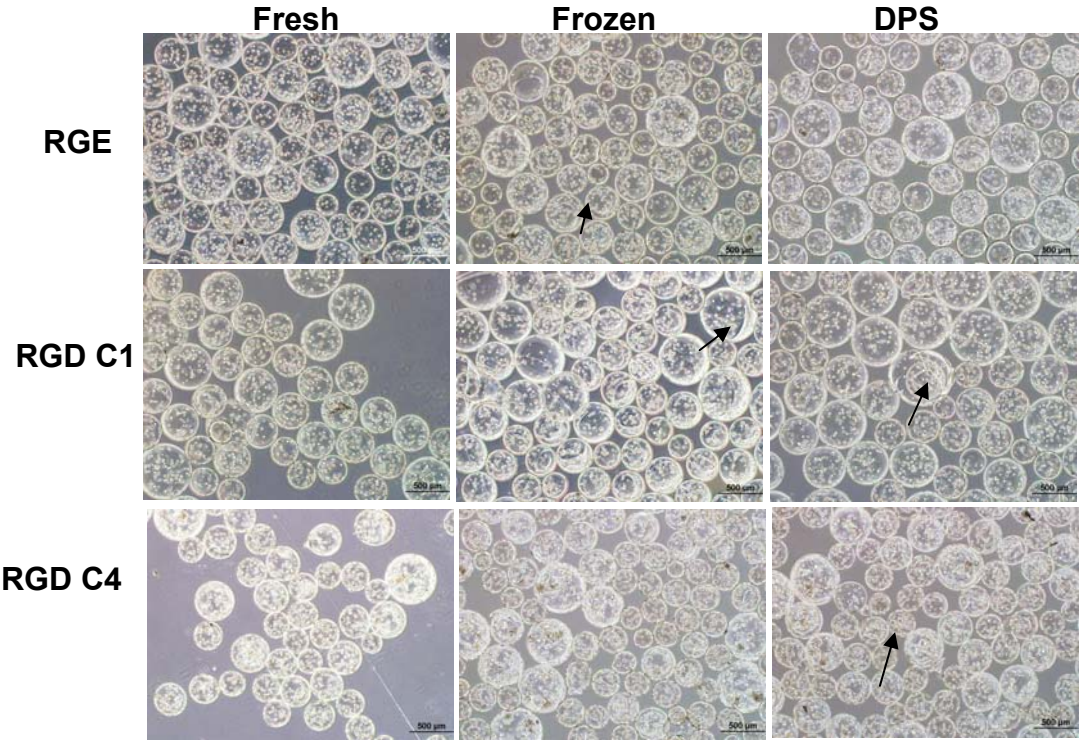

Figure 6.9. Representative phase contrast light micrographs (4x) of Cryopreserved beads and Fresh controls immediately post-warming. Arrows point to damaged beads. The scale bars represent 500 μm.

6.4.8 Actin/Nuclei Staining of Fresh RGD and RGE Beads at the Time of Cryopreservation

In order to assess cell morphology at the time of cryopreservation, Fresh beads from RGD C1, RGD C4, and RGE groups were stained for actin and counterstained with DAPI. Figure 6.10 shows representative confocal microscopy images of stained cells, and indicates that cells were overall rounded at the time of cryopreservation in the Fresh RGE group (Figure 6.10 E-F). Both adhesive groups (RGD C1 and RGD C4) exhibited more heterogeneity in cell morphology compared to the RGE group, with some spread cells as well as more rounded cells. Thus, elongated cells were present at the time of cryopreservation in the RGD-alginate groups, but not the RGE groups.

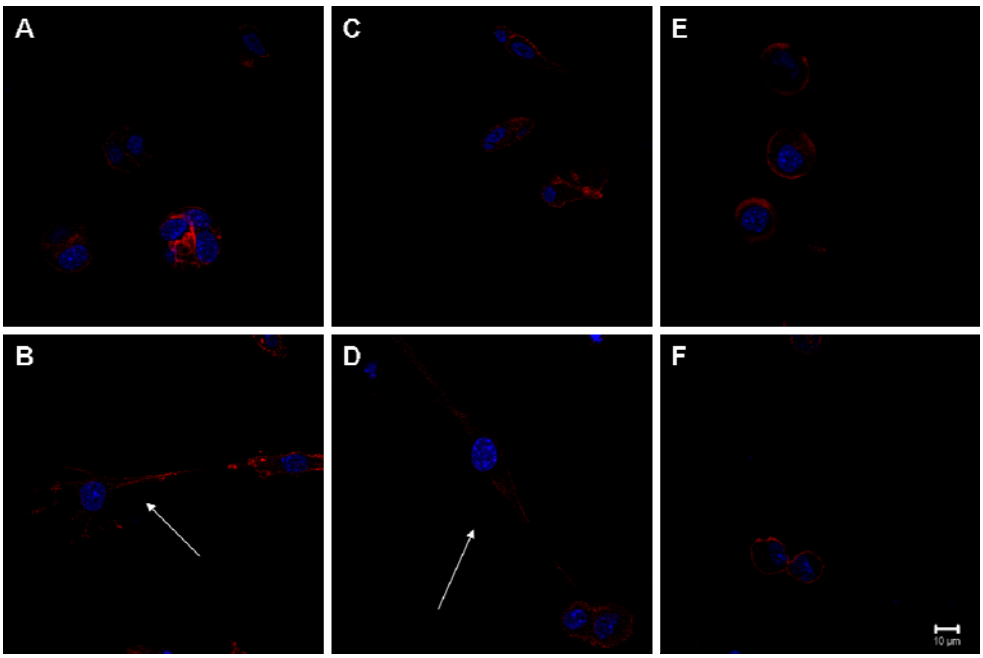

Figure 6.10 Representative confocal microscopy images (63x) of actin/nuclei stained encapsulated cells in Fresh RGD and RGE beads at the time of cryopreservation: A)-B). RGD C1, C)-D). RGD C4, E)-F). RGE. White arrows point to spread cells. Scale bar represents 10 um.

6.5 Discussion

Cryopreservation is important for clinical realization of tissue engineered constructs [5, 213]. Specifically, it is important to study cellular responses after exposure to different cryopreservation methods in a 3-D adhesive hydrogel environment, as cryopreservation with the added complexity of adhesion in 3-D may affect cellular response, but has not been extensively investigated. Indeed, studies have indicated that adhesion in 3-D may be beneficial for encapsulated insulin-secreting cells or islets [11, 12, 96], and may become necessary as different cell types are microencapsulated for a pancreatic substitute. Hydrogels containing the RGD adhesive peptide motif in particular have been used for encapsulation of a variety of cell types, including myoblasts [20, 103], bone marrow stromal cells [101], pre-osteoblasts [103], and human embryonic stem cells [104].

In this study, we have characterized cellular responses to cryopreservation in a 3-D adhesive RGD-alginate system, where cell-matrix interactions have been shown to be important for cell survival, as indicated by the comparison of metabolic activity over time for Stable C2C12 cells encapsulated in RGD vs. non-adhesive alginates. Specifically, the decline in metabolic activity for Stable C2C12 cells encapsulated in non-adhesive (RGE-modified and no peptide) alginate from Day 1 to Day 4, the higher metabolic activity in the RGD vs. non-adhesive hydrogels from Day 2 onward, and the maintenance of metabolic activity in the RGD-alginate beads from Day 1 to Day 4, all indicate that the encapsulated Stable C2C12 cells perform better in an adhesive environment at the given cell density used. Additionally, as there was no difference in metabolic activity between Stable C2C12 cells encapsulated in RGE and no peptide alginate hydrogels at any time

point assayed, there was likely no additional negative effect of incorporation of RGE into the alginate matrix. Due to the similarity in metabolic activity between RGE and no peptide alginates as well as RGE-alginate being a non-adhesive control closer in composition to an RGD-matrix, RGE-alginate was chosen as the non-adhesive control for subsequent cryopreservation experiments.

Although the Stable C2C12 cells used in this study perform better in an adhesive RGD-alginate matrix, as mentioned above, it is still important to understand how the presence of cell-matrix interactions affects cell response to cryopreservation in a 3-D hydrogel environment, as this information may be significant in helping to design strategies for cryopreservation of cells in 3-D hydrogels. Although recent evidence suggests that encapsulation in an adhesive matrix may result in higher viability compared to encapsulation in a non-adhesive matrix after freezing-warming [16], not all studies showing benefits of cryopreservation in adhesive matrices include a non-adhesive control to compare the effects of cryopreservation in non-adhesive vs. adhesive matrices [17]. A non-adhesive control would help in understanding if there is indeed an additional benefit to adhesion over encapsulation alone for cells, especially as encapsulation in a non-adhesive matrix has been shown to result in higher cell viability and reduction of apoptosis compared to cryopreservation of cells in suspension [229]. Additionally, no studies have simultaneously compared effects of both cryopreservation methods (i.e. vitrification and conventional freezing) in the context of adhesive vs. non-adhesive 3-D hydrogel environments. In the current study, early time points were chosen to assess the effect of cell-matrix interactions in 3-D, as the metabolic activity declined for cells encapsulated in non-adhesive alginates over time (Figure 6.2). As no differences in

insulin secretory response or metabolic activity (normalized to respective Fresh controls, Figure 6.3), were found after either freezing or vitrification up to one day post-warming, this indicated that the encapsulated cells responded similarly to both cryopreservation methods at early time points post-warming regardless of the presence of cell-matrix interactions. This is in contrast to Sambu et al.[16], who found that mouse embryonic stem cells encapsulated in RGD-functionalized alginate and subsequently frozen performed better in terms of viability and expression of the Oct-4 stem cell maker compared to cells encapsulated and frozen in non-adhesive alginate. However, the addition of adhesion in 3-D did not significantly improve all factors examined, as not all stem cell markers studied exhibited different expression levels after cryopreservation in unmodified alginate compared to RGD-functionalized alginate. Additionally, the authors did not include data from non-preserved controls, and thus were unable to account for possible differences in initial cell viability or physiological status prior to cryopreservation. Including data from the Fresh non-adhesive control is key, as we have shown that metabolic activity from cells in Fresh non-adhesive alginate beads is lower than that from cells in RGD-alginates (Figure 6.2).

Cell morphology was quantitatively assessed, via circularity measurements, after cryopreservation, as cell spreading of myoblasts encapsulated in partially oxidized, RGD-modified hydrogels has been associated with differentiation of and fusion of myoblasts into multinucleated myotubes [20]. For a model pancreatic substitute containing myoblasts, terminal differentiation of myoblasts and fusion into myotubes would be important prior to use *in vivo*, as this would prevent excessive cell growth after implantation. As expected, the circularity per bead for the Fresh RGE group was higher

than that for both the Fresh RGD-encapsulated groups. This is likely due to the inability of the cells to attach and subsequently spread in the RGE-functionalized matrix, as opposed to their ability to bind to the RGD-alginate. Soluble RGD peptide competition studies have indicated that C2C12 cells can bind in an RGD-specific manner to RGD-conjugated alginate [98, 99]. Additionally, the ability of C2C12 cells to bind to RGD-alginate is in accordance with the literature showing that myoblasts express integrins such as αvβ3[230-232] and αvβ1[231] that can bind to the RGD sequence [222].

Additionally, the cell circularity per bead was similar between the cryopreserved groups and the Fresh control for either the RGD groups or the RGE group one day post-warming. Although a quantitative measure of cell shape after cryopreservation in 3-D hydrogels is lacking in the literature, some studies have qualitatively assessed cell morphology after freezing and warming in collagen gels [225, 233]. Koebe et al. [225] reported that only approximately 30% of hepatocytes cultured in a collagen sandwich configuration and conventionally frozen had a morphology similar to CPA-treated, non-frozen controls 2 and 11 days post-warming. Teo et al. [233], showed that immediately after freezing-thawing, in addition to changes to the microstructure of the matrix, fibroblasts encapsulated in collagen matrices experienced damage to cellular extensions as well as cell detachment, indicating damage to cell-matrix adhesions. Differences in cell morphology may not have been seen in the current study, as we examined morphology one day post-warming, allowing for possible recovery of changes present immediately post-warming. Additionally, cell morphology may have been better maintained in the RGD-alginate as opposed to previous studies with cells encapsulated and cryopreserved in collagen gels, as stresses formed during the cryopreservation

procedure, such as ice formation and mechanical deformation during freezing, may have affected the RGD peptides to a smaller extent than collagen fibrils in the collagen matrix. Freezing has been shown to affect the matrix structure of collagen gels, specifically by increasing the mean void area, or porosity, of the matrix [233]. Similarly, the structure of collagen fibers from heart valve tissue has also been shown to be damaged after freezing and to a smaller extent by vitrification [234, 235]. Since we did not use a gel consisting of a structural protein, but rather a polysaccharide conjugated with a small peptide, the damage to the peptide itself after freezing or vitrification may be less than that to a gel containing a dense extracellular matrix protein structure. Another plausible reason for the maintenance in cell morphology in the current study, especially after freezing, is the possible decrease in ice formation. Indeed, polysaccharide gels such as dextran [236] and alginate [237] have been shown to reduce ice crystallization during cryopreservation. As such, encapsulation in alginate has been shown to better maintain morphology of cell clusters including islets [37] and neurospheres [42] after conventional freezing compared to non-encapsulated controls. The maintenance of cell morphology and bead integrity may have also been an important factor in preserving metabolic activity and insulin secretion from the Cryopreserved encapsulated Stable C2C12 cells in this study.

It is important to note that developing a 3-D hydrogel system that allowed for cell spreading in 3-D, while maintaining bead integrity in culture and after cryopreservation, was challenging. This was due to the requirement for cell spreading (likely due to less hydrogel resistance and/or decreased stiffness) in the matrix, while still having the beads robust enough to survive both methods of cryopreservation. After various preparations were tested (refer to Appendix D), it was determined that 3.5% oxidized RGD-LVM,

cross-linked with Ca^{2+} and coated with 0.1% PLL and unmodified alginate was the appropriate matrix to allow for both cell spreading and maintenance of bead integrity during culture and cryopreservation. Although there were some broken beads present immediately post-warming in the current experiments (less than 10%), the cause of the bead breakage is currently unclear. One possibility may be due in part to the agitation of the beads in the cell strainer during the CPA addition and removal procedure.

Importantly, we examined cryopreservation response in RGD-alginate hydrogels up to 3 days post-warming, to account for recovery over time and because results immediately post-thaw may give overestimates of cell viability due to delayed-onset cell death after cryopreservation [238]. As the metabolic activity for the DPS-vitrified group was lower than Fresh immediately post-warming ($p<0.05$), and there were no differences in metabolic activity between Fresh and Frozen constructs, metabolic activity was maintained throughout the study specifically in Frozen constructs. Overall, insulin secretion rate was also maintained in Frozen constructs. Additionally, we saw no difference in ISR between Fresh and Cryopreserved groups from the RGE-alginate encapsulated cells immediately post-warming (data not shown). This is in contrast to Murua et al. [44], who saw a 42% decrease in erythropoietin secretion, compared to the Fresh control, after freezing stably transfected C2C12 cells encapsulated in alginate-poly-L-lysine-alginate beads. However, the alginate type and freezing protocol used were different than those used in the current procedure, which may have contributed to the reduced secretion.

Interestingly, when directly comparing cryopreservation response for RGD-containing beads cultured one day (RGD C1) vs. four days (RGD C4) post-encapsulation

prior to cryopreservation (Figure 6.6), no differences were seen in metabolic activity or insulin secretion, except for a small difference in insulin secretion between RGD C1 and RGD C4 groups for the Frozen beads one day post-warming. Although the cell circularity per bead was lower for the cryopreserved RGD C4 groups compared to the cryopreserved RGD C1 groups one day post-warming (data not shown), they overall responded similarly to both cryopreservation methods in terms of metabolic activity, with a slight difference in insulin secretion for the Frozen group. Koebe et al. found a higher survival rate, better recovery, and greater albumin secretion for encapsulated rat hepatocytes cultured 7 or 11 days prior to freezing compared to constructs cultured only 3 days prior to cryopreservation. Additionally, Ji et al. [17] found that cryopreserving adherent human embryonic stem cell colonies 24 hours after placement of a top matrigel layer led to a higher viability compared to colonies that were cryopreserved only one hour after placement of the matrigel layer. However, no differences in viability were seen between the groups that were cryopreserved 24 hours after matrigel layer placement on top of cells and those that were cryopreserved 48 hours after matrigel layer placement [17]. Although we possibly may have seen a difference in cryopreservation response if we had waited longer than 4 days post-encapsulation to cryopreserve the RGD-alginate beads, large cell clusters were seen in beads at later time points (data not shown), leading to increased cell-cell interactions. This was undesirable in the current study, as the overall focus was on the effect of cell-matrix interactions more than cell-cell interactions on cryopreservation response.

6.6 Conclusions

In summary, at early time points post-warming, the presence of cell-matrix interactions did not affect cryopreservation response with respect to metabolic activity or insulin secretion after vitrification or freezing. Furthermore, when directly comparing the effect of pre-preservation culture period on RGD-alginate encapsulated Stable C2C12 cell response post-warming, there was no difference in metabolic activity or ISR, except for slightly higher ISR one day post-warming from the Frozen group cultured one day pre-preservation. Up to 3 days post-warming, metabolic activity and ISR from Frozen RGD-alginate encapsulated cells were maintained relative to Fresh controls, irrespective of one or four-day pre-preservation culture period. In spite of a transient decrease immediately post-warming, metabolic activity in DPS-vitrified RGD-alginate encapsulated cells was similar to Fresh controls up to 3 days post-warming, regardless of pre-preservation culture period. Insulin secretion rate from DPS-vitrified encapsulated Stable C2C12 cells was also similar to Fresh controls, except for a transient increase immediately post-warming in 4-day pre-preservation cultured encapsulated cells. Although differences were seen between Fresh RGD C1, RGD C4, and RGE groups, cell circularity per bead was maintained one day post-warming, respective to Fresh controls, after both freezing and vitrification in each type of alginate matrix. Except for differences immediately post-warming in metabolic activity and insulin secretion rate relative to Fresh controls for the DPS-vitrified group, overall, conventional freezing and DPS-vitrification maintain metabolic activity, insulin secretion rate, and cell morphology for Stable C2C12 cells encapsulated in RGD-alginate hydrogels. Due to simplicity of procedure and slightly superior results compared to vitrification, freezing appears

appropriate for cryopreservation of Stable C2C12 cells encapsulated in a partially oxidized, adhesive RGD-alginate matrix.

CHAPTER 7

CONCLUSIONS AND FUTURE DIRECTIONS

7.1 Conclusions

A tissue engineered pancreatic substitute consisting of insulin-secreting cells encapsulated in alginate hydrogels may provide more physiologic control of blood glucose levels compared to exogenous insulin therapy. For clinical translation of such a pancreatic substitute, long-term storage is critical, and cryopreservation is the most promising means of preservation. In particular, the two main cryopreservation methods that may be employed are conventional freezing and vitrification (ice-free cryopreservation). Although not necessarily damaging to single cells in suspension, ice formation during conventional freezing may be detrimental to a 3-D construct. Additionally, the high concentrations of cryoprotectants necessary for vitrification may lead to cell osmotic excursions as well as cytotoxicity. Thus, both cryopreservation methods must be carefully evaluated in determining the appropriate method of preservation for a pancreatic substitute consisting of insulin-secreting cells encapsulated in alginate hydrogels.

As different cell types are being explored for use in pancreatic substitutes, different requirements for anchorage-dependence in 3-D may become necessary upon encapsulation. Cell-matrix interactions are important for various processes, including cell survival, proliferation, and differentiation [221]. Indeed, recent studies have indicated the importance of adhesion in 3-D for encapsulated insulin-secreting cells [11, 12, 96]. Thus, it is important to study the effect of cryopreservation on cells encapsulated in non-

adhesive vs. adhesive alginate hydrogel environments. Therefore, we investigated the effects of both conventional freezing and vitrification on βTC-tet cells encapsulated in unmodified alginate, a model pancreatic substitute containing cells that have been shown to proliferate and function in a non-adhesive environment [18, 19]. Additionally, we investigated the effects of conventional freezing and vitrification on C2C12 cells, stably transfected to secrete insulin, encapsulated in RGD-modified, partially oxidized alginate. Stable C2C12 cells were encapsulated in an adhesive matrix, as C2C12 cells have been shown to proliferate and differentiate in an adhesive 3-D RGD-alginate environment [20].

In CHAPTER 4 of this thesis, the appropriate parameters and procedures for ^{13}C labeling, extraction, and isotopomer analysis from Fresh and Cryopreserved encapsulated βTC-tet cells were established. A volume of 6 ml of Fresh beads encapsulated at $7x10^7$ cells/ml was found to be appropriate for obtaining sufficient SNR in the NMR spectrum. Additionally, a pseudo isotopomer steady state was achieved at the 6 hour incubation period in the labeling medium. To interpret ^{13}C NMR-derived isotopomer patterns, a previously published model with a second non-pyruvate carboxylase anaplerotic entrance to the TCA cycle was found to represent the experimental data well. Using these established parameters and procedures, relative metabolic fluxes were determined in CHAPTER 5.

In CHAPTER 5 of this thesis, cryopreservation effects on intermediary metabolism in encapsulated βTC-tet cells were investigated using ^{13}C NMR and isotopomer analysis. Post-warming, secretory function after glucose and high K^+ induced secretion was studied from Frozen and DPS-vitrified beads. Relative carbon flow through the TCA cycle-associated pathways studied was found to be maintained after both

conventional freezing and vitrification. Although insulin secretory function was maintained in Conventionally Frozen constructs during the extraction experiments, it was impaired in the DPS-vitrified constructs. As a similar trend in decreased insulin secretion compared to Fresh controls was found in DPS-vitrified beads upon performing a small-scale GSIS test, with beads from a single cryopreservation batch, the scale-up of the vitrification procedure necessary for the extractions did not cause the decrease in insulin secretion. Upon exposure to high K^+, DPS-vitrified constructs secreted significantly less insulin compared to Fresh controls, although secretion from Frozen constructs was comparable to Fresh. Intracellular insulin content measured prior to depolarization was similar in Cryopreserved groups compared to Fresh controls. As DPS-vitrified beads exhibited reduced insulin secretion upon depolarization with high K^+ compared to Fresh controls, similar stimulation indices for glucose and high K^+ -induced insulin secretion, and similar intracellular insulin content to Fresh controls prior to depolarization, this indicates a possible defect in the late-stage insulin secretion/exocytosis machinery in these encapsulated cells.

In CHAPTER 6 of this thesis, Stable C2C12 cells were encapsulated in RGD and RGE-alginate hydrogels, cryopreserved, and assessed up to one day post-warming to examine the effect of cell-matrix interactions on cryopreservation response in terms of metabolic activity and insulin secretion. To address the longer-term response of Stable C2C12 cells encapsulated in an adhesive alginate environment, Stable C2C12 cells were encapsulated in RGD-alginate hydrogels, cultured either 1 or 4 days post-encapsulation, cryopreserved, and assessed up to 3 days post-warming. As myoblast spreading in partially oxidized, RGD-modified hydrogels has been associated with myoblast

differentiation and fusion into myotubes [20], and myoblast differentiation would be optimal for a pancreatic substitute prior to *in vivo* implantation, cell circularity in beads was also assessed after cryopreservation. Regardless of cryopreservation method, the presence of cell-matrix interactions did not affect the cellular response with respect to metabolic activity or insulin secretion at early time points post-warming. Direct comparison of pre-preservation culture time on cellular response post-warming indicated similar insulin secretion and metabolic activity for RGD-alginate encapsulated Stable C2C12 cells, except for a difference in ISR one day post-warming from the Frozen group cultured one day prior to preservation. Irrespective of one or four-day pre-preservation culture period, metabolic activity and ISR from Frozen RGD-alginate encapsulated Stable C2C12 cells were maintained relative to Fresh controls, up to 3 days post-warming. Except for a decrease immediately post-warming, metabolic activity in DPS-vitrified RGD-alginate encapsulated Stable C2C12 cells was maintained relative to Fresh controls up to 3 days post-warming, regardless of pre-preservation culture period. In addition, the insulin secretion rate from DPS-vitrified Stable C2C12 cells encapsulated in RGD-alginate was maintained relative to Fresh controls, except for an increase immediately post-warming in encapsulated cells that were cultured 4 days prior to cryopreservation. In terms of cell morphology, cell circularity per bead was maintained one day post-warming for cells cryopreserved in RGD-alginate hydrogels cultured either 1 or 4 days pre-preservation as well as RGE-encapsulated and Cryopreserved Stable C2C12 cells, relative to Fresh controls. Overall, both methods preserved metabolic activity, secretory function, and bead integrity, with freezing producing slightly superior outcomes.

In summary, the work in this thesis indicates that conventional freezing can be used to successfully cryopreserve and maintain intermediary metabolism and secretory function post-warming in βTC-tet cells encapsulated in unmodified alginate. Although intermediary metabolism is maintained in vitrified encapsulated βTC-tet cells, insulin secretory function in response to glucose and K^+-induced secretion is impaired. In addition, conventional freezing maintains metabolic activity, insulin secretory function, and cell morphology in Stable C2C12 cells encapsulated in partially oxidized, RGD-modified alginate. Although vitrification results in differences immediately post-warming in metabolic activity and insulin secretion, overall, metabolic activity, insulin secretory function, and cell morphology are maintained post-warming after vitrification for Stable C2C12 cells encapsulated in RGD-modified alginate hydrogels.

7.2 Future Directions

7.2.1 Cryopreservation Effects on Insulin Secretion from Vitrified Encapsulated βTC-tet Cells

Although results from CHAPTER 5 indicate that conventional freezing successfully maintains intermediary metabolism, as measured by ^{13}C NMR and isotopomer analysis, as well as glucose-stimulated and depolarization-induced insulin secretion from encapsulated βTC-tet cells, further investigation into the effects of vitrification on insulin secretion is still warranted, as vitrification may be beneficial for more complex systems such as encapsulated islets. Additionally, vitrification may be important for encapsulated insulin-secreting cell systems where the biomaterial

component may be damaged by conventional freezing, as has been shown previously for encapsulated islets [25] and beta cells [22].

Although glucose-stimulated as well as depolarization-induced insulin secretory function were affected immediately post-warming in the Vitrified beads, it is not clear if incubation for a longer time at 37^{o}C post-warming would allow for recovery of secretory function from the encapsulated cells. Indeed, the insulin secretory response 24 hours post-warming has been shown to be different than that obtained within 2 hours post-warming for Frozen and Vitrified islets in culture [239]. Thus, the Vitrified beads could be incubated for various periods immediately post-warming, such as 4-24 hours, prior to performing a glucose-stimulated or K^{+} induced depolarization/exocytosis test. If even after extended incubation at 37^{o}C the depolarization/exocytosis response is still impaired, further investigation into the mechanism responsible for the impaired secretion would be warranted.

As cryoprotectants alone have been shown to exhibit toxicity towards cells [163] and higher cryoprotectant concentrations are used in vitrification compared to freezing, an important test would be to see if the CPA addition/removal process itself affects insulin secretion from encapsulated βTC-tet cells. Cryoprotectants alone, for example, have been shown to cause reduced enzyme activity possibly due to denaturing of proteins [240] in addition to affecting the cytoskeletal network [241, 242]. Thus, it may be possible that affecting protein structure or activity may lead to problems with proper ion transport in channels and/or that cytoskeletal disruption may affect processes such as secretory granule transport. If CPA addition/removal does not impair secretion, then the cooling and warming steps of vitrification should be added and subsequent tests, as

described below, should be performed. If, however, secretion is impaired after just adding and removing CPAs, then areas in the insulin secretion pathway as well as their respective tests, as described below, should be examined after only CPA addition/removal.

One of the first steps in elucidating vitrification-induced secretion defects would involve determining if there is indeed an increase in intracellular calcium concentration after membrane depolarization by exposure to high K^+. A previous study has indicated impaired response to depolarization after high K^+ exposure in cryopreserved cells, where the rise in intracellular calcium was three times lower compared to fresh cells [209]. One method that could be used to assess this would be by loading vitrified beads post-warming with a fluorescent calcium indicator, such as fluo-4 AM, and then exposing the beads to a high concentration of K^+ to artificially induced membrane depolarization. Subsequently the change in intracellular calcium would be monitored by imaging the beads over time after K^+ exposure with confocal microscopy [209]. If there is impairment in the rise of intracellular calcium subsequent to addition of a high concentration of K^+, then steps upstream of the increase in intracellular calcium concentration should be investigated, such as the ability of the plasma membrane to depolarize or the opening of the voltage-gated calcium channels. The change in membrane potential after depolarization in the vitrified beta cells can be measured to see if membrane depolarization is actually occurring. Although exocytosis studies have been performed on beta cells from Conventionally Frozen free islets [243, 244], information from Vitrified islets is lacking in the literature.

If indeed the intracellular calcium concentration does increase, in spite of the reduced insulin secretion after high K^+ exposure, a further area of investigation could be the movement of the secretory granules to the plasma membrane or the process of fusion of secretory granules with the plasma membrane. The cellular cytoskeletal organization is important for glucose-stimulated insulin secretion in the beta cell [245, 246], and cryoprotectants have been shown to affect the cytoskeleton [241, 242]. For example, evidence in the literature suggests that cryoprotectants can affect the integrity of the microtubule network [242, 247, 248], and in the beta cell this could potentially affect recruitment of secretory granules from the various pools within the cytosol to the plasma membrane prior to fusion and exocytosis. This would be applicable for longer-term secretion from encapsulated beta cells as initial insulin release is likely due to fusion of secretory vesicles that are near the plasma membrane and likely not those that are located in the reserve pool that may need to be transported to the plasma membrane. Cytoskeletal integrity would likely be more affected by vitrification as opposed to conventional freezing, as higher concentrations of cryoprotectants are used for vitrification.

7.2.2 Cryopreservation Effects on Intermediary Metabolism in Encapsulated Islets

In addition, future metabolic studies can be performed on encapsulated islets as opposed to encapsulated insulinoma cells, as encapsulated islets represent a more clinically relevant system. As previous studies of freezing and vitrification of encapsulated islets have indicated impaired insulin secretion post-warming [24, 25, 53], determining the effect of cryopreservation on the metabolism of the viable cells in the islets would be beneficial in understanding how cryopreservation affects fundamental

processes in GSIS in encapsulated islets. However, obtaining a sufficient signal-to-noise ratio may be challenging, as a previous ^{13}C NMR and isotopomer analysis study indicated lower SNR in the ^{13}C NMR spectrum obtained from porcine islets compared to spectra obtained from insulinoma cells [36]. Possible methods to increase signal-to-noise ratio in the NMR spectrum include using a higher field strength NMR magnet than that used in CHAPTER 5 (11.7 T) or a cryoprobe.

7.2.3 Examination of First and Second Phases of Insulin Secretion to Measure Dynamic Insulin Secretory Response Post-Preservation

Although the static insulin secretory response from encapsulated βTC-tet cells was evaluated in CHAPTER 4 of this thesis, the dynamic response would provide real-time insulin secretory kinetics and better provide a response that mimics *in vivo* conditions. A single-pass perfusion system could be used to determine the effect of cryopreservation on different phases of the insulin secretory response [249]. This could be especially useful in elucidating if any particular phase of the insulin secretory response is affected post-vitrification.

7.2.4 Effects of Longer-Term Culture of Encapsulated βTC-tet cells on the Cryopreservation Outcome

As evidence in the literature has suggested differences in cell survival and function depending on culture period pre-cryopreservation for cells encapsulated under [17] or within hydrogels [225], it would be beneficial to understand how cell response is affected by culture time of encapsulated βTC-tet cells prior to cryopreservation. Although

in CHAPTER 5 freezing was found to be appropriate for cryopreservation of encapsulated βTC-tet cells cultured overnight prior to cryopreservation, changes such as the formation of cell clusters and deposition of a more dense extracellular matrix may render cells more susceptible to ice formation. In a broader application sense, it is also important to study cryopreservation response at different time points after encapsulation to find the ideal time of culture prior to cryopreservation for long-term storage at an industrial facility.

7.2.5 Cryopreservation of Encapsulated Islets

Although encapsulated βTC-tet cells represent an appropriate model pancreatic substitute for animal studies, encapsulated islets would represent a more clinically relevant system. Although studies with Conventionally Frozen alginate-poly-L-lysine-alginate (APA) encapsulated islets have indicated glucose responsiveness *in vitro* and *in vivo* with reversal of hyperglycemia in rodent models [37, 53], the presence of the PLL layer may elicit an inflammatory response [82], leading to possible failure of the implant. Thus, islets encapsulated in barium alginate may represent a more biocompatible system, compared to APA-encapsulated islets. Although implantation of Conventionally Frozen barium alginate encapsulated rat islets resulted in restoration of normoglycemia in a diabetic rat model [52], investigation into other islet species, such as porcine, encapsulated in barium alginate, is still warranted. Encapsulated porcine islets are promising as potential pancreatic substitutes, as porcine insulin is similar to human insulin, and the porcine islet supply is ample. Evidence suggests that APA-encapsulated porcine islets may be more prone to damage after freezing compared to APA-

encapsulated rat islets [37, 53], in spite of using the same freezing procedure, indicating that encapsulated islet response to cryopreservation protocols can be species-specific [37, 53]. This would also warrant investigations of vitrification of encapsulated porcine islets.

7.2.6 Long-Term Storage of Encapsulated Insulin-Secreting Cells

The studies in this thesis have evaluated cryopreservation effects on encapsulated cells stored overnight prior to warming. Although metabolic processes should be halted below temperatures of -130^{o}C, it would be important to see how long-term storage (i.e. weeks, months, years) affects cellular response, as not many studies have compared the effect of storage time from different cryopreservation methods. This is particularly important for the Vitrified samples, as maintaining glass stability is important for long-term storage. Reports in the literature vary from days, months, and even up to a year in long-term storage, but often only examine one type of cryopreservation method. Studies examining insulin secretion and viability from encapsulated insulin-secreting cells for time scales of days to a year would help in understanding how long microencapsulated cells can be stored without any major effects on cell viability or function.

7.2.7 Effects of Cryopreservation on Encapsulated Differentiated Myoblasts

In order to use the encapsulated myoblasts *in vivo*, it would be beneficial to differentiate them prior to implantation to prevent excessive cell growth. Thus, it would be important to investigate the effects of cryopreservation on insulin secretion from myotubes derived from differentiation of myoblasts in RGD-alginate hydrogels; indeed,

myotubes may respond differently to cryopreservation as compared to undifferentiated myoblasts.

APPENDICES

APPENDIX A

PRELIMINARY CRYOPROTECTANT (CPA) ADDITION/REMOVAL AND VITRIFICATION STUDIES FROM ENCAPSULATED βTC-TET CELLS

In order to determine the appropriate cryopreservation solution for vitrification, various pre-formulated cryoprotectant (CPA) solutions were tested on encapsulated βTC-tet cells. Baseline protocols for addition and removal of CPAs were created using a previously developed math model [28]. CPAs were added and removed in a stepwise fashion at 4^{o}C and 22^{o}C, respectively, from βTC-tet cells encapsulated at 3x10^{7} cells/ml in 500-600 μm calcium alginate beads. The following solutions were tested: 7 M 1,2 propanediol (PD), VS55 (3.1 M dimethylsulfoxide (DMSO), 3.1 M formamide, 2.2 M PD), PEG 400 (5 M PD, 1 M DMSO, 12% PEG 400), DP6 (3 M DMSO, 3 M PD) + 0.3 M sucrose, 5.5 M PD + 1 M sucrose. The CPA-treated groups were compared to the carrier solution 1X EuroCollins and the Fresh control.

Post-treatment, beads were cultured for 3 days and assayed immediately post-treatment (day 0) and at days 1 and 3 for metabolic activity using alamarBlue® at each time point. For the alamarBlue® incubation, 100 μl of alamarBlue® stock solution was added to 0.1 ml beads and 1 ml fully supplemented DMEM. Beads were subsequently incubated at 37^{o}C for 3 hours prior to reading fluorescence (Excitation: 544 nm/Emission: 590 nm). As indicated in Figure A.1, the DP6+0.3 M sucrose group was comparable to Fresh and 1X EC at every time point ($p>0.05$). The PEG400 group was

similar to 1X EC at all time points ($p>0.05$). Recovery was apparent, and all groups exhibited an increase in metabolic activity and were comparable to Fresh on Day 3 ($p>0.05$). Based on these results, two solutions, PEG400 and DP6 + 0.3 M sucrose, were chosen as the top two solutions in terms of metabolic activity after CPA addition/removal studies.

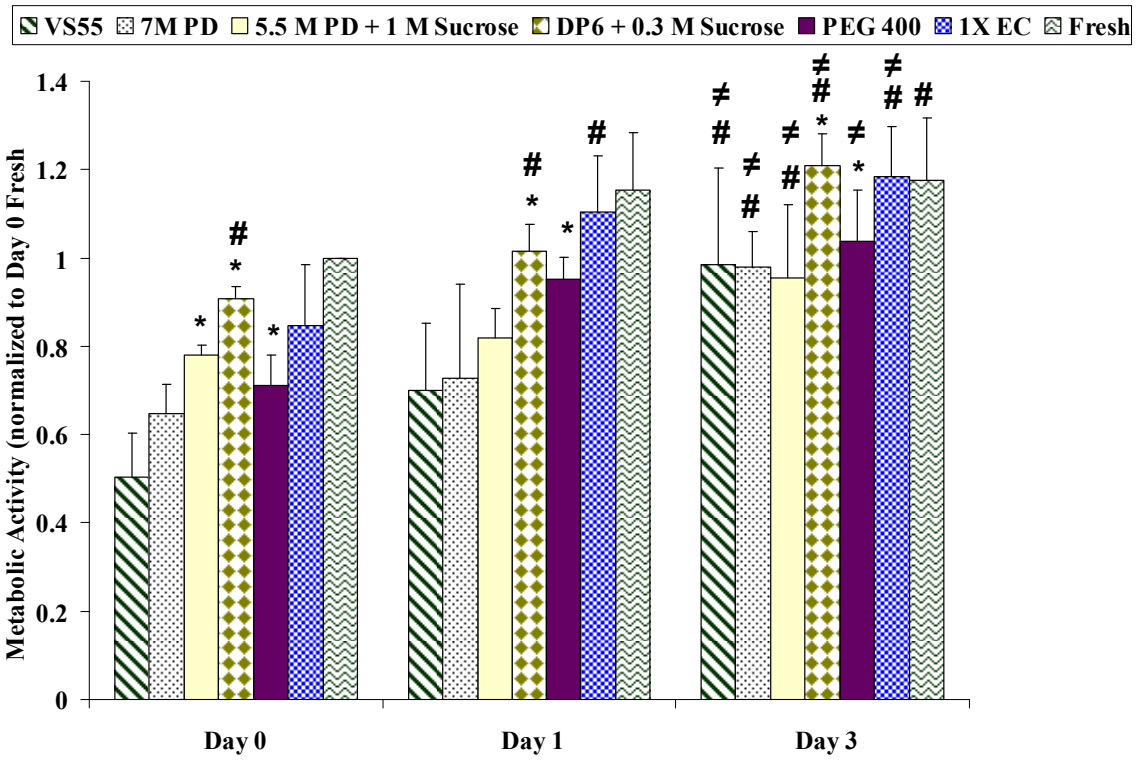

Figure A.1 CPA addition/removal from encapsulated βTC-tet cells. *no statistical difference vs. 1X EC on same day; ($p>0.05$); #no statistical difference vs. Fresh on same day ($p>0.05$); ≠indicates a statistically significant increase in metabolic activity relative to the same group on Day 0 ($p<0.05$). *n=3-12*

Initial vitrification studies were performed using a benchtop apparatus. However, to allow for overnight storage as well as allow for scale-up of the vitrification process, subsequent vitrification studies were performed in a mechanical freezer. However, upon performing vitrification studies in the mechanical freezer, DP6 + 0.3 M sucrose

devitrified upon warming. Thus, the sucrose concentration was increased to 0.5 M to prevent devitrification, and the new vitrification solution was named DPS. Subsequent vitrification studies indicated that although DPS and PEG400-vitrified groups gave lower metabolic activity compared to Fresh controls (Figure A.2), there was no difference in normalized ISR between DPS-vitrified and the Fresh control (Figure A.3). Thus, DPS was chosen as the vitrification solution for the studies in this thesis.

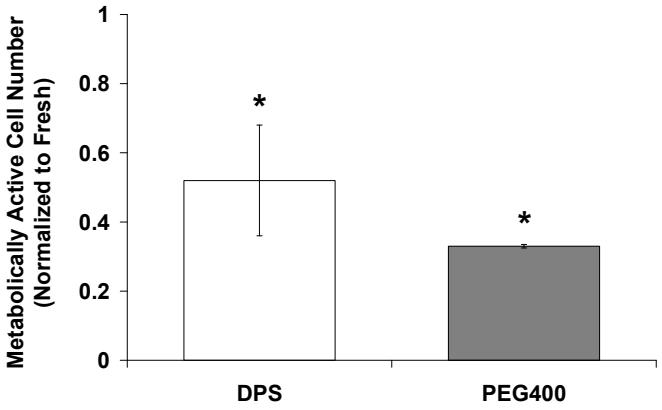

Figure A.2 Metabolic activity (normalized to Fresh Controls) after vitrification of encapsulated βTC-tet cells. Note: for the DPS group, cells were encapsulated in alginate-poly-L-lysine-alginate (APA) beads. βTC insulinomas encapsulated in alginate coated with poly-L-lysine (PLL) have been shown to exhibit similar metabolic activity and function compared to controls without PLL [134]. *p<0.05 compared to Fresh. *n=3*

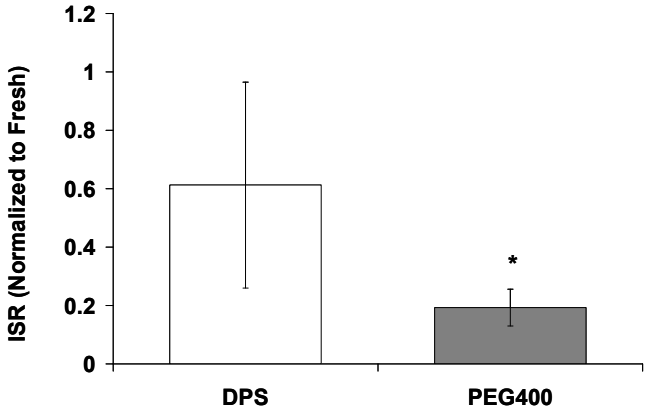

Figure A.3 ISR (normalized to Fresh Controls) after vitrification of encapsulated βTC-tet cells. Note: For the DPS group, cells were encapsulated in alginate-poly-L-lysine-alginate beads.*p<0.05 compared to Fresh control. *n=3*

APPENDIX B

METAL VS. PLASTIC GENERATOR PROBE: POTENTIAL PARAMAGNETIC ION EFFECTS ON ^{13}C NMR SPECTRA

As paramagnetic ions can lead to severe line broadening in the NMR spectrum, thus reducing resolution and potentially making it difficult to distinguish isotopomer patters, special precautions were taken during the development of the perchloric acid extraction procedure to minimize potential contamination. Specifically, the standard metal homogenizer probe used initially was replaced with a plastic Omni Tip™ generator probe to help minimize potential paramagnetic ion contamination. Switching to the plastic probe led to better resolution in the NMR spectrum, as indicated below in Figure B.1. Although it is not entirely clear if paramagnetic ions were the cause of the line broadening, it is a plausible explanation, as these ions are known to lead to line broadening and can come from metals.

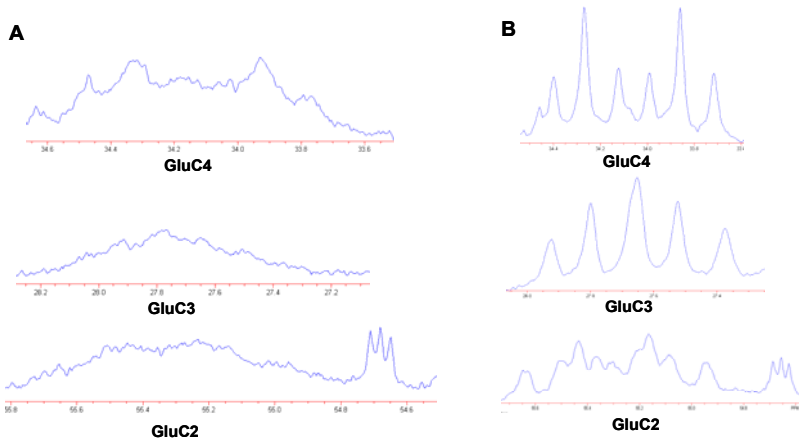

Figure B.1 Glutamate resonances from ^{13}C NMR spectra obtained from extractions using A). metal generator probe and B). a plastic Omin Tip™ generator probe. Prior to each extraction, a 6 ml bead volume of Fresh beads was incubated in 0 mM glucose DMEM for 1 hour followed by 12 hour incubation in ^{13}C-glucose medium.

APPENDIX C

PRELIMINARY STUDIES WITH ALGINATE MODIFICATION

In order to allow for cell attachment and spreading in 3-D, various alginates were modified with the RGD peptide at a density of 10 mg/g alginate, using aqueous carbodiimide chemistry [98]. Stable C2C12 cells were then encapsulated on Day 0 in RGD-modified and unmodified alginates (controls) at a low cell density of $1x10^6$ cells/ml in order to promote cell-matrix interactions and cultured for 10 days. Metabolically active cell number was assessed with alamarBlue™. An increase in cell number was apparent only in the RGD-modified LVM group (Figure C.1). Cells encapsulated in other alginates experienced a decrease in cell number over time. Although light microscopy pictures indicated that cell proliferation was likely occurring in the 2% RGD-LVM group, significant cell spreading was not evident within gels (Figure C.2).

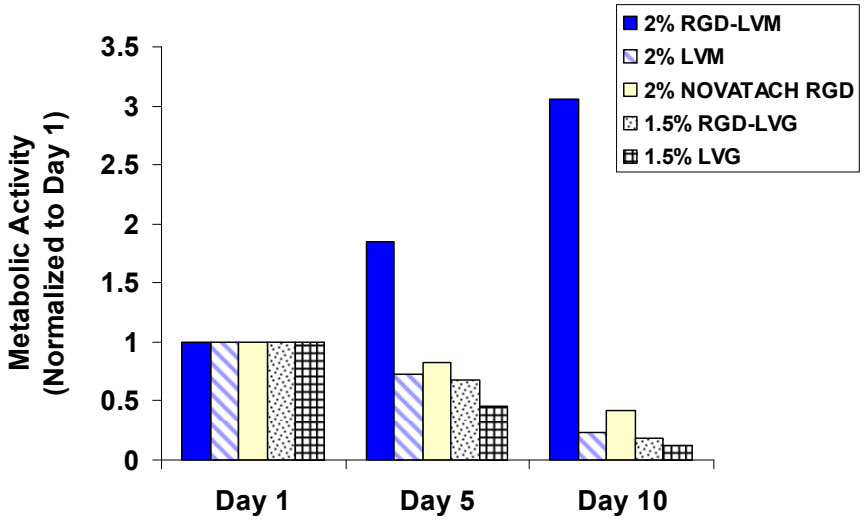

Figure C.1 Metabolic activity of Stable C2C12 cells encapsulated in different alginates at a density of $1x10^6$ cells/ml on Day 0. Beads were cultured for 10 days and sampled for metabolic activity via alamarBlue® and normalized to Day 1 values. Data shown represent one independent encapsulation from each group. *n=1*

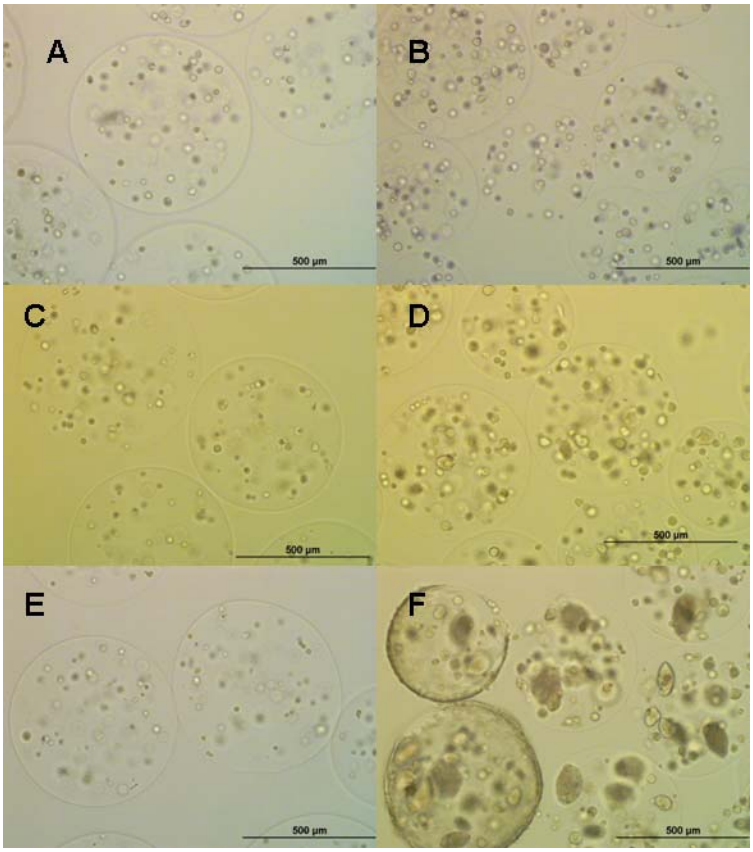

Figure C.2 Stable C2C12 cells encapsulated at $1x10^6$ cells/ml in 2% LVM or 2% RGD-LVM. A)., C)., and E). represent 2% unmodified LVM on days 1, 5, and 10, respectively. B)., D)., and F). represent 2% RGD-LVM on days 1,5, and 10, respectively. All pictures were taken with a 10x objective on an Olympus IX71 inverted microscope.

In order to produce weaker gels that may allow for cell spreading in 3-D, alginates were oxidized prior to RGD modification. Partial oxidation was performed as previously described [111]. After oxidation, alginates were modified with RGD peptide at a density of 10 mg/g alginate as before. Stable C2C12 cells were encapsulated in RGD-modified oxidized alginates at a density of $1x10^6$ cells/ml on Day 0 and beads were assessed with alamarBlue™ over five days (Figure C.3). The highest metabolic activity (Figure C.4) and cell spreading were observed in the 2% RGD-modified oxidized LVM group. However, in order to increase the cell density for assay purposes to $3x10^6$ cells/ml,

and still maintain bead integrity immediately post-encapsulation, the concentration of alginate was increased from 2% to 3%. A control of 3% oxidized LVM without RGD was also included to assess the effect of the softer gels on the encapsulated cells. Initial results indicate cells encapsulated at the higher density in 3% RGD-modified oxidized LVM also experienced an increase in the alamarBlue® reading with cell spreading apparent by 3 days post-encapsulation (Figures C.3 and C.4). It is unclear if the alamarBlue® increase was due to cell proliferation and/or spreading.

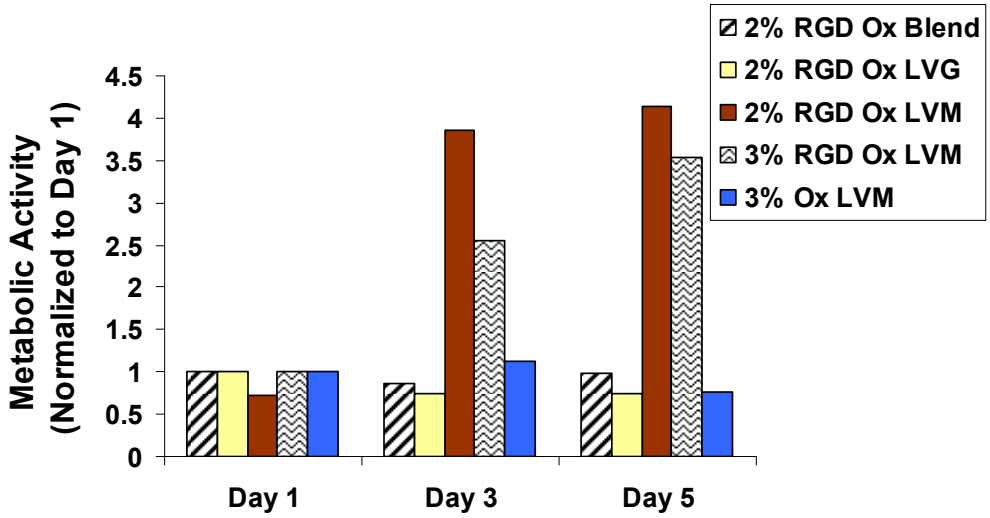

Figure C.3 Metabolic activity measured by alamarBlue® of Stable C2C12 cells encapsulated in different types of RGD-modified oxidized alginates at $1x10^6$ cells/ml (3% alginate groups were encapsulated at $3x10^6$ cells/ml) and normalized to Day 1 values. The blend represents 2% RGD-modified oxidized LVM and 2% RGD-modified oxidized LVG in a 1:1 ratio. Data shown represent one independent encapsulation from each group. *n=1*

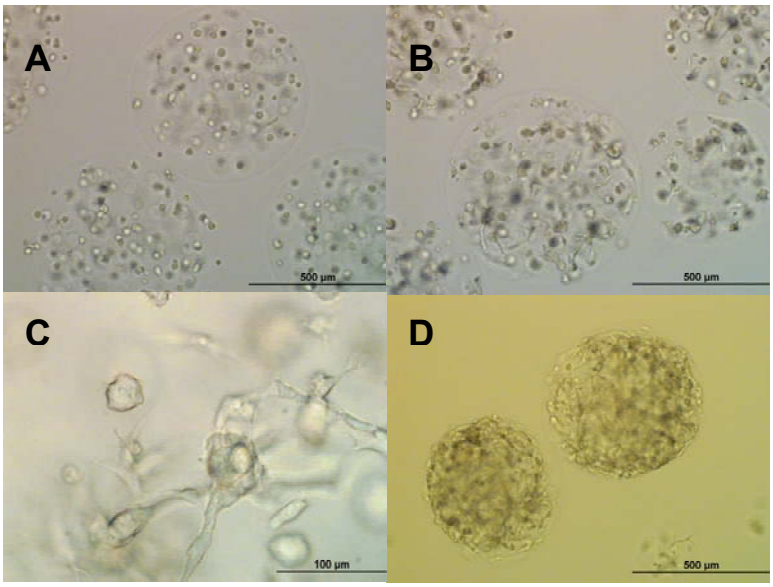

Figure C.4 Light microscopy pictures of Stable C2C12 cells encapsulated in 3% RGD-modified oxidized LVM at $3x10^6$ cells/ml. A). Day 1, 10x; B). Day 3, 10x; C). Day 3, 40x; D).Day 6, 10x. All pictures were taken with an Olympus IX71 inverted microscope.

APPENDIX D

STUDIES TO DETERMINE THE APPROPRIATE 3-D ADHESIVE ALGINATE SYSTEM

Various bead formulations were tested in order to determine the best system to allow for spreading in 3-D RGD-alginate while still being robust enough for surviving time in culture and the cryopreservation procedure. Although various preparations were tried, this section highlights some of the key preparations tried to determine the appropriate 3-D adhesive matrix. Figure D.1 summarizes the different approaches taken and their corresponding results.

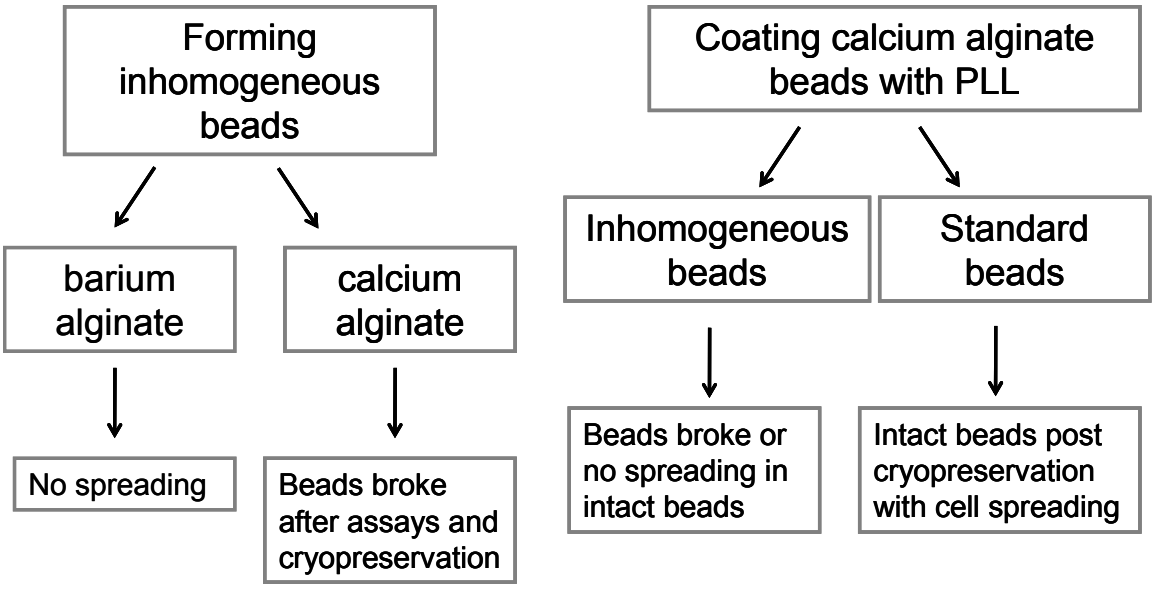

Figure D.1 Flow chart summarizing approaches and results obtained after trying different preparations of Stable C2C12 cells encapsulated in partially oxidized, RGD-modified alginate hydrgels.

Stable C2C12 cells encapsulated in 3.5% oxidized RGD-LVM and crossinked in Ca^{2+} resulted in broken beads after culture in T-flasks. Thus, various approaches were taken to improve bead integrity during culture. These approaches included the formation

of inhomogeneous calcium alginate beads, barium alginate beads, and poly-L-lysine coated calcium alginate beads.

D.1 Inhomogeneous Calcium Alginate Beads

Inhomogeneous calcium alginate beads were tested, as they are known to result in a higher concentration of alginate at the periphery of the bead compared to the center, possibly creating a more stable bead. To form inhomogeneous beads, alginate was dissolved in mannitol and subsequently crosslinked in 100 mM $CaCl_2$ adjusted to 300 mOsm. Although the inhomogeneous calcium alginate beads exhibited nice, spherical geometry post-encapsulation, and overall bead integrity during 4 days in culture (Figure D.2), they did not survive the LIVE/DEAD® procedure (Figure D.3).

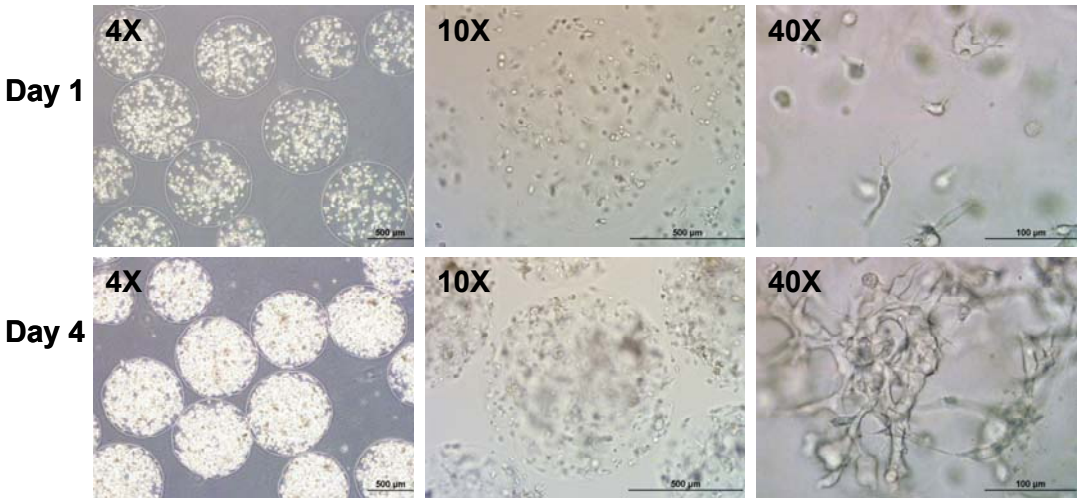

Figure D.2 Fresh inhomogeneous calcium alginate beads (3.5% oxidized, RGD-modified LVM).

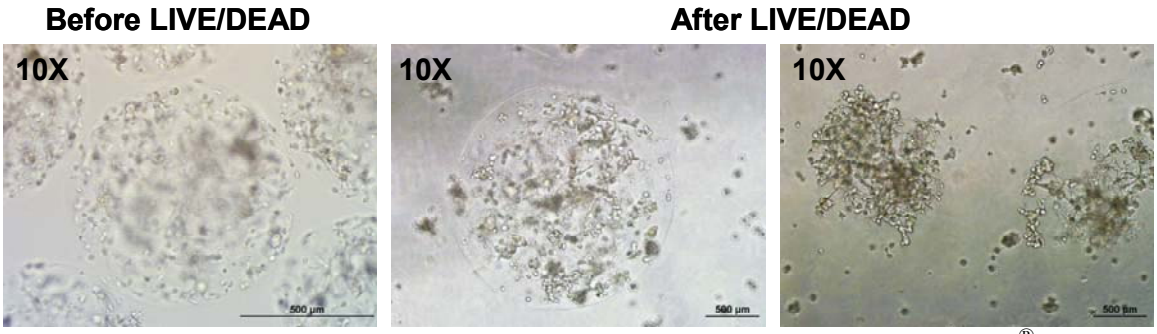

Figure D.3 Fresh inhomogeneous calcium alginate beads after LIVE/DEAD® staining. Beads are damaged after the LIVE/DEAD® staining and imaging procedure.

D.2 Inhomogeneous Barium Alginate Beads

Additionally, inhomogeneous barium-alginate beads were also formed to see if stiffer beads could be formed compared to using calcium alginate beads. Concentrations of 20-50 mM Ba^{2+} were tried, but led to no spreading in beads. As indicated in Figure D.4, crosslinking beads in 20 mM $BaCl_2$ led to maintenance of bead integrity up to 4 days in culture, but did not result in cell spreading. This may have been due to the stiffness of the beads, but it is unclear. Beads crosslinked using lower concentrations of barium (i.e. 10 mM Ba^{2+}) resulted in irregular bead formation. Additionally, homogeneous barium alginate beads were also tested, and led to similar results of maintenance of bead integrity in culture over time with no major cell spreading apparent.

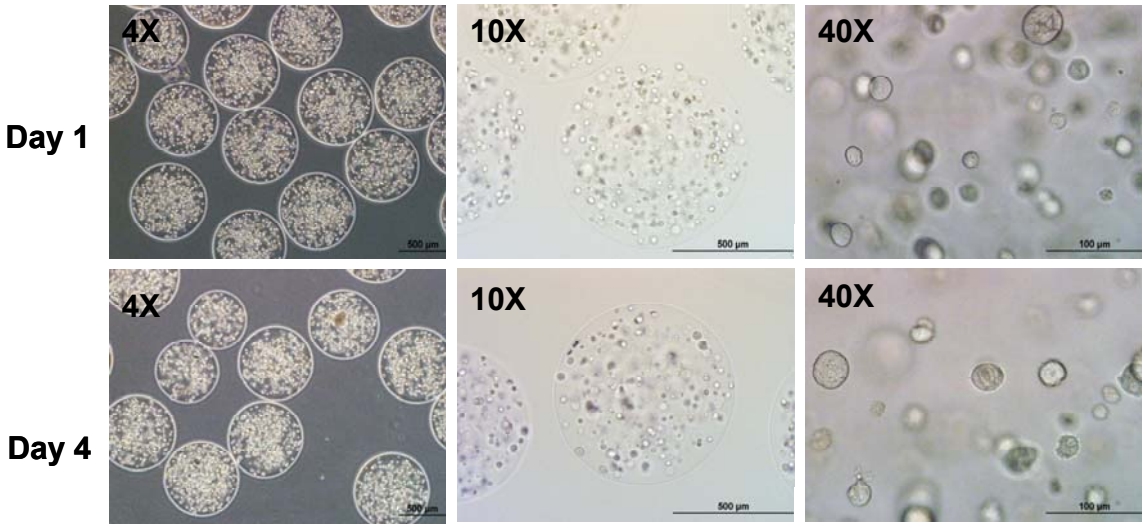

Figure D.4 Fresh Stable C2C12 cells encapsulated in 3.5% oxidized RGD-modified LVM and crosslinked in 20 mM $BaCl_2$ in mannitol (inhomogeneous bead formation). Beads were cultured up to 4 days post-encapsulation.

D.3 Poly-L-lysine-Alginate Coating of Standard Calcium Alginate Beads

Another approach was to coat beads with poly-L-lysine (PLL) (and a final coating of unmodified alginate) in order to help mechanically stabilize the beads. It was thought that the PLL would form a thin shell at the periphery of the beads to help stabilize them. Standard beads, using alginate dissolved in 0.85% NaCl for encapsulation, and crosslinked in 300 mOsm $CaCl_2$ (without NaCl), were formed. However, the base coating protocol, of incubating beads in 0.05% PLL in 0.85% NaCl for 6 minutes [227], resulted in broken beads. Thus, various modifications, as described in Table D.1, were performed.

Table D.1 Modifications made to base protocol for coating standard calcium alginate beads and subsequent results. The base protocol involved coating 3.5% oxidized RGD-modified LVM beads in 0.05% PLL in 0.85% NaCl for 6 minutes. Alginate was dissolved in 0.85% NaCl.

Modification	Result
Increase [alginate] to 3.8%	Majority Beads Broken
Increase [PLL] to 0.1% for 10 min	Intact beads, appear very coated
Increase [PLL] to 0.1% for 5 min	Intact beads, appear very coated
Increase [PLL] to 0.1% for 5 min with one less 0.85% wash	Intact beads, cell spreading

The best option was found to be increasing the PLL concentration to 0.1% for 5 minutes with one less 0.85% NaCl wash. It was desirable to reduce the number of washes in 0.85% NaCl in order to reduce the likelihood of bead destabilization from sodium ions. These beads were able to maintain integrity in culture over 4 days and exhibited cell spreading (Figure D.5). After 4 days in culture, bead integrity was maintained after cryopreservation of small volumes of beads (0.2-0.3 ml) (Figure D.6).

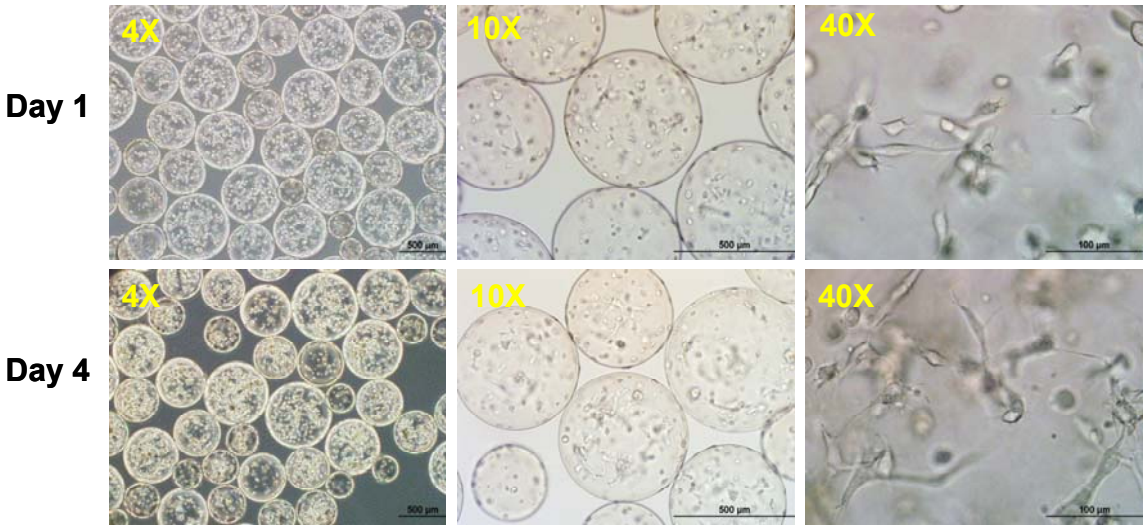

Figure D.5 Fresh Stable C2C12 cells encapsulated in 3.5% oxidized RGD-LVM and coated with 0.1% PLL (Standard coated beads) after 1 and 4 days in culture.

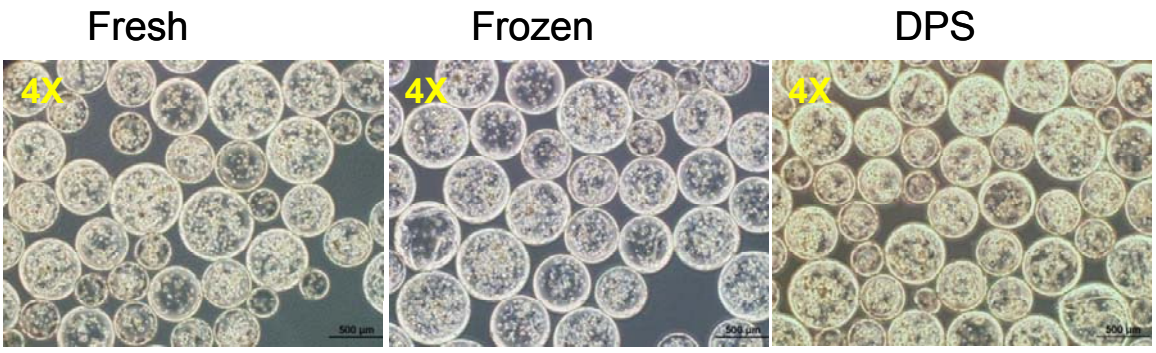

Figure D.6 Stable C2C12 cells encapsulated in 3.5% oxidized RGD-LVM and coated with 0.1% PLL and alginate, before and after cryopreservation. Beads were cultured for 4 days prior to cryopreservation. Light micrographs represent images from beads immediately post-warming (Day 5) as well as the respective Fresh control (Day 4)

D.4 Poly-L-lysine-Alginate Coating of Inhomogeneous Calcium Alginate Beads

Inhomogeneous, PLL-alginate-coated calcium alginate beads were also tested, as they did not require 0.85% NaCl washes, and the exclusion of these washes was thought to possibly help stabilize the alginate matrix. Additionally, inhomogenous beads may be more stable than standard coated beads due to the higher concentration of alginate at the periphery. The alginate was dissolved in 300 mOsm mannitol as opposed to 0.85% NaCl. The base protocol described in Table D.2 resulted in 30-40% broken beads. Thus, the modifications listed in Table D.2 were performed. As none of the modifications were deemed appropriate, inhomogeneous beads were not used for subsequent studies.

Table D.2 Modifications made to base protocol for coating inhomogeneous calcium alginate beads and subsequent results. The base protocol involved coating beads in 0.1% PLL in 300 mOsm mannitol for 6 minutes. The alginate was dissolved in mannitol.

Modification	Result
Coat in 50/50 0.85% NaCl and 300 mOsm mannitol	Majority of beads broken
Remove CHES and CaCl2 washes	Majority of beads broken
Coat in 0.85% NaCl for 5 minutes	Beads intact, but no spreading
Coat in 0.85% NaCl for 2.5 minutes	Majority of beads broken
Decrease [PLL] to 0.05% in 0.85% NaCl	Majority of beads broken
Decrease [PLL] to 0.05% and remove CaCl2 and CHES	Had ~40-50% broken beads

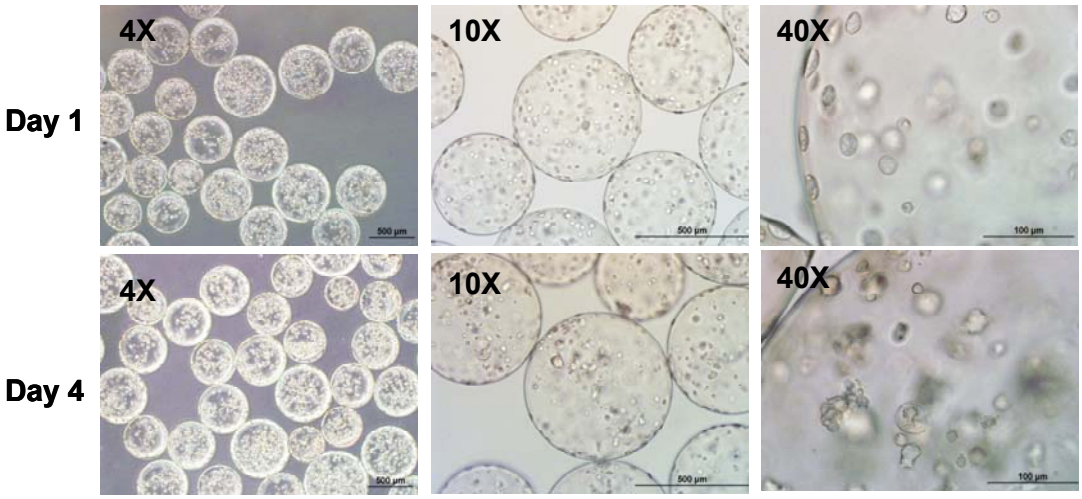

Figure D.7 Fresh inhomogeneous coated beads maintained bead integrity in culture but lacked spreading. Beads were coated in 0.1% PLL in 0.85% NaCl for 5 minutes.

REFERENCES

1. *National Diabetes Fact Sheet, 2011*, C.f.D.C.a. Prevention, Editor. 2011: Atlanta.

2. Ryan, E.A., et al., *Five-year follow-up after clinical islet transplantation.* Diabetes, 2005. **54**(7): p. 2060-9.

3. Sambanis, A., *Bioartificial Pancreas*, in *Principles of Tissue Engineering, 3rd Edition*, L.R. Lonza R, and Vacanti, J, Editor. 2007: Burlington, MA.

4. Fahy, G.M., B. Wowk, and J. Wu, *Cryopreservation of complex systems: The missing link in the regenerative medicine supply chain (vol 9, pg 279, 2006).* Rejuvenation Research, 2006. **9**(4): p. 509-509.

5. Brockbank, K.G.M., Walsh, J.R., Song, Y.C., and Taylor, M.J., *Vitrification: Preservation of Celluar Implants*, in *Topics in Tissue Engineering*, N. Ashammakhi, and Ferretti, P., Editor. 2003. p. 2-26.

6. Fowler, A. and M. Toner, *Cryo-injury and biopreservation.* Cell Injury: Mechanisms, Responses, and Repair, 2005. **1066**: p. 119-135.

7. Acker, J.P., Chen, T, Fowler, A, and Toner M, *Engineering Desiccation Tolerance in Mammalian Cells: Tools and Techniques*, in *Life in the Frozen State*, B. Fuller, Lane, N, and Benson, E, Editor. 2004, CRC Press: Washington, DC. p. 563-580.

8. Narang, A.S. and R.I. Mahato, *Biological and biomaterial approaches for improved islet transplantation.* Pharmacological Reviews, 2006. **58**(2): p. 194-243.

9. Uludag, H., P. De Vos, and P.A. Tresco, *Technology of mammalian cell encapsulation.* Advanced Drug Delivery Reviews, 2000. **42**(1-2): p. 29-64.

10. Weber, L.M. and K.S. Anseth, *Hydrogel encapsulation environments functionalized with extracellular matrix interactions increase islet insulin secretion.* Matrix Biol, 2008. **27**(8): p. 667-73.

11. Weber, L.M., K.N. Hayda, and K.S. Anseth, *Cell-matrix interactions improve beta-cell survival and insulin secretion in three-dimensional culture.* Tissue Eng Part A, 2008. **14**(12): p. 1959-68.

12. Weber, L.M., et al., *The effects of cell-matrix interactions on encapsulated beta-cell function within hydrogels functionalized with matrix-derived adhesive peptides.* Biomaterials, 2007. **28**(19): p. 3004-3011.

13. Geiger, B., et al., *Transmembrane crosstalk between the extracellular matrix--cytoskeleton crosstalk.* Nat Rev Mol Cell Biol, 2001. **2**(11): p. 793-805.

14. Armitage, W.J. and B.K. Juss, *The influence of cooling rate on survival of frozen cells differs in monolayers and in suspensions.* Cryo-Letters, 1996. **17**(4): p. 213-218.

15. Pegg, D.E., *Cryopreservation of vascular endothelial cells as isolated cells and as monolayers.* Cryobiology, 2002. **44**(1): p. 46-53.

16. Sambu, S., et al., *Rgds-Fuctionalized Alginates Improve the Survival Rate of Encapsulated Embryonic Stem Cells during Cryopreservation.* Cryoletters, 2011. **32**(5): p. 389-401.

17. Ji, L., J.J. de Pablo, and S.P. Palecek, *Cryopreservation of adherent human embryonic stem cells.* Biotechnology and Bioengineering, 2004. **88**(3): p. 299-312.

18. Simpson, N.E., et al., *Effects of growth regulation on conditionally-transformed alginate-entrapped insulin secreting cell lines in vitro.* Biomaterials, 2005. **26**(22): p. 4633-41.

19. Goh, F., et al., *Limited beneficial effects of perfluorocarbon emulsions on encapsulated cells in culture: experimental and modeling studies.* J Biotechnol, 2010. **150**(2): p. 232-9.

20. Boontheekul, T., et al., *Regulating myoblast phenotype through controlled gel stiffness and degradation.* Tissue Engineering, 2007. **13**(7): p. 1431-42.

21. Cheng, S.Y., I. Constantinidis, and A. Sambanis, *Use of glucose-responsive material to regulate insulin release from constitutively secreting cells.* Biotechnology and Bioengineering, 2006. **93**(6): p. 1079-1088.

22. Mukherjee, N., et al., *Effects of cryopreservation on cell viability and insulin secretion in a model tissue-engineered pancreatic substitute (TEPS).* Cell Transplant, 2005. **14**(7): p. 449-56.

23. Song, Y.C., et al., *Vitrification of tissue engineered pancreatic substitute.* Transplant Proc, 2005. **37**(1): p. 253-5.

24. Agudelo, C.A., Y. Teramura, and H. Iwata, *Cryopreserved Agarose-Encapsulated Islets As Bioartificial Pancreas: A Feasibility Study.* Transplantation, 2009. **87**(1): p. 29-34.

25. Agudelo, C.A. and H. Iwata, *The development of alternative vitrification solutions for microencapsulated islets.* Biomaterials, 2008. **29**(9): p. 1167-1176.

26. Acker, J.P., et al., *Intracellular ice formation is affected by cell interactions.* Cryobiology, 1999. **38**(4): p. 363-71.

27. Choi, J. and J.C. Bischof, *Cooling rate dependent biophysical and viability response shift with attachment state in human dermal fibroblast cells.* Cryobiology, 2011. **63**(3): p. 285-91.

28. Mukherjee, I.N., Y.C. Song, and A. Sambanis, *Cryoprotectant delivery and removal from murine insulinomas at vitrification-relevant concentrations.* Cryobiology, 2007. **55**(1): p. 10-18.

29. Song, Y.C., et al., *Vitrification of tissue engineered pancreatic substitute.* Transplantation Proceedings, 2005. **37**(1): p. 253-255.

30. Mukherjee, N., et al., *Effects of cryopreservation on cell viability and insulin secretion in a model tissue-engineered pancreatic substitute (TEPS).* Cell Transplantation, 2005. **14**(7): p. 449-456.

31. Matschinsky, F.M., *A lesson in metabolic regulation inspired by the glucokinase glucose sensor paradigm.* Diabetes, 1996. **45**(2): p. 223-241.

32. Jensen, M.V., et al., *Metabolic cycling in control of glucose-stimulated insulin secretion.* American Journal of Physiology-Endocrinology and Metabolism, 2008. **295**(6): p. E1287-E1297.

33. Jitrapakdee, S., et al., *Regulation of insulin secretion: role of mitochondrial signalling.* Diabetologia, 2010. **53**(6): p. 1019-1032.

34. Lu, D., et al., *13C NMR isotopomer analysis reveals a connection between pyruvate cycling and glucose-stimulated insulin secretion (GSIS).* Proc Natl Acad Sci U S A, 2002. **99**(5): p. 2708-13.

35. Cline, G.W., et al., *C-13 NMR isotopomer analysis of anaplerotic pathways in INS-1 cells.* Journal of Biological Chemistry, 2004. **279**(43): p. 44370-44375.

36. Simpson, N.E., et al., *Insights into the role of anaplerosis in insulin secretion: a C-13 NMR study.* Diabetologia, 2006. **49**(6): p. 1338-1348.

37. Inaba, K., et al., *Normalization of diabetes by xenotransplantation of cryopreserved microencapsulated pancreatic islets - Application of a new strategy in islet banking.* Transplantation, 1996. **61**(2): p. 175-179.

38. Schneider, S. and H.H. Klein, *Preserved insulin secretion capacity and graft function of cryostored encapsulated rat islets.* Regulatory Peptides, 2011. **166**(1-3): p. 135-138.

39. Stiegler, P.B., et al., *Cryopreservation of insulin-producing cells microencapsulated in sodium cellulose sulfate.* Transplantation Proceedings, 2006. **38**(9): p. 3026-3030.

40. Zhou, D.B., I. Vacek, and A.M. Sun, *Cryopreservation of microencapsulated porcine pancreatic islets - In vitro and in vivo studies.* Transplantation, 1997. **64**(8): p. 1112-1116.

41. Stensvaag, V., et al., *Cryopreservation of alginate-encapsulated recombinant cells for antiangiogenic therapy.* Cell Transplantation, 2004. **13**(1): p. 35-44.

42. Malpique, R., et al., *Alginate encapsulation as a novel strategy for the cryopreservation of neurospheres.* Tissue Eng Part C Methods, 2010. **16**(5): p. 965-77.

43. Umemura, E., et al., *Viable cryopreserving tissue-engineered cell-biomaterial for cell banking therapy in an effective cryoprotectant.* Tissue Eng Part C Methods, 2011. **17**(8): p. 799-807.

44. Murua, A., et al., *Cryopreservation based on freezing protocols for the long-term storage of microencapsulated myoblasts.* Biomaterials, 2009. **30**(20): p. 3495-3501.

45. Heng, B.C., H. Yu, and S.C. Ng, *Strategies for the cryopreservation of microencapsulated cells.* Biotechnology and Bioengineering, 2004. **85**(2): p. 202-213.

46. Bhakta, G., et al., *Cryopreservation of alginate-fibrin beads involving bone marrow derived mesenchymal stromal cells by vitrification.* Biomaterials, 2009. **30**(3): p. 336-43.

47. Wu, Y., et al., *Vitreous cryopreservation of cell-biomaterial constructs involving encapsulated hepatocytes.* Tissue Eng, 2007. **13**(3): p. 649-58.

48. Jones, P.M., et al., *Cell-based treatments for diabetes.* Drug Discovery Today, 2008. **13**(19-20): p. 888-893.

49. Aguayo-Mazzucato, C. and S. Bonner-Weir, *Stem cell therapy for type 1 diabetes mellitus.* Nature Reviews Endocrinology, 2010. **6**(3): p. 139-148.

50. Bhakta, G., et al., *Cryoreservation of alginate-fibrin beads involving bone marrow derived mesenchymal stromal cells by vitrification.* Biomaterials, 2009. **30**(3): p. 336-343.

51. Wu, Y.N., et al., *Vitreous cryopreservation of cell-biomaterial constructs involving encapsulated hepatocytes.* Tissue Engineering, 2007. **13**(3): p. 649-658.

52. Schneider, S. and H.H. Klein, *Preserved insulin secretion capacity and graft function of cryostored encapsulated rat islets.* Regul Pept, 2011. **166**(1-3): p. 135-8.

53. Zhou, D., I. Vacek, and A.M. Sun, *Cryopreservation of microencapsulated porcine pancreatic islets: in vitro and in vivo studies.* Transplantation, 1997. **64**(8): p. 1112-6.

54. *National diabetes fact sheet: general information and national estimates on diabetes in the United States, 2007*, C.f.D.C.a.P. U.S. Department of Health and Human Services, Editor. 2008: Atlanta.

55. Eriksson, K.F. and F. Lindgarde, *Prevention of Type-2 (Non-Insulin-Dependent) Diabetes-Mellitus by Diet and Physical Exercise - the 6-Year Malmo Feasibility Study.* Diabetologia, 1991. **34**(12): p. 891-898.

56. Goh, S.Y. and M.E. Cooper, *Clinical review: The role of advanced glycation end products in progression and complications of diabetes.* J Clin Endocrinol Metab, 2008. **93**(4): p. 1143-52.

57. *The effect of intensive treatment of diabetes on the development and progression of long-term complications in insulin-dependent diabetes mellitus. The Diabetes Control and Complications Trial Research Group.* N Engl J Med, 1993. **329**(14): p. 977-86.

58. Haitoglou, C.S., et al., *Altered cellular interactions between endothelial cells and nonenzymatically glucosylated laminin/type IV collagen.* Journal of Biological Chemistry, 1992. **267**(18): p. 12404-7.

59. Zieman, S.J., V. Melenovsky, and D.A. Kass, *Mechanisms, pathophysiology, and therapy of arterial stiffness.* Arterioscler Thromb Vasc Biol, 2005. **25**(5): p. 932-43.

60. Cooper, M.E., et al., *Mechanisms of diabetic vasculopathy: an overview.* Am J Hypertens, 2001. **14**(5 Pt 1): p. 475-86.

61. Alsaleh, F.M., et al., *Insulin pumps: from inception to the present and toward the future.* Journal of Clinical Pharmacy and Therapeutics, 2010. **35**(2): p. 127-138.

62. Bode, B.W., R.D. Steed, and P.C. Davidson, *Reduction in severe hypoglycemia with long-term continuous subcutaneous insulin infusion in type I diabetes.* Diabetes Care, 1996. **19**(4): p. 324-327.

63. Boland, E.A., et al., *Continuous subcutaneous insulin infusion - A new way to lower risk of severe hypoglycemia, improve metabolic control, and enhance coping in adolescents with type 1 diabetes.* Diabetes Care, 1999. **22**(11): p. 1779-1784.

64. Conwell, L.S., et al., *Dermatological complications of continuous subcutaneous insulin infusion in children and adolescents.* Journal of Pediatrics, 2008. **152**(5): p. 622-628.

65. Lam, V.W.T., et al., *Evolution of pancreas transplant surgery.* Anz Journal of Surgery, 2010. **80**(6): p. 411-418.

66. White, S.A., J.A. Shaw, and D.E.R. Sutherland, *Pancreas transplantation.* Lancet, 2009. **373**(9677): p. 1808-1817.

67. Frank, A., et al., *Transplantation for type I diabetes: comparison of vascularized whole-organ pancreas with isolated pancreatic islets.* Ann Surg, 2004. **240**(4): p. 631-40; discussion 640-3.

68. Shapiro, A.M., et al., *Islet transplantation in seven patients with type 1 diabetes mellitus using a glucocorticoid-free immunosuppressive regimen.* N Engl J Med, 2000. **343**(4): p. 230-8.

69. Ryan, E.A., et al., *Five-year follow-up after clinical islet transplantation.* Diabetes, 2005. **54**(7): p. 2060-2069.

70. Sambanis, A., et al., *Core technologies in tissue engineering and their application to the bioartificial pancreas.* Tissue Engineering for Therapeutic Use 6, 2002. **1243**: p. 5-18.

71. Uludag, H., P. De Vos, and P.A. Tresco, *Technology of mammalian cell encapsulation.* Adv Drug Deliv Rev, 2000. **42**(1-2): p. 29-64.

72. Sambanis, A.e.a., *Core technologies in tissue engineering and their application to the bioartificial pancreas*, in *Tissue engineering for therapeutic use* Y. Ikada, Umakoshi, Y., and T. Hotta, Editor. 2002. p. 5-18.

73. Lanza, R.P., J.L. Hayes, and W.L. Chick, *Encapsulated cell technology.* Nature Biotechnology, 1996. **14**(9): p. 1107-1111.

74. Orive, G., et al., *Biocompatibility of alginate-poly-L-lysine microcapsules for cell therapy.* Biomaterials, 2006. **27**(20): p. 3691-700.

75. Lim, F. and A.M. Sun, *Microencapsulated islets as bioartificial endocrine pancreas.* Science, 1980. **210**(4472): p. 908-10.

76. Wijsman, J., et al., *Histological and Immunopathological Analysis of Recovered Encapsulated Allogeneic Islets from Transplanted Diabetic Bb/W Rats.* Transplantation, 1992. **54**(4): p. 588-592.

77. Oshea, G.M. and A.M. Sun, *Encapsulation of Rat Islets of Langerhans Prolongs Xenograft Survival in Diabetic Mice.* Diabetes, 1986. **35**(8): p. 943-946.

78. Fritschy, W.M., et al., *The Capsular Overgrowth on Microencapsulated Pancreatic-Islet Grafts in Streptozotocin and Autoimmune Diabetic Rats.* Transplant International, 1994. **7**(4): p. 264-271.

79. Black, S.P., et al., *Immune responses to an encapsulated allogeneic islet beta-cell line in diabetic NOD mice.* Biochemical and Biophysical Research Communications, 2006. **340**(1): p. 236-243.

80. Aoki, T., et al., *Intrasplenic transplantation of encapsulated genetically engineered mouse insulinoma cells reverses streptozotocin-induced diabetes in rats.* Cell Transplantation, 2005. **14**(6): p. 411-421.

81. Juste, S., et al., *Effect of poly-L-lysine coating on macrophage activation by alginate-based microcapsules: Assessment using a new in vitro method.* Journal of Biomedical Materials Research Part A, 2005. **72A**(4): p. 389-398.

82. King, A., S. Sandler, and A. Andersson, *The effect of host factors and capsule composition on the cellular overgrowth on implanted alginate capsules.* Journal of Biomedical Materials Research, 2001. **57**(3): p. 374-383.

83. Strand, B.L., et al., *Poly-L-lysine induces fibrosis on alginate microcapsules via the induction of cytokines.* Cell Transplantation, 2001. **10**(3): p. 263-275.

84. Duvivier-Kali, V.F., et al., *Complete protection of islets against allorejection and autoimmunity by a simple barium-alginate membrane.* Diabetes, 2001. **50**(8): p. 1698-1705.

85. Cui, H., et al., *Long-Term Metabolic Control of Autoimmune Diabetes in Spontaneously Diabetic Nonobese Diabetic Mice by Nonvascularized Microencapsulated Adult Porcine Islets.* Transplantation, 2009. **88**(2): p. 160-169.

86. Omer, A., et al., *Survival and maturation of microencapsulated porcine neonatal pancreatic cell clusters transplanted into immunocompetent diabetic mice.* Diabetes, 2003. **52**(1): p. 69-75.

87. Omer, A., et al., *Long-term normoglycemia in rats receiving transplants with encapsulated islets.* Transplantation, 2005. **79**(1): p. 52-58.

88. Smidrsod, O.a.S.-B., G, *Alginate as immobilization matrix for cells.* Tibtech, 1990. **8**: p. 71-77.

89. Grant, G.T., et al., *Biological Interactions between Polysaccharides and Divalent Cations - Egg-Box Model.* Febs Letters, 1973. **32**(1): p. 195-198.

90. Martinsen, A., G. Skjakbraek, and O. Smidsrod, *Alginate as Immobilization Material .1. Correlation between Chemical and Physical-Properties of Alginate Gel Beads.* Biotechnology and Bioengineering, 1989. **33**(1): p. 79-89.

91. Constantinidis, I., et al., *Effects of alginate composition on the metabolic, secretory, and growth characteristics of entrapped beta TC3 mouse insulinoma cells.* Biomaterials, 1999. **20**(21): p. 2019-2027.

92. Stabler, C., et al., *The effects of alginate composition on encapsulated beta TC3 cells.* Biomaterials, 2001. **22**(11): p. 1301-1310.

93. Simpson, N.E., et al., *The role of the CaCl2-guluronic acid interaction on alginate encapsulated beta TC3 cells.* Biomaterials, 2004. **25**(13): p. 2603-2610.

94. Simpson, N.E., et al., *NMR properties of alginate microbeads.* Biomaterials, 2003. **24**(27): p. 4941-4948.

95. Price, L.S., *Morphological control of cell growth and viability.* Bioessays, 1997. **19**(11): p. 941-943.

96. Weber, L.M. and K.S. Anseth, *Hydrogel encapsulation environments functionalized with extracellular matrix interactions increase islet insulin secretion.* Matrix Biology, 2008. **27**(8): p. 667-673.

97. Boontheekul, T., et al., *Quantifying the relation between bond number and myoblast proliferation.* Faraday Discussions, 2008. **139**: p. 53-70.

98. Rowley, J.A., G. Madlambayan, and D.J. Mooney, *Alginate hydrogels as synthetic extracellular matrix materials.* Biomaterials, 1999. **20**(1): p. 45-53.

99. Rowley, J.A. and D.J. Mooney, *Alginate type and RGD density control myoblast phenotype.* Journal of Biomedical Materials Research, 2002. **60**(2): p. 217-223.

100. Boontheekul, T., et al., *Regulating myoblast phenotype through controlled gel stiffness and degradation.* Tissue Eng, 2007. **13**(7): p. 1431-42.

101. Connelly, J.T., A.J. Garcia, and M.E. Levenston, *Inhibition of in vitro chondrogenesis in RGD-modified three-dimensional alginate gels.* Biomaterials, 2007. **28**(6): p. 1071-1083.

102. Orive, G., et al., *Bioactive cell-hydrogel microcapsules for cell-based drug delivery.* Journal of Controlled Release, 2009. **135**(3): p. 203-210.

103. Kong, H.J., T. Boontheekul, and D.J. Mooney, *Quantifying the relation between adhesion ligand-receptor bond formation and cell phenotype.* Proc Natl Acad Sci U S A, 2006. **103**(49): p. 18534-9.

104. Hwang, N.S., et al., *Chondrogenic differentiation of human embryonic stem cell-derived cells in arginine-glycine-aspartate modified hydrogels.* Tissue Engineering, 2006. **12**(9): p. 2695-2706.

105. Pierschbacher, M.D. and E. Ruoslahti, *Cell Attachment Activity of Fibronectin Can Be Duplicated by Small Synthetic Fragments of the Molecule.* Nature, 1984. **309**(5963): p. 30-33.

106. Ruoslahti, E., *RGD and other recognition sequences for integrins.* Annu Rev Cell Dev Biol, 1996. **12**: p. 697-715.

107. van der Flier, A. and A. Sonnenberg, *Function and interactions of integrins.* Cell and Tissue Research, 2001. **305**(3): p. 285-298.

108. Hermanson, G.T., *Bioconjugate techniques*. 1996, San Diego: Academic Press. xxv, 785 p.

109. Huebsch, N., et al., *Harnessing traction-mediated manipulation of the cell/matrix interface to control stem-cell fate.* Nature Materials, 2010. **9**(6): p. 518-526.

110. Friedl, P. and E.B. Brocker, *The biology of cell locomotion within three-dimensional extracellular matrix.* Cellular and Molecular Life Sciences, 2000. **57**(1): p. 41-64.

111. Boontheekul, T., H.J. Kong, and D.J. Mooney, *Controlling alginate gel degradation utilizing partial oxidation and bimodal molecular weight distribution.* Biomaterials, 2005. **26**(15): p. 2455-2465.

112. Painter, T. and B. Larsen, *Formation of Hemiacetals between Neighbouring Hexuronic Acid Residues during Periodate Oxidation of Alginate.* Acta Chemica Scandinavica, 1970. **24**(3): p. 813-&.

113. Smidsrod, O. and T. Painter, *Effect of Periodate Oxidation Upon Stiffness of Alginate Molecule in Solution.* Carbohydrate Research, 1973. **26**(1): p. 125-132.

114. Bouhadir, K.H., et al., *Degradation of partially oxidized alginate and its potential application for tissue engineering.* Biotechnology Progress, 2001. **17**(5): p. 945-950.

115. Kristiansen, K.A., H.B. Tomren, and B.E. Christensen, *Periodate oxidized alginates: Depolymerization kinetics.* Carbohydrate Polymers, 2011. **86**(4): p. 1595-1601.

116. Kim, W.S., et al., *Adipose tissue engineering using injectable, oxidized alginate hydrogels.* Tissue Eng Part A, 2012. **18**(7-8): p. 737-43.

117. Silva, E.A. and D.J. Mooney, *Effects of VEGF temporal and spatial presentation on angiogenesis.* Biomaterials, 2010. **31**(6): p. 1235-1241.

118. Safley, S.A., et al., *Biocompatibility and immune acceptance of adult porcine islets transplanted intraperitoneally in diabetic NOD mice in calcium alginate poly-L-lysine microcapsules versus barium alginate microcapsules without poly-L-lysine.* J Diabetes Sci Technol, 2008. **2**(5): p. 760-7.

119. Duvivier-Kali, V.F., et al., *Survival of microencapsulated adult pig islets in mice in spite of an antibody response.* Am J Transplant, 2004. **4**(12): p. 1991-2000.

120. Sun, Y.L., et al., *Normalization of diabetes in spontaneously diabetic cynomologus monkeys by xenografts of microencapsulated porcine islets without immunosuppression.* Journal of Clinical Investigation, 1996. **98**(6): p. 1417-1422.

121. van der Laan, L.J., et al., *Infection by porcine endogenous retrovirus after islet xenotransplantation in SCID mice.* Nature, 2000. **407**(6800): p. 90-4.

122. Heneine, W., *No evidence of infection with porcine endogenous retrovirus in recipients of porcine islet-cell xenografts (vol 352, pg 695, 1998).* Lancet, 1998. **352**(9138): p. 1478-1478.

123. D'Amour, K.A., et al., *Production of pancreatic hormone-expressing endocrine cells from human embryonic stem cells.* Nat Biotechnol, 2006. **24**(11): p. 1392-401.

124. Kroon, E., et al., *Pancreatic endoderm derived from human embryonic stem cells generates glucose-responsive insulin-secreting cells in vivo.* Nat Biotechnol, 2008. **26**(4): p. 443-52.

125. Limbert, C., et al., *Beta-cell replacement and regeneration: Strategies of cell-based therapy for type 1 diabetes mellitus.* Diabetes Research and Clinical Practice, 2008. **79**(3): p. 389-399.

126. Tateishi, K., et al., *Generation of Insulin-secreting Islet-like Clusters from Human Skin Fibroblasts.* Journal of Biological Chemistry, 2008. **283**(46): p. 31601-31607.

127. Maehr, R., et al., *Generation of pluripotent stem cells from patients with type 1 diabetes.* Proc Natl Acad Sci U S A, 2009. **106**(37): p. 15768-73.

128. Sapir, T., et al., *Cell-replacement therapy for diabetes: Generating functional insulin-producing tissue from adult human liver cells.* Proc Natl Acad Sci U S A, 2005. **102**(22): p. 7964-9.

129. Zalzman, M., L. Anker-Kitai, and S. Efrat, *Differentiation of human liver-derived, insulin-producing cells toward the beta-cell phenotype.* Diabetes, 2005. **54**(9): p. 2568-75.

130. Efrat, S., *Cell replacement therapy for type 1 diabetes.* Trends in Molecular Medicine, 2002. **8**(7): p. 334-339.

131. Papas, K.K., et al., *Development of a bioartificial pancreas: I. Long-term propagation and basal and induced secretion from entrapped beta TC3 cell cultures.* Biotechnology and Bioengineering, 1999. **66**(4): p. 219-230.

132. Papas, K.K., et al., *Role of ATP and P-i in the mechanism of insulin secretion in the mouse insulinoma beta TC3 cell line.* Biochemical Journal, 1997. **326**: p. 807-814.

133. Sambanis, A., Papas, K.K., Flanders, P.C., Long, R.C., Kang, H., Constantinidis, I., *Towards the development of a bioartificial pancreas: immunoisolation and NMR monitoring of mouse insulinomas.* Cytotechnology, 1994. **15**: p. 351-363.

134. Benson, J.P., et al., *Towards the development of a bioartificial pancreas: Effects of poly-L-lysine on alginate beads with BTC3 cells.* Cell Transplantation, 1997. **6**(4): p. 395-402.

135. Papas, K.K., et al., *Development of a bioartificial pancreas: II. Effects of oxygen on long-term entrapped beta TC3 cell cultures.* Biotechnology and Bioengineering, 1999. **66**(4): p. 231-237.

136. Long, R.C., et al., *In vitro monitoring of total choline levels in a bioartificial pancreas: H-1 NMR spectroscopic studies of the effects of oxygen level.* Journal of Magnetic Resonance, 2000. **146**(1): p. 49-57.

137. Efrat, S., *Development of engineered pancreatic beta-cell lines for cell therapy of diabetes.* Advanced Drug Delivery Reviews, 1998. **33**(1-2): p. 45-52.

138. Efrat, S., et al., *Conditional Transformation of a Pancreatic Beta-Cell Line Derived from Transgenic Mice Expressing a Tetracycline-Regulated Oncogene.* Proceedings of the National Academy of Sciences of the United States of America, 1995. **92**(8): p. 3576-3580.

139. Simpson, N.E., et al., *Effects of growth regulation on conditionally-transformed alginate-entrapped insulin secreting cell lines in vitro.* Biomaterials, 2005. **26**(22): p. 4633-4641.

140. Thule, P.M., J. Liu, and L.S. Phillips, *Glucose regulated production of human insulin in rat hepatocytes.* Gene Therapy, 2000. **7**(3): p. 205-214.

141. Kozlowski, M., et al., *Adeno-associated viral delivery of a metabolically regulated insulin transgene to hepatocytes.* Molecular and Cellular Endocrinology, 2007. **273**(1-2): p. 6-15.

142. Bara, H. and A. Sambanis, *Insulin-secreting L-cells for the treatment of insulin-dependent diabetes.* Biochemical and Biophysical Research Communications, 2008. **371**(1): p. 39-43.

143. Han, J., et al., *Engineered enteroendocrine cells secrete insulin in response to glucose and reverse hyperglycemia in diabetic mice.* Molecular Therapy, 2007. **15**(6): p. 1195-1202.

144. Zhang, Y.Q., et al., *Genetically engineered K cells provide sufficient insulin to correct hyperglycemia in a nude murine model.* Acta Biochimica Et Biophysica Sinica, 2008. **40**(2): p. 149-157.

145. Gros, L., et al., *Insulin production by engineered muscle cells.* Human Gene Therapy, 1999. **10**(7): p. 1207-1217.

146. Wilson, M.O., et al., *Tetracycline-regulated secretion of human (pro)insulin following plasmid-mediated transfection of human muscle.* Journal of Molecular Endocrinology, 2005. **34**(2): p. 391-403.

147. Simonson, G.D., et al., *Synthesis and processing of genetically modified human proinsulin by rat myoblast primary cultures.* Human Gene Therapy, 1996. **7**(1): p. 71-8.

148. Ito, M., et al., *Implantation of primary cultured adipocytes that secrete insulin modifies blood glucose levels in diabetic mice.* Diabetologia, 2005. **48**(8): p. 1614-1620.

149. Knudsen, K.A., *Cell adhesion molecules in myogenesis.* Curr Opin Cell Biol, 1990. **2**(5): p. 902-6.

150. Groskreutz, D.J., M.X. Sliwkowski, and C.M. Gorman, *Genetically-Engineered Proinsulin Constitutively Processed and Secreted as Mature, Active Insulin.* Journal of Biological Chemistry, 1994. **269**(8): p. 6241-6245.

151. Brems, D.N., et al., *Improved Insulin Stability through Amino-Acid Substitution.* Protein Engineering, 1992. **5**(6): p. 519-525.

152. Schwartz, G.P., G.T. Burke, and P.G. Katsoyannis, *A Superactive Insulin - [B10-Aspartic Acid]Insulin(Human).* Proceedings of the National Academy of Sciences of the United States of America, 1987. **84**(18): p. 6408-6411.

153. Polge, C., A.U. Smith, and A.S. Parkes, *Revival of Spermatozoa after Vitrification and Dehydration at Low Temperatures.* Nature, 1949. **164**(4172): p. 666-666.

154. Karlsson, O.M., and Toner, M., *Cryopreservation*, in *Principles of Tissue Engineering*, R.P. Lanza, Langer, R., and J. Vacanti, Editor. 2000, Academic Press: San Diego. p. 293-307.

155. Pegg, D.E., *The history and principles of cryopreservation.* Semin Reprod Med, 2002. **20**(1): p. 5-13.

156. Beattie, G.M., et al., *Trehalose: A cryoprotectant that enhances recovery and preserves function of human pancreatic islets after long-term storage.* Diabetes, 1997. **46**(3): p. 519-523.

157. Pegg, D., *Principles of Tissue Preservation*, in *Progress in Transplantation*, P.a.N. Morris, Tilney, Editor. 1985, Churchill Livingstone: New York. p. 69-105.

158. Mazur, P., S.P. Leibo, and E.H. Chu, *A two-factor hypothesis of freezing injury. Evidence from Chinese hamster tissue-culture cells.* Exp Cell Res, 1972. **71**(2): p. 345-55.

159. Karlsson, J.O.M., E.G. Cravalho, and M. Toner, *Intracellular Ice Formation - Causes and Consequences.* Cryo-Letters, 1993. **14**(6): p. 323-336.

160. Brockbank, K.G., Walsh, J.R., Song, Y.C., and M.J. Taylor, *Vitrification: Preservation of Cellular Implants*, in *Topics in Tissue Engineering*, N.a.P.F. Ashammakhi, Editor. 2003. p. 1-26.

161. Kaiser, J., *New prospects for putting organs on ice.* Science, 2002. **295**(5557): p. 1015.

162. Dahl, S.L.M., et al., *Feasibility of vitrification as a storage method for tissue-engineered blood vessels.* Tissue Engineering, 2006. **12**(2): p. 291-300.

163. Lawson, A., H. Ahmad, and A. Sambanis, *Cytotoxicity effects of cryoprotectants as single-component and cocktail vitrification solutions.* Cryobiology, 2011. **62**(2): p. 115-122.

164. Wang, X., et al., *Cryopreservation of tissue-engineered dermal replacement in Me2SO: Toxicity study and effects of concentration and cooling rates on cell viability.* Cryobiology, 2007. **55**(1): p. 60-5.

165. Macfarlane, D.R., *Physical Aspects of Vitrification in Aqueous Solutions.* Cryobiology, 1987(24): p. 181-195.

166. Ulhmann, D.R., *A kinetic treatment of glass formation.* Journal of Non-Crystalline Solids, 1972(7): p. 337-348.

167. Schneider, S. and H.H. Klein, *Long-Term Graft Function of Cryostored Alginate Encapsulated Rat Islets.* European Journal of Medical Research, 2011. **16**(9): p. 396-400.

168. Rajotte, R.V., et al., *Cryopreservation of microencapsulated canine islets.* Transplantation Proceedings, 1995. **27**(6): p. 3389-3389.

169. Taylor, M.J. and M.J. Benton, *Interaction of cooling rate, warming rate, and extent of permeation of cryoprotectant in determining survival of isolated rat islets of Langerhans during cryopreservation.* Diabetes, 1987. **36**(1): p. 59-65.

170. Rajotte, R.V., et al., *Transplantation of Cryopreserved and Fresh Rat Islets and Canine Pancreatic Fragments - Comparison of Cryopreservation Protocols.* Cryobiology, 1983. **20**(2): p. 169-184.

171. Newsholme, P., C. Gaudel, and N.H. McClenaghan, *Nutrient regulation of insulin secretion and beta-cell functional integrity.* Adv Exp Med Biol, 2010. **654**: p. 91-114.

172. Straub, S.G. and G.W. Sharp, *Glucose-stimulated signaling pathways in biphasic insulin secretion.* Diabetes Metab Res Rev, 2002. **18**(6): p. 451-63.

173. Newgard, C.B. and J.D. McGarry, *Metabolic coupling factors in pancreatic beta-cell signal transduction.* Annu Rev Biochem, 1995. **64**: p. 689-719.

174. Bratanova-Tochkova, T.K., et al., *Triggering and augmentation mechanisms, granule pools, and biphasic insulin secretion.* Diabetes, 2002. **51**: p. S83-S90.

175. Henquin, J.C., *Regulation of insulin secretion: a matter of phase control and amplitude modulation.* Diabetologia, 2009. **52**(5): p. 739-51.

176. Henquin, J.C., et al., *Hierarchy of the beta-cell signals controlling insulin secretion.* Eur J Clin Invest, 2003. **33**(9): p. 742-50.

177. MacDonald, M.J., et al., *Perspective: emerging evidence for signaling roles of mitochondrial anaplerotic products in insulin secretion.* Am J Physiol Endocrinol Metab, 2005. **288**(1): p. E1-15.

178. Jeffrey, F.M.H., et al., *C-13-Nmr - a Simple yet Comprehensive Method for Analysis of Intermediary Metabolism.* Trends in Biochemical Sciences, 1991. **16**(1): p. 5-10.

179. Sherry, A.D., F.M.H. Jeffrey, and C.R. Malloy, *Analytical solutions for C-13 isotopomer analysis of complex metabolic conditions: substrate oxidation, multiple pyruvate cycles, and gluconeogenesis.* Metabolic Engineering, 2004. **6**(1): p. 12-24.

180. Papas, K.K., et al., *NMR spectroscopy in beta cell engineering and islet transplantation.* Ann N Y Acad Sci, 2001. **944**: p. 96-119.

181. Malloy, C.R., A.D. Sherry, and F.M.H. Jeffrey, *Evaluation of Carbon Flux and Substrate Selection through Alternate Pathways Involving the Citric-Acid Cycle of the Heart by C-13 Nmr-Spectroscopy.* Journal of Biological Chemistry, 1988. **263**(15): p. 6964-6971.

182. Lu, D.H., et al., *C-13 NMR isotopomer analysis reveals a connection between pyruvate cycling and glucose-stimulated insulin secretion (GSIS).* Proceedings of the National Academy of Sciences of the United States of America, 2002. **99**(5): p. 2708-2713.

183. Simpson, N.E., et al., *Biochemical consequences of alginate encapsulation: A NMR study of insulin-secreting cells.* Biomaterials, 2006. **27**(12): p. 2577-2586.

184. Jeffrey, F.M., et al., *Substrate selection in the isolated working rat heart: effects of reperfusion, afterload, and concentration.* Basic Res Cardiol, 1995. **90**(5): p. 388-96.

185. Jeffrey, F.M., et al., *13C isotopomer model for estimation of anaplerotic substrate oxidation via acetyl-CoA.* American Journal of Physiology, 1996. **271**(4 Pt 1): p. E788-99.

186. Malloy, C.R., *Analysis of substrate utilization by 13C NMR Spectroscopy.* Stuctural and Organizational Aspects of Metabolic Regulation, 1990: p. 363-374.

187. Simpson, N.E. and I. Constantinidis, *13C NMR isotopomeric analysis and its application in the study of endocrine cell metabolism and function.* Acta Biomed, 2007. **78 Suppl 1**: p. 99-112.

188. Malloy, C.R., A.D. Sherry, and F.M.H. Jeffrey, *Analysis of Tricarboxylic-Acid Cycle of the Heart Using C-13 Isotope Isomers.* American Journal of Physiology, 1990. **259**(3): p. H987-H995.

189. Jeffrey, F.M., et al., *13C-NMR: a simple yet comprehensive method for analysis of intermediary metabolism.* Trends Biochem Sci, 1991. **16**(1): p. 5-10.

190. Breitmaier, E.a.V., Wolfgang, *13C NMR Spectroscopy: Methods and Applications*. Monographs in Modern Chemstry, ed. H.F. Ebel. 1974. 303.

191. Efrat, S., et al., *Conditional transformation of a pancreatic beta-cell line derived from transgenic mice expressing a tetracycline-regulated oncogene.* Proc Natl Acad Sci U S A, 1995. **92**(8): p. 3576-80.

192. Sambanis, A., I.N. Mukherjee, and Y.C. Song, *Cryoprotectant delivery and removal from murine insulinomas at vitrification-relevant concentrations.* Cryobiology, 2007. **55**(1): p. 10-18.

193. Kelly, A.E., et al., *Low-conductivity buffers for high-sensitivity NMR measurements.* J Am Chem Soc, 2002. **124**(40): p. 12013-9.

194. Tyagi, R.K., et al., *Simultaneous extraction of cellular lipids and water-soluble metabolites: Evaluation by NMR spectroscopy.* Magnetic Resonance in Medicine, 1996. **35**(2): p. 194-200.

195. Zhou, D., et al., *In vitro and in vivo evaluation of insulin-producing beta TC6-F7 cells in microcapsules.* American Journal of Physiology-Cell Physiology, 1998. **274**(5): p. C1356-C1362.

196. Duvivier-Kali, V.F., et al., *Complete protection of islets against allorejection and autoimmunity by a simple barium-alginate membrane.* Diabetes, 2001. **50**(8): p. 1698-705.

197. Kizilel, S., M. Garfinkel, and E. Opara, *The bioartificial pancreas: progress and challenges.* Diabetes Technol Ther, 2005. **7**(6): p. 968-85.

198. Cui, H., et al., *Long-term metabolic control of autoimmune diabetes in spontaneously diabetic nonobese diabetic mice by nonvascularized microencapsulated adult porcine islets.* Transplantation, 2009. **88**(2): p. 160-9.

199. Iwata, H. and Y. Teramura, *Bioartificial pancreas Microencapsulation and conformal coating of islet of Langerhans.* Advanced Drug Delivery Reviews, 2010. **62**(7-8): p. 827-840.

200. Beck, J., et al., *Islet encapsulation: strategies to enhance islet cell functions.* Tissue Eng, 2007. **13**(3): p. 589-99.

201. Mallett, A.G. and G.S. Korbutt, *Alginate modification improves long-term survival and function of transplanted encapsulated islets.* Tissue Eng Part A, 2009. **15**(6): p. 1301-9.

202. Veriter, S., et al., *In vivo selection of biocompatible alginates for islet encapsulation and subcutaneous transplantation.* Tissue Eng Part A, 2010. **16**(5): p. 1503-13.

203. Dabos, K.J., et al., *1H NMR spectroscopy as a tool to evaluate key metabolic functions of primary porcine hepatocytes after cryopreservation.* NMR Biomed, 2002. **15**(3): p. 241-50.

204. Loven, A.D., et al., *Phase I and II metabolism and carbohydrate metabolism in cultured cryopreserved porcine hepatocytes.* Chem Biol Interact, 2005. **155**(1-2): p. 21-30.

205. Cline, G.W., et al., *13C NMR isotopomer analysis of anaplerotic pathways in INS-1 cells.* Journal of Biological Chemistry, 2004. **279**(43): p. 44370-5.

206. Weiss, A.D., et al., *Statistical prediction of the vitrifiability and glass stability of multi-component cryoprotective agent solutions.* Cryobiology, 2010. **61**(1): p. 123-7.

207. Malloy, C.R., A.D. Sherry, and F.M. Jeffrey, *Analysis of tricarboxylic acid cycle of the heart using 13C isotope isomers.* Am J Physiol, 1990. **259**(3 Pt 2): p. H987-95.

208. Fleischer, N., et al., *Functional analysis of a conditionally transformed pancreatic beta-cell line.* Diabetes, 1998. **47**(9): p. 1419-1425.

209. Kim, J.C., et al., *Effects of Cryopreservation on Ca(2+) Signals Induced by Membrane Depolarization, Caffeine, Thapsigargin and Progesterone in Boar Spermatozoa.* Molecules and Cells, 2008. **26**(6): p. 558-565.

210. Muller-Schweinitzer, E., et al., *The mechanism of cryoinjury: In vitro studies on human internal mammary arteries.* British Journal of Pharmacology, 2000. **130**(3): p. 636-640.

211. Muller-Schweinitzer, E., et al., *Activated Rho/Rho kinase and modified calcium sensitivity in cryopreserved human saphenous veins.* Cryobiology, 2008. **57**(1): p. 37-45.

212. Song, Y.C., et al., *Vitreous cryopreservation maintains the function of vascular grafts.* Nat Biotechnol, 2000. **18**(3): p. 296-9.

213. Karlsson, J.O.M. and M. Toner, *Long-term storage of tissues by cryopreservation: Critical issues.* Biomaterials, 1996. **17**(3): p. 243-256.

214. Kuleshova, L.L., S.S. Gouk, and D.W. Hutmacher, *Vitrification as a prospect for cryopreservation of tissue-engineered constructs.* Biomaterials, 2007. **28**(9): p. 1585-1596.

215. Song, Y.C., et al., *Vitreous cryopreservation maintains the function of vascular grafts.* Nature Biotechnology, 2000. **18**(3): p. 296-299.

216. Brockbank, K.G.M., et al., *Quantitative analyses of vitrified autologous venous arterial bypass graft explants.* Cell Preservation Technology, 2007. **5**(2): p. 68-76.

217. Drury, J.L. and D.J. Mooney, *Hydrogels for tissue engineering: scaffold design variables and applications.* Biomaterials, 2003. **24**(24): p. 4337-4351.

218. Hernandez, R.M., et al., *Microcapsules and microcarriers for in situ cell delivery.* Adv Drug Deliv Rev, 2010. **62**(7-8): p. 711-30.

219. Jabbari, E., *Bioconjugation of hydrogels for tissue engineering.* Curr Opin Biotechnol, 2011. **22**(5): p. 655-60.

220. Lutolf, M.P. and J.A. Hubbell, *Synthetic biomaterials as instructive extracellular microenvironments for morphogenesis in tissue engineering.* Nature Biotechnology, 2005. **23**(1): p. 47-55.

221. Berrier, A.L. and K.M. Yamada, *Cell-matrix adhesion.* Journal of Cellular Physiology, 2007. **213**(3): p. 565-573.

222. Ruoslahti, E., *RGD and other recognition sequences for integrins.* Annual Review of Cell and Developmental Biology, 1996. **12**: p. 697-715.

223. Place, E.S., et al., *Strontium- and Zinc-Alginate Hydrogels for Bone Tissue Engineering.* Tissue Engineering Part A, 2011. **17**(21-22): p. 2713-2722.

224. Magalhaes, R., et al., *Influence of cell culture configuration on the post-cryopreservation viability of primary rat hepatocytes.* Biomaterials, 2012. **33**(3): p. 829-36.

225. Koebe, H.G., et al., *A new approach to the cryopreservation of hepatocytes in a sandwich culture configuration.* Cryobiology, 1990. **27**(5): p. 576-84.

226. Bouhadir, K.H., D.S. Hausman, and D.J. Mooney, *Synthesis of cross-linked poly(aldehyde guluronate) hydrogels.* Polymer, 1999. **40**(12): p. 3575-3584.

227. Sun, A.M., *Microencapsulation of Pancreatic-Islet Cells - a Bioartificial Endocrine Pancreas.* Methods in Enzymology, 1988. **137**: p. 575-580.

228. Box, G., Cox, DRT, *An analysis of transformations.* Journal of the Royal Statistical Society Series B, 1964(26): p. 211-252.

229. Mahler, S., et al., *Hypothermic storage and cryopreservation of hepatocytes: the protective effect of alginate gel against cell damages.* Cell Transplantation, 2003. **12**(6): p. 579-92.

230. Garcia, A.J., M.D. Vega, and D. Boettiger, *Modulation of cell proliferation and differentiation through substrate-dependent changes in fibronectin conformation.* Mol Biol Cell, 1999. **10**(3): p. 785-98.

231. Gullberg, D., et al., *Analysis of fibronectin and vitronectin receptors on human fetal skeletal muscle cells upon differentiation.* Exp Cell Res, 1995. **220**(1): p. 112-23.

232. Lan, M.A., et al., *Myoblast proliferation and differentiation on fibronectin-coated self assembled monolayers presenting different surface chemistries.* Biomaterials, 2005. **26**(22): p. 4523-31.

233. Teo, K.Y., et al., *Effects of freezing-induced cell-fluid-matrix interactions on the cells and extracellular matrix of engineered tissues.* Biomaterials, 2011. **32**(23): p. 5380-5390.

234. Schenke-Layland, K., et al., *Optimized preservation of extracellular matrix in cardiac tissues: implications for long-term graft durability.* Ann Thorac Surg, 2007. **83**(5): p. 1641-50.

235. Votteler, M., et al., *Raman spectroscopy for the non-contact and non-destructive monitoring of collagen damage within tissues.* Journal of Biophotonics, 2012. **5**(1): p. 47-56.

236. Murase, N., et al., *Two-dimensional diffraction study of ice crystallisation in polymer gels.* Cryo Letters, 2004. **25**(3): p. 227-34.

237. Zhang, W., et al., *Preferential vitrification of water in small alginate microcapsules significantly augments cell cryopreservation by vitrification.* Biomed Microdevices, 2010. **12**(1): p. 89-96.

238. Baust, J.M., et al., *A molecular basis of cryopreservation failure and its modulation to improve cell survival.* Cell Transplantation, 2001. **10**(7): p. 561-71.

239. Taylor, M.J. and S. Baicu, *Review of vitreous islet cryopreservation Some practical issues and their resolution.* Organogenesis, 2009. **5**(3): p. 155-166.

240. Adam, M., Rana, J., and McAndrew, B, *Effect of Cryoprotectants on Activity of Selected Enzymes in Fish Embryos.* Cryobiology, 1995. **32**(1): p. 92-104.

241. Pajot-Augy, E., *Comparative effects of cryosolvents on tubulin association, thermal stability, and binding of microtubule-associated proteins.* Cryobiology, 1993. **30**(3): p. 286-98.

242. Vincent, C., et al., *Solvent effects on cytoskeletal organization and in-vivo survival after freezing of rabbit oocytes.* J Reprod Fertil, 1989. **87**(2): p. 809-20.

243. Lakey, J.R.T., et al., *Secretion from islets and single islet cells following cryopreservation.* Cell Transplantation, 1999. **8**(6): p. 691-698.

244. Misler, S., A. Dickey, and D.W. Barnett, *Maintenance of stimulus-secretion coupling and single beta-cell function in cryopreserved-thawed human islets of Langerhans.* Pflugers Archiv-European Journal of Physiology, 2005. **450**(6): p. 395-404.

245. Orci, L., K.H. Gabbay, and W.J. Malaisse, *Pancreatic Beta-Cell Web - Its Possible Role in Insulin-Secretion.* Science, 1972. **175**(4026): p. 1128-&.

246. Wang, Z.X. and D.C. Thurmond, *Mechanisms of biphasic insulin-granule exocytosis - roles of the cytoskeleton, small GTPases and SNARE proteins.* Journal of Cell Science, 2009. **122**(7): p. 893-903.

247. Dobrinsky, J.R., *Cellular approach to cryopreservation of embryos.* Theriogenology, 1996. **45**(1): p. 17-26.

248. Johnson, M.H. and S.J. Pickering, *The Effect of Dimethylsulfoxide on the Microtubular System of the Mouse Oocyte.* Development, 1987. **100**(2): p. 313-324.

249. Cheng, S.Y., I. Constantinidis, and A. Sambanis, *Insulin secretion dynamics of free and alginate-encapsulated insulinoma cells.* Cytotechnology, 2006. **51**(3): p. 159-170.